1984

Kinetics of coal fly ash chlorination by phosgene

Douglas John Adelman
Iowa State University

INFORMATION TO USERS

This reproduction was made from a copy of a document sent to us for microfilming. While the most advanced technology has been used to photograph and reproduce this document, the quality of the reproduction is heavily dependent upon the quality of the material submitted.

The following explanation of techniques is provided to help clarify markings or notations which may appear on this reproduction.

1. The sign or "target" for pages apparently lacking from the document photographed is "Missing Page(s)". If it was possible to obtain the missing page(s) or section, they are spliced into the film along with adjacent pages. This may have necessitated cutting through an image and duplicating adjacent pages to assure complete continuity.

2. When an image on the film is obliterated with a round black mark, it is an indication of either blurred copy because of movement during exposure, duplicate copy, or copyrighted materials that should not have been filmed. For blurred pages, a good image of the page can be found in the adjacent frame. If copyrighted materials were deleted, a target note will appear listing the pages in the adjacent frame.

3. When a map, drawing or chart, etc., is part of the material being photographed, a definite method of "sectioning" the material has been followed. It is customary to begin filming at the upper left hand corner of a large sheet and to continue from left to right in equal sections with small overlaps. If necessary, sectioning is continued again—beginning below the first row and continuing on until complete.

4. For illustrations that cannot be satisfactorily reproduced by xerographic means, photographic prints can be purchased at additional cost and inserted into your xerographic copy. These prints are available upon request from the Dissertations Customer Services Department.

5. Some pages in any document may have indistinct print. In all cases the best available copy has been filmed.

University Microfilms International
300 N. Zeeb Road
Ann Arbor, MI 48106

Adelman, Douglas John

KINETICS OF COAL FLY ASH CHLORINATION BY PHOSGENE

Iowa State University PH.D. 1984

PLEASE NOTE:

In all cases this material has been filmed in the best possible way from the available copy. Problems encountered with this document have been identified here with a check mark ✓.

1. Glossy photographs or pages ✓
2. Colored illustrations, paper or print _____
3. Photographs with dark background ✓
4. Illustrations are poor copy _____
5. Pages with black marks, not original copy _____
6. Print shows through as there is text on both sides of page _____
7. Indistinct, broken or small print on several pages ✓
8. Print exceeds margin requirements _____
9. Tightly bound copy with print lost in spine _____
10. Computer printout pages with indistinct print _____
11. Page(s) _____ lacking when material received, and not available from school or author.
12. Page(s) _____ seem to be missing in numbering only as text follows.
13. Two pages numbered _____. Text follows.
14. Curling and wrinkled pages _____
15. Other _____

Kinetics of coal fly ash chlorination by phosgene

by

Douglas John Adelman

A Dissertation Submitted to the
Graduate Faculty in Partial Fulfillment of the
Requirements for the Degree of
DOCTOR OF PHILOSOPHY

Major: Chemical Engineering

Approved:

Signature was redacted for privacy.

In Charge of Major Work

Signature was redacted for privacy.

For the Major Department

Signature was redacted for privacy.

For the Graduate College

Iowa State University
Ames, Iowa

1984

TABLE OF CONTENTS

LIST OF FIGURES

LIST OF TABLES

SYMBOLS

A_I = fly ash inert phase specific surface area, $m^2 g^{-1}$

A_N = area per nitrogen molecule, 16.2 $\mathring{A}^2$

A_o = initial fly ash specific surface area, $m^2 g^{-1}$

A_s = area of sample, cm^2

b = stoichiometric coefficient, $g_{\text{fly ash}} (g_{COCl_2})^{-1}$

B'(X) = derivative of alumina versus fly ash conversion expression

c = B.E.T. equation constant

C = ratio of alumina to silica initial weight percent composition in fly ash

C_A = phosgene local concentration, g-M cm^{-3}

C_T = total gaseous molar concentration, kg-M m^{-3}

d_i = average diameter of component i of the fly ash grain size distribution, cm

D = pellet diameter, cm

D_e = effective diffusion coefficient, $cm^2 s^{-1}$

D_{ek} = effective Knudsen diffusion coefficient, $cm^2 s^{-1}$

D_{eM} = effective molecular diffusion coefficient, $cm^2 s^{-1}$

D_M = molecular diffusion coefficient, $cm^2 s^{-1}$

E'(X) = derivative of silica versus fly ash conversion expression

f_m = friction factor

F_A = phosgene reactor input rate, kg hr^{-1}

$F_{A_{as}}$ = phosgene mass input rate required for reaction of alumina and silica, kg hr^{-1}

$F_{A_{nsa}}$ = phosgene mass input rate for reaction of nonsilica-alumina components, kg hr^{-1}

F_I = fly ash reactor input rate, kg hr^{-1}

F_N = flow rate of nitrogen into nitrogen-rich side of diffusion cell, $cm^3 s^{-1}$

F_T = total gaseous flow entering diffusion cell, $cm^3 s^{-1}$

F_{T_2} = flow rate of gas exiting the helium-rich side of diffusion cell, $cm^3 s^{-1}$

g = gravity acceleration constant, m hr^{-2}

G = gaseous superficial mass velocity through chlorination reactor, kg $hr^{-1} m^{-2}$

ΔH_{rxn} = heat of reaction of the alumina-silica fly ash fraction, kcal kg^{-1}

J_i = number of grains in component i of the fly ash grain size distribution

k = fly ash-phosgene reaction rate constant, cm s^{-1}

k_{ad} = phosgene adsorption rate constant, g-M $cm^{-2} atm^{-1} s^{-1}$

k_{de} = phosgene desorption rate constant, g-M $cm^{-2} s^{-1}$

K = thermal conductivity of reactor wall material, kcal m^{-1} hr^{-1} $^oC^{-1}$

L = fly ash pellet half-thickness, cm

m = exponent in equation 54

M = molecular weight, g g-M^{-1}

n = reaction order with respect to phosgene concentration

N = gaseous flux, g-M $cm^{-2} s^{-1}$

N_o = Avogadro's number, molecules g-M^{-1}

N'_{Re} = modified Reynolds number defined in equation 55

P = total pressure, atm

ΔP = reactor bed pressure drop, kg m^{-2}

P_A = phosgene partial pressure, atm

P_{ad} = pressure of nitrogen in contact with fly ash, torr

P_s = saturated vapor pressure of nitrogen in contact with fly ash, torr

Q_C = heat generation rate, kcal hr^{-1}m^{-2}

Q_L = wall heat loss rate, kcal hr^{-1}m^{-2}

r = average reactive core radius of fly ash grains, cm

r_{ad} = phosgene adsorption rate, g-M cm^{-2}s^{-1}

r_{de} = phosgene desorption rate, g-M cm^{-2}s^{-1}

r_o = average radius of unreacted fly ash grains, cm

R = molar reaction or production rate, kg-M hr^{-1}

R_{A_d} = phosgene molar dissociation rate per reactor slice volume, kg-M hr^{-1}

$R_{A_{dv}}$ = phosgene molar dissociation rate, g-M liter^{-1}s^{-1}

R_{A_i} = phosgene local reaction rate in pellet, g-M cm^{-2}s^{-1}

R_F = fly ash reaction rate, kg hr^{-1}

R_G = gas constant

$R_{i,o}$ = chlorination reactor inner, outer radius, m

S = fly ash specific surface area, m^{2}g^{-1}

t = time, s

T = temperature, K

T_b = boiling point temperature, K

$T_{i,o}$ = chlorination reactor inner, outer reactor wall temperature, ^oC

T_s = temperature of liquid nitrogen bath, K

V = chlorination reactor slice volume, m^3

V_A = phosgene local mass reaction rate per unit mass fly ash, g_{COCl_2} $(g_{fly\ ash})^{-1}s^{-1}$

V_{ad} = volume of nitrogen adsorbed on fly ash surface, cm^3

V_b = gaseous molar volume, $cm^3g\text{-}M^{-1}$

V_m = volume of nitrogen monolayer, cm^3

W = weight of clean fly ash sample, g

W_i = initial fly ash sample weight, g

X = fly ash conversion

X_A = conversion of fly ash reactive phase

X_F = fly ash final conversion

Y = gaseous mole fraction

$\bar{Y}$ = gaseous mass fraction

z = position in fly ash pellet axial direction, cm

ΔZ = chlorination reactor slice thickness, m

Greek

α = defined by equation 23

ϵ_b = interpellet bed porosity

ϵ_p = pellet porosity

ϵ_{p_o} = initial pellet porosity

ϵ_T = total porosity of chlorination reactor bed

θ = fraction of fly ash surface covered by phosgene

μ = viscosity of gaseous component i, micropoise

μ_m = viscosity of chlorination reactor gaseous mixture, kg $m^{-1}hr^{-1}$

ρ_g = chlorination reactor gaseous density, kg m^{-3}

ρ_s = density of fly ash grains, g cm^{-3}

σ = reaction modulus defined in equation 8

τ = tortuosity factor

Subscripts

A = phosgene

Al = aluminum chloride

Ca = calcium oxide

Cl_2 = chlorine

CO = carbon monoxide

CO_2 = carbon dioxide

H = helium

N = nitrogen

Si = silicon tetrachloride

Ti = titania

INTRODUCTION

In 1982, 65.4 million tons of coal combustion ashes, over three-fourths of which were fly ash, were collected in the United States. Only 20.7 percent of the total ash was utilized and this amount predominantly in the construction industry (6). Disposal of the remainder may create environmental problems because of the leaching of heavy metals into the ground water. As an alternative to disposal, processes are under development that are to be used to recover metals, primarily aluminum and titanium, from these ashes. They are based on lime-soda sintering (48), acid/base leaching (50), or gaseous chlorination (2,54).

The objective of the Ames Laboratory chlorination project is to collect and correlate data required for the development of the proposed HiChlor process. The research effort is divided into two parts dealing with the chlorination reaction and with product separation. Results of the former are reported here.

The kinetics of the reaction between phosgene and a fly ash, composed primarily of alumina and silica, were characterized. A reaction model has been developed which predicts fly ash conversions as a function of time for the reaction of fly ash with phosgene at partial pressures of 0.03 to 0.96 atm and temperatures of 450 to 675 ^{o}C. The results of the kinetic study were used in the design of a chlorination reactor.

A gas-solid reaction kinetics approach was applied in the study of

the phosgene-fly ash reaction. Values of intrinsic kinetic parameters were determined along with data which physically and chemically characterized fly ash as a function of its conversion. Fly ash was used in this work since it represents a large fraction of the coal combustion ashes collected and is available in uniform supply. The choice of phosgene as a primary reactant will be discussed later.

LITERATURE REVIEW

In developing an experimental approach, chlorination studies and gas-solid reaction techniques were reviewed. Literature from each of these categories considered to be pertinent to the study of the chlorination of fly ash will be discussed.

Chlorination Studies

The chlorination of alumina and titania containing materials has been the subject of many experimental investigations. The alumina work has involved the study of the pure alpha form (39,44,62), and gamma form (3,4,11,12,14,39,44,46), and other materials such as clays (39,40,62) and bauxite (33,38,39,44,46,52). The titania studies involved the chlorination of rutile (10,23,24,25) and ilmenite (23,24,25). Some fly ash chlorination results have also been reported recently (1,33,42). The information provided by these studies was used in the planning of this research project.

The following list of experimental variables was compiled and then choices were made and ranges set based on the literature findings. A discussion of each item will follow.

1. Carbon and chlorine sources
2. Reactant concentrations
3. Fly ash physical state; powder or pellets
4. Temperature
5. Total pressure

6. Additives

7. Silicon tetrachloride recycle

Carbon and chlorine sources

Alumina and titania react with the carbon and chlorine sources to produce the respective metal chlorides and carbon oxides. The carbon source acts as an oxygen sink and is required since thermodynamically these oxides will not react with chlorine directly within the temperature range (up to 900 ^{o}C) chosen for this work (1). The forms of carbon and chlorine typically used in chlorination work include: solid carbon and chlorine, carbon monoxide and chlorine, and phosgene. A discussion of the use of each combination follows.

Carbon and chlorine In a carbon/chlorine reaction system, carbon and the metal oxides are contacted in one of two ways: carbon, in the form of graphite, coke, or activated charcoal, is admixed with the oxide or the carbon is pyrolytically coated on the oxide surface. This coating is obtained by exposing oxides, at elevated temperatures, to hydrocarbons (e.g. methane) in a reducing atmosphere (3,46).

The distance between the carbon and oxides has a strong effect on the oxide chlorination rate (8,10,46). The carbon appears to catalyze the formation of reactive chlorine intermediates (8). However, the catalytic effect is seen only if the carbon-metal oxide separation is less than 30 microns. Since the carbon and the metal oxides react to form gaseous products, chlorination proceeds at a high rate until a separation distance of 30 microns develops. High chlorination rates can

be reattained only if the partially reacted metal oxide is recoated with carbon (46). Simple admixing of carbon and chlorine will not result in appreciable carbon-metal oxide contact. High-surface area materials then are good candidates for the coating option as their use will maximize the carbon contact. The establishment of initial contact between a large weight fraction of the fly ash and carbon will not be possible due to the low specific surface area of fly ash (3 m^2/g).

If, as fly ash reacts, a pore structure develops, coating and chlorination cycles can be considered. The economics of this approach, however, are questionable. In an earlier study (1), it was determined that components, such as quartz, which exist in fly ash, do not chlorinate. This appears to result in the development of an inert matrix as reaction proceeds. If the coating/chlorination approach were employed, it seems that most carbon coated onto the inert surface would be wasted. In addition, if admixed fly ash/carbon systems were reacted with chlorine, the outer inert fly ash layer, which develops after a period of reaction, would possibly adsorb chlorine reactive intermediates travelling from the carbon surface toward the fly ash inner reactive surface.

Carbon monoxide and chlorine Gaseous carbon sources maintain one advantage over solid sources in that they will possibly be able to penetrate the inert matrix developed during the reaction of fly ash. Support for this mechanism is found in the literature. Admixed gamma-alumina-carbon samples chlorinate at much higher rates if oxygen is introduced into the system (39). The oxygen reacts to form carbon

monoxide, which along with the chlorine, can penetrate at least some of the gamma-alumina pore structure to react. In another study (42), the direct addition of carbon monoxide to admixed carbon-fly ash samples enhanced the chlorination rate. Fly ash has a very limited pore structure but that which is available and which develops during reaction is better utilized if carbon monoxide is present.

Under comparable conditions, pyrolytically carbon coated gamma-alumina samples have been shown to chlorinate at a higher rate than samples exposed to carbon monoxide and chlorine (46). With fly ash not being a good candidate for the coating approach and the carbon monoxide/chlorine kinetics appearing to be poor, a third carbon/chlorine source, phosgene, has been considered.

Phosgene Phosgene is thought to hold a kinetic advantage over carbon monoxide/chlorine because it has the oxygen sink and chlorine in the same molecule (10,39). Bertoti et al. (13) report that phosgene molecules were detected on the surface of gamma-alumina samples exposed to carbon tetrachloride. In addition, results of Knudsen-cell mass spectrometry measurements, done as part of this study, indicate that phosgene molecules desorb from the surface of partially reacted fly ash samples. If the formation of surface phosgene species is necessary for chlorination to occur, the direct use of phosgene would eliminate one or more reaction steps. A kinetic advantage is reflected by the lower reaction temperatures needed when using phosgene. Landsberg (39) presents data for the chlorination of aluminous clay which indicate that a temperature of 1050 ^{o}C is required when carbon monoxide and chlorine

are used to produce reaction rates comparable to those attained at 700 ^{o}C with phosgene.

While phosgene holds a significant kinetic advantage, it would appear to be the least practical choice in terms of process development. Phosgene is very toxic (31) and would be the most expensive to obtain. Based on the same criteria, carbon and chlorine would be the best choice. However, to maintain an anhydrous reaction system, a hydrogen-free carbon source would be required. Compositions of coke, one possible carbon source, indicate the presence of a volatile fraction (19). Since this fraction would probably contain some hydrogen bearing compounds, the use of coke would introduce hydrogen to the chlorination system. Carbon monoxide could be produced and dried prior to its use in chlorination. However, for comparable conditions the kinetics when using carbon monoxide and chlorine are so poor relative to those with phosgene that the expense of producing the latter could probably be justified.

The production of phosgene, outlined in several patents (22,41,47,50), does not appear difficult. For example, an equimolar stream of carbon monoxide and chlorine are passed over activated charcoal at 200 ^{o}C and a total pressure of 1 atm to produce nearly pure phosgene (100 ppm carbon tetrachloride) (47). The kinetics of the phosgene synthesis have been thoroughly investigated in a series of papers (58,59,60). It would appear, considering the large number of patents published concerning the phosgene production, that phosgene is used industrially. Methods of dealing with its toxicity then have

certainly been developed.

The complexity of the resulting reaction system also affected the carbon/chlorine choice. The reaction of one solid with one gas (phosgene) is a much easier system to control and monitor than the reaction of two solids with a gas (carbon/chlorine) or two gases with a solid (carbon monoxide/chlorine).

Alternatives Other oxygen sink and chlorine sources were considered. Hydrogen chloride gas (45) and a sulfur dioxide/carbon monoxide mixture (29) have been investigated for the pretreatment of bauxite to remove iron. However, results of thermodynamic calculations published by Kellog (36) indicate that hydrogen chloride gas will not react with either alumina or silica at temperatures of 500 to 1000 ^{o}C. In addition, the use of a sulfur containing compound to chlorinate fly ash in a flow system does not seem to be consistent with treatments to remove sulfur from the coal and the stack gases.

Phosgene was chosen then to serve as the oxygen sink and chlorine source for several reasons. First, being gaseous it could potentially penetrate the inert matrix of fly ash. Phosgene was also found to be kinetically superior to the other options. Finally, phosgene does not appear to be prohibitively expensive to produce and it is accepted in industry. A thorough kinetic study using each option would have been desirable but this was considered to be beyond the scope of this project.

Phosgene concentration, temperature, and total pressure

In considering the operation of a chlorination reactor, it seems likely that the fly ash will be exposed to a wide phosgene concentration range. For this reason, phosgene partial pressures of 0.1 to 0.96 atm were used in the experiments. A temperature range of 400 to 800 ^{o}C was chosen as this is very similar to that used in other phosgene chlorination studies (14,39). The total pressure of the reactor was held at atmospheric pressure for safety reasons. The possible advantages or disadvantages of operating at higher pressures will be discussed later.

Fly ash form

To optimize gas-solid contact, powdered fly ash would be reacted with phosgene. However, since fly ash is a very finely divided material (90 percent, -325 mesh), elutriation from a fluidized bed or a large pressure drop across a static bed may make the use of powder impractical. Since the reaction of fly ash agglomerates may be necessary, it was decided that some pellets would be used in the experimental work.

Additives

The presence of alkali and alkaline earth chlorides in an alumina chlorination reaction system have been usually shown to enhance aluminum chloride production rates (38,40,62). Sodium chloride has been found to enhance these rates most dramatically (40,62). The reasons for the improved reaction rates are not completely understood (40,62); however,

they are thought to be related to the formation of sodium aluminum chloride on the alumina surface (40).

Contrary to the above findings, the authors (42) of a recent fly ash chlorination study report that sodium, potassium, magnesium, and calcium oxides, present in fly ash, readily chlorinate to form solid or liquid products which gradually block the fly ash surface. Decreases in the fly ash specific reaction rate and surface area with conversion are cited as evidence. The interpretation of these results appears questionable since it is also reported (62) that the addition of 2 moles of sodium chloride per mole of alumina significantly enhances the reaction rates and final conversions of alumina. This concentration of sodium chloride is much greater than the combined concentrations of all alkali and alkaline earth oxides present in any fly ash.

In another fly ash chlorination study (1), samples from which 90 weight percent of the alkali and alkaline earth oxides had been removed chlorinated at the same rate as samples bearing the oxides. Based then on the majority of the literature findings, it appears that the addition of alkali and alkaline earth chlorides could dramatically enhance the chlorination rate of fly ash. However, the need to limit the scope of this project precluded a confirmation of their effects.

Silicon tetrachloride recycle

Fly ash typically contains about 60 weight percent silica, present in mullite and in a glass with alumina and balancing ions (30). Since silicon tetrachloride nor silica are of great value, suppression of

silica chlorination is desirable. However, since almost all alumina in fly ash is associated with silica (30), it seems likely that the suppression of the silica reaction would be detrimental to the alumina reaction rates and final recoveries.

The effects of silicon tetrachloride recycle have been examined for the chlorination of bauxite (43) and clays (40). Recycle over bauxite reduced both the silica and alumina chlorination rates and final conversions. Similar results are reported for the clay experiments. Both authors then advised against the use of a silicon tetrachloride recycle. An additional reason for possibly not using $SiCl_4$ recycle in the fly ash chlorination scheme is related to the chemical and physical properties of fly ash. The silica and alumina in bauxite and clay likely exist as separate entities or combined as crystalline minerals with an appreciable surface area. However, the alumina and silica in fly ash are chemically combined in a low surface area solid making reaction of some silica necessary to expose the alumina. Chlorine will have to be recovered from the silicon tetrachloride formed in order to make the process economical.

Gas-Solid Reaction Kinetics

Surface reaction control was verified before intrinsic kinetic parameters were calculated for the fly ash-phosgene reaction system. A discussion of the techniques employed in testing for surface reaction control follows a list of potential reaction rate limiting mechanisms (64). The reaction of a pellet composed of individual particles

(grains) is considered.

1. Mass transfer rates of gaseous reactants or products through the stagnant gas layer surrounding the pellet.
2. Pore diffusion rates of the reactants or products between and within grains.
3. Chemical reaction rates of reactants on the grain surfaces.
4. Adsorption-desorption rates of the reactants or products on the grain surfaces.

The influence of the first two effects are usually eliminated by adjusting experimental conditions. To detect mass transfer limitations, reaction gas velocities are varied over a ten-fold range past identical samples. Constant specific reaction rates as a function of velocity suggests the absence of mass transfer limiting effects.

Pore diffusion limitations can result if the molecular or Knudsen diffusion rates are less than the surface reaction rate. In either a pellet or a powder sample, molecular diffusion often predominates in the intergrain spaces and Knudsen diffusion in the intragrain pores. If the pellet micropore and grain size distributions are available, intragrain and intergrain Knudsen diffusion rates can be estimated, respectively (64). One method useful in detecting diffusion effects involves varying the sample porosity. If the reaction rate decreases with porosity for equal weight samples, diffusion limitations are implied. Diffusion effects can sometimes be eliminated by decreasing the reaction temperature or by reacting thin powder layers.

Intragrain diffusion effects must also be considered. If grain micropores are very small or few in number such that little reaction occurs within them, the grains will react as shrinking solid objects and the intrinsic reaction rates determined can be based on the external surface area of the grains. Intrinsic reaction parameters will result also if the grain pore sizes are large enough to allow rapid diffusion of reactants and products. However, if a large number of pores small enough to cause diffusion rate limitations exist within the grains, temperature adjustment may not eliminate diffusion effects making it impossible to determine intrinsic kinetic parameters. Destruction of the micropores by sintering can jeopardize the accuracy of the kinetic parameters due to chemical changes in the solid.

The magnitude of the activation energy is often used to decide which mechanism limits the solid reaction rate. This approach must be used with caution. If a value of 10 kcal/mole or less is calculated, strong mass transfer or pore diffusion effects are to be suspected. However, a value of 35 kcal/mole, while suggesting surface reaction control, can still be somewhat influenced by the transport mechanisms. Other techniques, mentioned above, must be used to verify the absence of these effects.

Adsorption-desorption effects are often not addressed (64) and are instead usually combined under the third item of the above list. Suggestions concerning the influence of adsorption and desorption rates can be made only if adsorption and desorption kinetic parameters are available. As will be explained later, it did not appear as though

these parameters could be determined for the reaction of fly ash with phosgene.

REACTION MODEL

The grain model has been used in the analysis of many gas-solid reaction systems (40). The model assumes that a pellet consists of a collection of grains, each of which reacts as a shrinking-solid sphere. The grain model is easiest to apply if the initial pellet and grain shapes persist throughout the reaction.

Implications of Fly Ash Physical and Chemical Properties

The physical and chemical characteristics of the fly ash chosen for this study were reviewed prior to deciding whether the grain model could be applied. A microporosity of 0.005, measured using gas adsorption techniques, indicated that fly ash satisfied the first condition of being composed of very nearly solid grains. The maintenance of pellet and grain shapes during reaction seemed likely since, in a previous study (1) and in this work, it was found that only 40 weight percent of the fly ash reacted.

An unreacted fly ash sample along with samples reacted to conversions of 0.05, 0.1, 0.2, and 0.3 were examined with a scanning electron microscope (SEM) so changes resulting from reaction in the shape and morphology of the grains could be observed. A large area of each sample was scanned to ensure that the pictures, presented in Figures 1 and 2, accurately represent the samples. The pictures a-d in Figure 2, are magnifications of a central section of the corresponding lettered pictures of Figure 1.

Figure 1. Scanning electron microscope pictures of fly ash powder chlorinated by phosgene at 625 °C to conversions of: A - 0.0, B - 0.05, C - 0.20, and D - 0.30. Magnification = 1000X (1 cm = 10 microns)

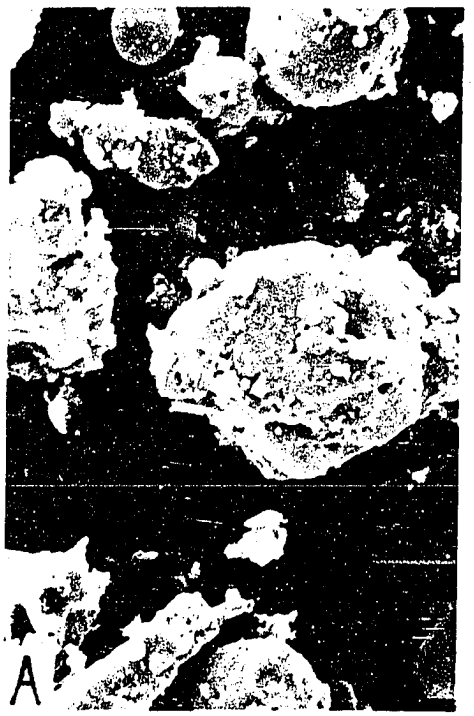
A

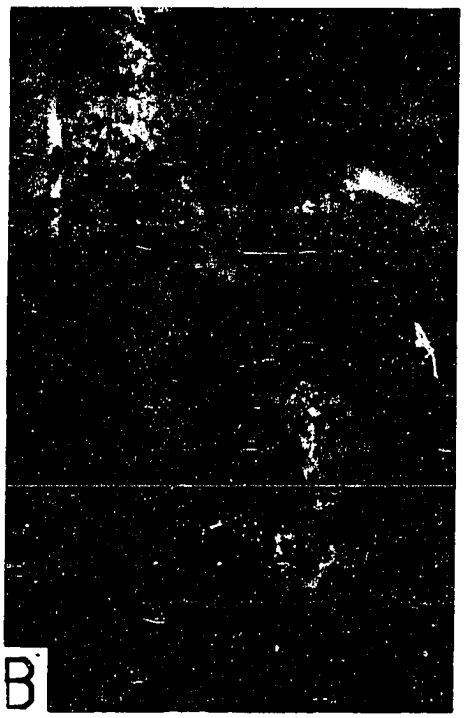
B

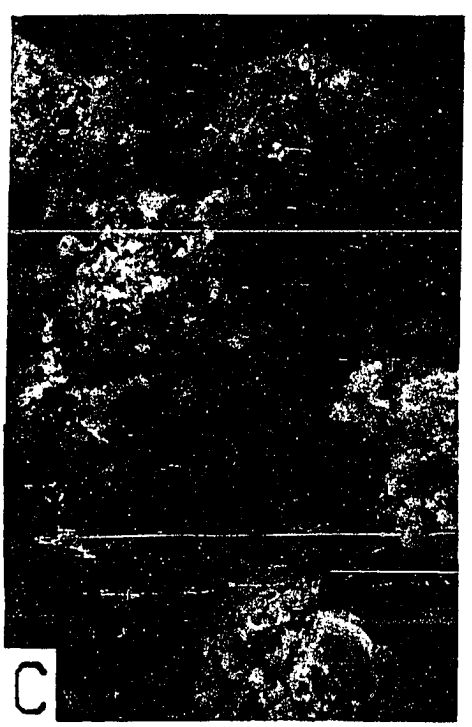
C

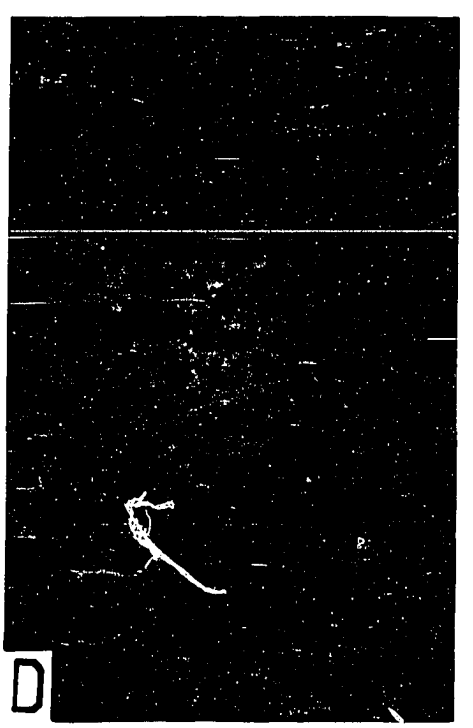
D

Figure 2. Scanning electron microscope pictures of fly ash powder chlorinated by phosgene at 625 °C to conversions of: A - 0.0, B - 0.05, C - 0.20, and D - 0.30. Magnification = 5000X (1 cm = 2 microns)


A

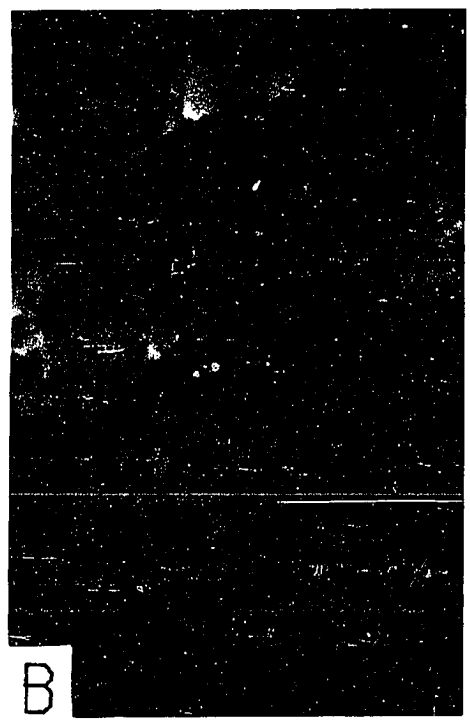
B

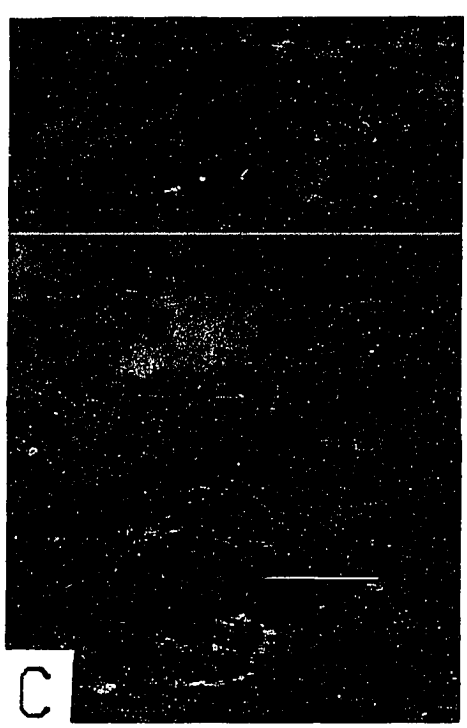
C

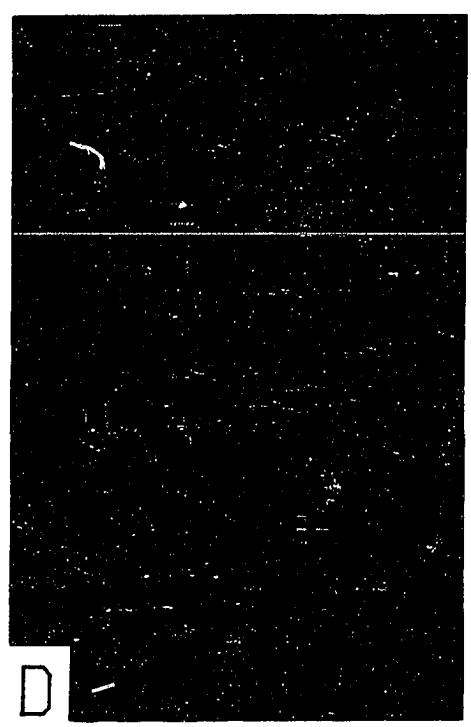
D

The unreacted particles of Figure 1a are varied with respect to shape and size. The large central particle is approximately 140 microns across while others shown are less than 1 micron. The grains are not perfect spheres but other general shapes such as cylinders and flat plates would appear to be less descriptive.

Evidence of the shrinking-core mode of reaction was also sought. As shown by Figure 1b, the surface became extremely rough after only 5 percent of the fly ash was reacted. Most reaction appears to have occurred starting near the outer surface since this degree of degradation throughout a grain would represent much more than a 5 percent weight loss.

In Figures 1c and 1d, it appears that individual particles, originally inside the grains are exposed as conversion increases. The inert matrix, referred to earlier, then develops as the reaction proceeds. The "glue" which holds the small particles together to form grains seems to react. The grain shown in Figure 2a appears to have some of these particles embedded just below its surface. Figures 2b-d give a magnified view of the individual surface particles which are uncovered. Holes or pores leading to the interiors of the grains are apparent in these same pictures suggesting that the reaction zone is quite diffuse.

The overall implication is that application of the grain model seems reasonable. Even though the reaction zone is diffuse, it still appears to move from the outer surface toward the center of the grains. While the grains undergo a dramatic surface change, they maintain the

same general shape.

The results of the SEM investigation are interesting for additional reasons. The chlorination of fly ash in an abrasive environment, such as in a fluidized bed, may cause a severe dusting problem. An alternative, the processing of pellets in a fixed bed could also be troublesome. If the "glue" holding the individual grains together is removed, the whole pellet could degrade. This was considered in the chlorination reactor design to follow. The uncovering of individual particles supports one of the theories of fly ash formation (69). It is thought that dust-like particles of high-melting point minerals stick to molten materials as they pass up the stack together. Many of the grains in Figure 1a appear to have been molten droplets prior to cooling.

The fly ash chemical composition was also considered during development of the reaction model. A typical fly ash (48) contains four major (greater than 5 weight percent) components: silica, alumina, iron oxide, and calcium oxide. Obtaining the data necessary for application of the grain model to such a solid is difficult. Previous work shows that the presence of nonsilica-alumina components (CaO and Fe_2O_3) does not significantly affect the reaction rate or final conversion of alumina in fly ash (1). Since the primary interest was in the reaction of alumina, and with alumina largely present only in combination with silica in mullite and in a glass (30), an attempt was made to obtain a fly ash composed of only alumina and silica. Such an ash (97 weight percent silica and alumina) was found and used in this work. While this simplified the reaction system, the following two reactions still had to

be considered:

$$3COCl_{2(g)} + Al_2O_{3(s)} = 3CO_{2(g)} + 2AlCl_{3(g)}$$

$$2COCl_{2(g)} + SiO_{2(s)} = 2CO_{2(g)} + SiCl_{4(g)}$$

All of the products are volatile gases over the temperature and pressure ranges chosen so product layer diffusion effects were omitted from the model.

Assumptions

The specification of a reaction stoichiometric coefficient was complicated by the presence of both silica and alumina. Since a mole of fly ash is a rather arbitrary quantity, it was decided that the coefficient would be defined as the ratio of the masses of fly ash to phosgene reacted. Any change in the differential molar reaction ratio of silica to alumina would cause a change in the coefficient. The SEM pictures seem to indicate that the fly ash grains reacted from the outer surface toward the center leaving behind an inert phase. This being true, the inert and reacting compositions would be constant and a constant stoichiometric coefficient would result. Variation of the coefficient as a function of fly ash conversion would indicate that a reactive fraction was preferentially removed first throughout the grains followed by a slower reaction of less reactive components. Since such behavior would signify nonadherence to the grain model, it was assumed initially and later verified experimentally that the stoichiometric coefficient was constant as a function of conversion.

Other assumptions adopted include reaction irreversibility and equimolar counterdiffusion within the pellet. Neither is necessarily valid, especially the latter, considering the difference between the number of moles of gaseous products and reactants. With respect to the first assumption, it has been shown that the formation of the oxychloride is the rate limiting step in the chlorination of titania (34). If this is also true for the reaction of alumina and silica, product concentrations within the pellets would be small making irreversibility an accurate assumption.

Some additional assumptions applied during the development of the reaction model include isothermal reaction conditions and the absence of external mass transfer resistance. The validity of the first assumption was never verified directly. Instead, thin pellets and powder layers were reacted to facilitate heat dissipation. When reaction rates became available, calculations were done which indicated that external mass transfer rates never limited the fly ash powder or pellet chlorination rates.

Phosgene and Fly Ash Mass Balances

Cylindrical pellets with a diameter to thickness ratio of 13 to 1 were reacted during the experiments and then modelled as flat plates (70). The mass balance for the movement of phosgene (A) across a differential slice of such a pellet is:

$$D_{e_A} \frac{\partial^2 C_A}{\partial z^2} - \frac{V_A \rho_s (1 - \epsilon_p)}{M_A} = 0 \qquad (1)$$

where D_{e_A} = phosgene effective diffusion coefficient, $cm^2 s^{-1}$;

C_A = phosgene local concentration, g-M cm^{-3};

z = position in pellet axial direction, cm;

V_A = local phosgene mass reaction rate per unit mass fly ash, $g_{COCl_2} (g_{fly\ ash})^{-1} s^{-1}$;

ρ_s = density of fly ash grains, g cm^{-3};

ϵ_p = pellet porosity;

M_A = phosgene molecular weight, g $g\text{-}M^{-1}$.

The accumulation term is set equal to zero since it is assumed that the amount of phosgene within the pellet void space is small compared to the reaction and net input rates of phosgene. The phosgene local reaction rate is given as:

$$R_{A_i} = kC_A^n \tag{2}$$

where R_{A_i} = phosgene local reaction rate, g-M $cm^{-2} s^{-1}$;

k = rate constant, cm s^{-1};

n = reaction order with respect to the phosgene concentration.

It was further assumed and verified experimentally that the reaction is first order with respect to phosgene. The rate at which the reactive core of a grain shrinks can be related to the phosgene local reaction rate by:

$$bM_A R_{A_i} = -\rho_s \frac{dr}{dt} \tag{3}$$

where b = reaction stoichiometric coefficient, $g_{\text{fly ash}}\ (g_{COCl_2})^{-1}$;

r = reactive core radius, cm;

t = time, s.

Combining equations 2 and 3 yields the following equation relating the rate at which the radius of a grain shrinks to the fly ash chlorination rate.

$$\frac{\partial r}{\partial t} = - \frac{bkM_A C_A}{\rho_s} \tag{4}$$

The equation for V_A, the phosgene mass reaction rate, is written according to its definition (equation 1) to give:

$$V_A = \frac{3r^2 kM_A C_A}{\rho_s r_o^3} \tag{5}$$

where r_o = initial average grain radius, cm.

A combination of equations 1 and 5 yields the following phosgene mass balance equation:

$$\frac{\partial^2 C_A}{\partial z^2} = \frac{3(1 - \epsilon_p) r^2 k C_A}{D_{e_A} r_o^3} \tag{6}$$

A dimensionless reaction modulus, σ, defined in a manner consistent with the literature (64), can be incorporated into equation 6 to give:

$$\frac{\partial^2 C_A}{\partial z^2} = \frac{6\sigma^2 r^2 M_A C_A}{L^2 \rho_s r_o^2} \tag{7}$$

with $$\sigma = L\frac{((1 - \epsilon_p)k)^{1/2}}{(2D_{e_A} r_o)^{1/2}} \qquad (8)$$

where σ = reaction modulus;

L = pellet half-thickness, cm.

The reaction modulus represents the ratio of the ability of the pellet to react to its capacity for gas transport. A modulus of less than 0.3 indicates that diffusion resistance is negligible and that all exposed surface within the pellet is available for reaction (65). The conversion rate of an average sized grain is then equal to that of the whole pellet. If the modulus is greater than 3, the intergrain diffusion rate limits the pellet reaction rate. Values between 0.3 and 3 indicate joint control which, for modelling, requires the numerical solution of equations 4 and 7. Pertinent initial and boundary conditions are:

1. At $t = 0$ $\quad r = r_o \quad$ for $0 \geq z \geq L$

2. At $z = 0$ $\quad C_A = C_{Ao} \quad$ for $t > 0$

3. At $z = L$ $\quad \frac{\partial C_A}{\partial z} = 0 \quad$ for $t > 0$

The initial condition implies that all grains are unreacted at time zero. The first boundary condition, item 2, dispenses with external mass transfer resistance by assuming that the phosgene concentration next to the external surface is the same as that in the bulk (C_{Ao}). The

third condition implies that there is no net flow of phosgene across the pellet centerline.

If diffusion and external mass transfer do not limit the fly ash reaction rate, the reaction can be modelled using a very simple expression (equation 4). To predict the presence of diffusion effects, rate constants, calculated from data known not to be influenced by diffusion effects, and estimated effective diffusion coefficients were used to compute reaction modulus values. These results and the final form of the reaction model equation will be presented later.

Effective Diffusion Coefficient Determination

Effective diffusion coefficients are either measured experimentally at reaction conditions or are calculated. The former method is thought to yield the most accurate values (68) but, for simplicity, the latter was used here. The summary of the procedure employed for the calculation of effective diffusion coefficients follows.

The Bosanquet interpolation formula represents an effective diffusion coefficient as the sum of the effective molecular (D_{eM}) and Knudsen (D_{ek}) diffusion contributions (65).

$$\frac{1}{D_e} = \frac{1}{D_{eM}} + \frac{1}{D_{ek}} \qquad (9)$$

where D_e = effective diffusion coefficient, $cm^2 s^{-1}$;

D_{eM} = effective molecular diffusion coefficient, $cm^2 s^{-1}$;

D_{ek} = effective Knudsen diffusion coefficient, $cm^2 s^{-1}$.

The effective Knudsen diffusion coefficient is calculated according to the following equation adapted from the dusty gas model (65):

$$\tau D_{ek} = \frac{r_o \epsilon_p}{(1 - \epsilon_p)(1 + \frac{\pi}{8})(\frac{8M}{\pi R_G T})^{1/2}} \qquad (10)$$

where τ = tortuosity factor;

M = molecular weight of gas, g $g\text{-}M^{-1}$;

R_G = gas constant, Joules $g\text{-}M^{-1}K^{-1}$;

T = temperature, K.

The molecular diffusion coefficient is determined using the Chapman-Enskog equation (15) and then the effective molecular diffusion coefficient is obtained according to:

$$\tau D_{eM} = \epsilon_p D_M \qquad (11)$$

where D_M = molecular diffusion coefficient, $cm^2 s^{-1}$.

A value for the tortuosity factor in equations 10 and 11 must be obtained before equation 9 can be used to calculate an effective diffusion coefficient. The tortuosity is defined as being a function of only the solid structure (64). It is possible, therefore, to measure an effective diffusion coefficient using an inert gas pair at ambient conditions and then to calculate a tortuosity factor according to equations 9, 10, and 11 and the Chapman-Enskog equation (15). This value of the tortuosity factor can then be used to estimate effective diffusion coefficients of other gases at reaction conditions. The

application of this approach in determining a fly ash pellet tortuosity factor is described in Appendix B.

Chemisorption Considerations

It has been assumed in writing equation 2 that the phosgene dependence can be represented by an integer power of its concentration. In homogeneous reactions, this approach is often satisfactory. In heterogeneous systems, however, the dependences are more complex since the reaction sequence involves the interactions between the different phases along with rearrangement of the reactants to form products. The surface reaction rate is limited by the rate of one of three steps; reactant adsorption, molecular rearrangement to form products, and product desorption. The rates of these steps are directly proportional to the fractions of the solid surface covered by the reactants and products. It is best, therefore, to use a kinetic expression which contains a term that relates the gas phase composition to the surface fractional coverages. The use of this approach was considered but the data requirements and the nature of the reaction system made a successful application seem unlikely. A discussion of some of the complicating factors follows.

Assume that the adsorption rate of phosgene onto the fly ash surface controls the overall reaction rate of fly ash. The Langmuir-Hinshelwood treatment of adsorption and desorption rates is given as (66):

$$r_{ad} = k_{ad}(1 - \theta)P_A \qquad (12)$$

and

$$r_{de} = k_{de}\theta \tag{13}$$

where r_{ad} = phosgene adsorption rate, g-M $cm^{-2}s^{-1}$;

k_{ad} = adsorption rate constant, g-M $cm^{-2}atm^{-1}s^{-1}$;

θ = fraction of fly ash surface covered by phosgene;

P_A = phosgene partial pressure, atm;

r_{de} = phosgene desorption rate, g-M $cm^{-2}s^{-1}$;

k_{de} = desorption rate constant, g-M $cm^{-2}s^{-1}$;

It is assumed, in writing these equations, that:

1. Each site adsorbs one molecule;
2. There is no interaction between neighboring adsorbed molecules;
3. All sites are of equal energy;
4. Phosgene adsorbs nondissociatively.

These assumptions are not realistic, especially the third, when applied to a multicomponent solid such as fly ash.

If Arrhenius expressions are used to calculate values of both rate constants, the determination of frequency factors and activation energies for adsorption and desorption is required. Combination of equations 12 and 13 gives the following coverage rate expression:

$$\frac{d\theta}{dt} = k_{ad}(1 - \theta)P_A - k_{de}\theta \tag{14}$$

The measurement of initial adsorption rates at zero conversion and desorption rates at known coverages, both as a function of temperature,

allows for the determination of the activation energies and frequency factors. The two Arrhenius expressions substituted into equation 14 will yield an expression which predicts phosgene coverage as a function of temperature and phosgene partial pressure at equilibrium.

As described thus far, implementation of this approach would not be difficult. Unfortunately, the assumptions associated with the Langmuir-Hinshelwood treatment are not applicable. The frequency factors and activation energies are often functions of coverages (64,67) so other largely empirical isotherms, Freudlich and Tempkin isotherms (67), must be employed if the relationship between surface coverage and temperature and gaseous partial pressures is to be described satisfactorily. The complexity then becomes much greater with the rate constants functions of coverage. Reaction rates have to be measured at equal coverages over a range of temperatures for the determination of activation energies and frequency factors as a function of coverage. Doing so may not be insurmountable, but the situation is further complicated by the fly ash being consumed. The surface characteristics will be changing so that the rate constants will be a function of both conversion and coverage.

The greatest deterrent to using such an approach arises, however, when the effect of the inert matrix is considered. Since phosgene can chemisorb onto the inert phase, adsorption or desorption rates measured will not be useful in determining active surface kinetic parameters. The possibility of phosgene chemisorption onto the inert phase along with the prospect of the surface characteristics changing with

conversion, are the main reasons for dropping the adsorption-desorption approach and adopting the simple power rate law approach.

EXPERIMENTAL WORK

General data requirements used in the development and testing of the reaction model have been mentioned. A more complete list of the data sets collected along with their purpose will follow. Data not used directly in the reaction model are included as they were important in characterizing fly ash chemical and physical changes resulting from reaction. A description of the equipment used in collecting the data is also included.

Data Sets Collected and Their Purpose

1. A set of initial fly ash conversion rates for phosgene partial pressures in the range, 0.1-0.96 atm, at each temperature, 525, 575, and 625 ^{o}C: to determine the reaction order with respect to the phosgene partial pressure.
2. Initial reaction rates at temperatures in the range, 400-800 ^{o}C, all at an input phosgene partial pressure of 0.48 atm: to prepare an Arrhenius plot to be used to determine an initial activation energy and frequency factor.
3. Conversion versus time data at input phosgene partial pressures of 0.24, 0.48, and 0.96 atm over the temperature range of 525-625 ^{o}C: to prepare an Arrhenius plot for the determination of an activation energy and a frequency factor.
4. Gas chromatographic measurement of exit gas composition at experimental conditions: to determine the extent of phosgene dissociation.

5. Nitrogen adsorption isotherms as a function of fly ash conversion: to determine fly ash specific surface areas as a function of conversion.
6. Phosgene adsorption isotherms as a function of conversion: to determine specific phosgene chemisorption weights as a function of fly ash conversion.
7. Steady-state diffusion cell measurements: to calculate a tortuosity factor.
8. Weight percent silica, alumina, and iron oxide removed from reacted samples: to determine silica to alumina molar reaction ratio as a function of fly ash conversion and to establish whether the iron oxide presence significantly affects the reaction rates measured.
9. Knudsen-cell mass spectrometry: to identify surface gaseous species.
10. Scanning electron microscope pictures: to determine fly ash grain morphology as a function of conversion.
11. Coulter counter grain size distribution: to determine an average fly ash grain diameter.
12. X-ray diffraction analysis of reacted and unreacted fly ash samples: to identify alumina containing components.

Equipment

A Cahn model 2000 microbalance was the major component used in the collection of data for the first five items above. There were

advantages and disadvantages to using a balance for this work. One disadvantage was that the balance was not capable of distinguishing between silica and alumina weight losses making elemental analyses of samples reacted to different conversions necessary for the determination of an alumina to silica molar reaction ratio. Gas chromatographic measurement of the product stream composition would be a more direct way of determining the individual reaction rates of fly ash components. However, reviews (5,56) of metal chloride gas chromatography literature indicated that the development of a workable separation scheme would be a research project in itself. Also, measurement of initial reaction rates with a gas chromatograph would be difficult.

Electrobalance flow system

The balance was utilized in both a flow and a closed configuration. The two arrangements were incorporated into one system represented by the schematic in Figure 3. The flow system was used to collect data needed in the calculation of initial reaction rates and phosgene chemisorption isotherms. The balance was operated at a sensitivity of 10 micrograms per chart paper division for reaction rate measurements and at 1 microgram per division for phosgene adsorption measurements.

The major components of the flow system were the glass jar which contained the balance mechanism, the quartz reaction tube, gas flow system, vacuum system, and furnace. The balance mechanism was protected from phosgene by purging the jar continuously with an inert gas. Helium entered the jar and flowed down through the narrow venturi (2 mm I.D.)

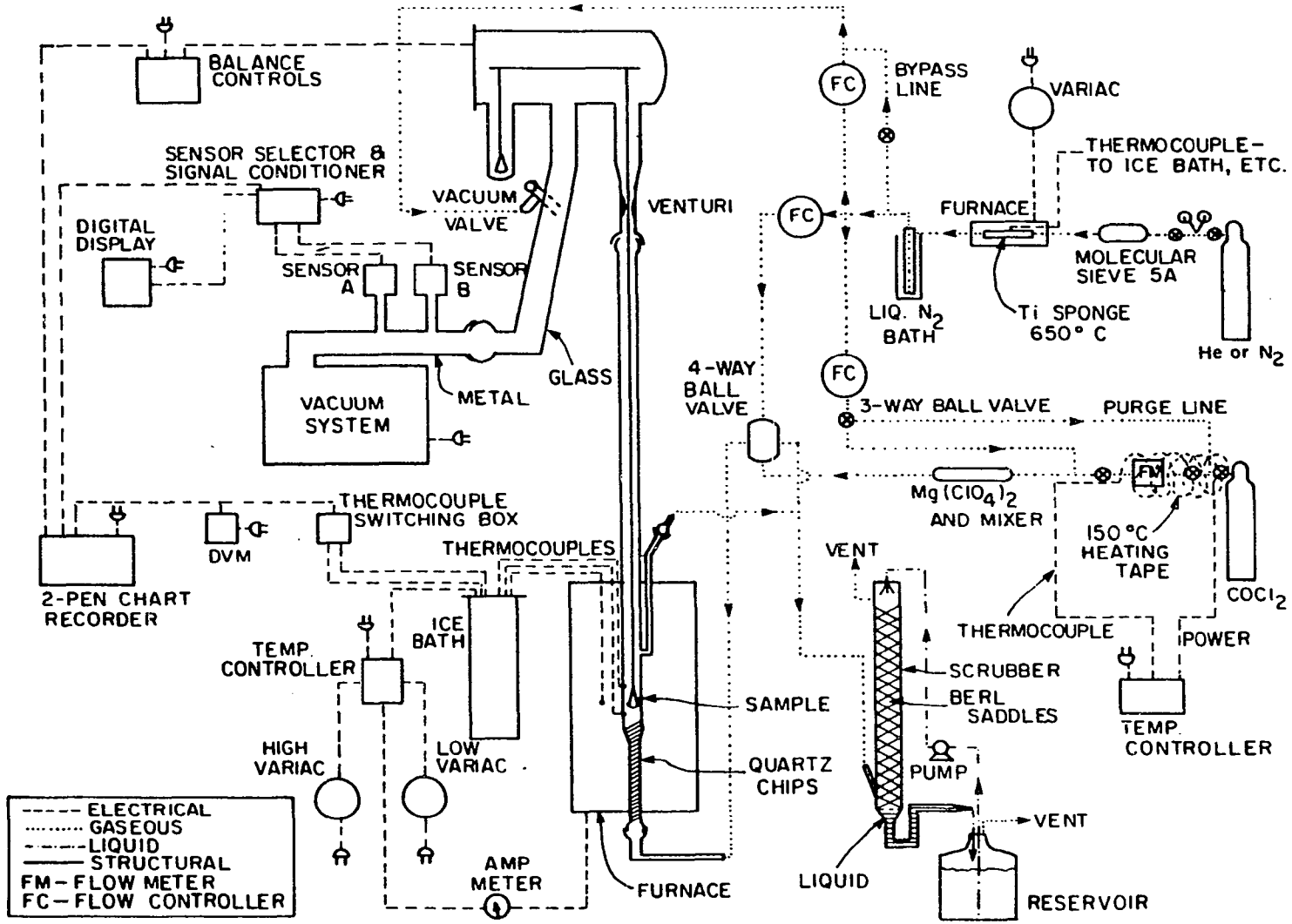

Figure 3. Gravimetric system used in gas-solid reaction experiments

shown in the schematic. Calculations indicated that at ambient conditions, with a flow of 60 cm^3/min helium, the diffusive flux of phosgene in stagnant helium would be 20 times less than that due to the flow of helium through the venturi. During preliminary work involving the reaction of carbon monoxide and chlorine with alpha-alumina, an Interscan portable chlorine detector was used to sample the gas above the venturi. No chlorine was ever detected.

Reactor geometry Two reactor designs were utilized during the flow experiments. The reactor shown in Figure 3 was used most frequently. After the reaction gases (phosgene and helium) were mixed, they enter the bottom, were heated, contacted the sample, and then exited out the side. The purge stream flowed down through the tube and also exited out the side. The exit was positioned within the furnace to prevent the condensation of chloride products on the sample support fiber.

The alternate design is shown in Figure 4 wherein the reaction gases entered above the sample, mixed with the purge gas, were heated, contacted the sample, and then exited out the bottom. With this design, samples could not be exposed to pure phosgene nor was the degree of purge gas-phosgene mixing known. Following recommendations of previous investigators (17), the main body of each reactor was constructed of 16 mm I.D. quartz tubing about 4.5 feet long. This length was used so the balance would be thermally isolated from the furnace.

Sample supports Powder or pellet samples were used in the flow experiments. Schematics of the supports for each are shown in Figure 4.

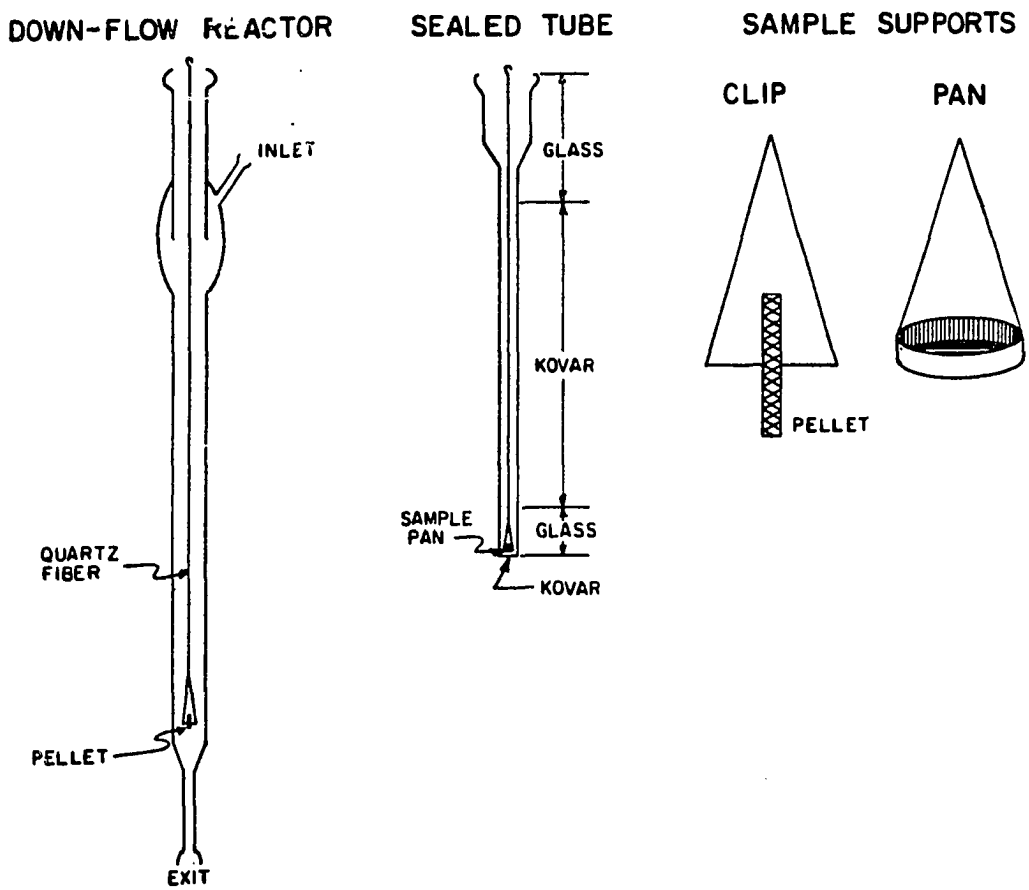

Figure 4. Alternate flow reactor, closed tube, and pellet and powder sample supports

The boat was formed by removing the upper three-fourths of the central section of a 3 mm thick by 15 mm in diameter quartz frit. It was very porous, providing little mass transfer resistance and had a maximum capacity of 100 mg fly ash. Pellets were held in a clip made of 1 mm diameter quartz rod. The samples and supports were suspended from the balance beam by 0.1 mm diameter quartz fiber.

Temperature control A clam-shell electric resistance furnace was used to heat the samples. A temperature controller, received a

millivolt signal from a thermocouple positioned inside the furnace and switched between high and low furnace power supplies, to give sensitive control (+/- 2 ^{o}C). The sample temperature was monitored by two chromel-alumel thermocouples placed in wells above and below the sample. The thermocouples were referenced to the triple point of water and their output was read using a switching box and a digital voltmeter.

Since a layer of quartz lay between the thermocouples and the sample, tests were conducted to ensure the accuracy of the sample temperature readings. One thermocouple was placed on the outside of the tube and another was placed in the reactor tube at the normal sample position. Carbon dioxide was used as the testing gas. The complete range of temperatures and flows were tested and the offsets were negligible.

Gaseous flow measurement A Union Carbide model FM-4550 four channel flow system was used to monitor and control the flow rates of the three inert gas (helium) streams. The first of those was the balance jar purge stream discussed previously. The second flowed past the sample before and after reaction gas exposure to establish sample weight reference points. Total weight loss or gain was then readily determined. This same stream was also used to sweep reaction gases out of the tube at the end of chlorination or chemisorption experiments. A third helium stream was mixed with phosgene to obtain desired partial pressures. Phosgene flows were monitored using a Matheson model 8116-0252 monel flow sensor and controlled manually with a needle valve. It was necessary that all flows be stable as any fluctuations or gradual

changes yielded erroneous sample weights. Gradual drifts were the greatest concern since some experiments spanned a 36-hour period.

Before entering the system, the helium passed through 5A molecular sieve, then titanium sponge at 650 ^{o}C, and finally a cold finger submerged in a liquid nitrogen bath. The nitrogen used in the adsorption experiments was exposed to all but the latter and the phosgene was passed through magnesium perchlorate.

Scrubber Several precautions were taken to prevent the escape of phosgene to the atmosphere. All gases exiting the flow system were passed through a scrubber which consisted of a 3 inch in diameter by 3.5 foot tall pyrex tube packed with 1 inch ceramic Berl saddles. An aqueous solution containing 5 weight percent sodium hydroxide and 1 weight percent ammonia (31) was circulated through the scrubber by pumping continuously from a reservoir. As an additional precaution, any part of the experimental system which could contain phosgene was housed inside a walk-in hood. Finally, the entire gaseous flow network was constructed of monel, stainless steel, glass, or teflon to prevent potentially dangerous line blockages or leaks due to corrosion.

Vacuum system A Veeco type RG vacuum system, connected to the balance jar, was used to clean samples prior to reaction or adsorption experiments. The link between the metal vacuum system and the glass jar consisted of a stainless steel socket and a glass ball. Pressures of 10^{-6} to 10^{-7} torr and temperatures of 25 to 900 ^{o}C could be used for sample cleaning. Samples to be used for chlorination or phosgene chemisorption experiments were cleaned in the flow reactor tube simply

by capping the two ports with blanks prior to evacuation. When nitrogen adsorption experiments were to be conducted, the flow tube was replaced by a sealed tube prior to cleaning the sample. The system pressure was monitored by MKS model 170M pressure transducers to four digit accuracy over a pressure range of 1000 to 10^{-4} torr and by a Veeco type RG-3A vacuum ionization gauge to three digit accuracy for pressures of 10^{-4} to 10^{-8} torr.

Electrobalance closed system

The balance closed configuration was used in the collection of data needed for the calculation of nitrogen physical adsorption isotherms. Samples were supported from the beam in an aluminum boat inside the sealed tube shown in Figure 4. A Dewar flask with a window was used as the sample constant temperature bath during the experiments. The temperature of this bath was measured using a thermistor. The balance was operated at a sensitivity of 1 microgram per chart division for measurements at pressures of greater than 350 torr and at 0.1 microgram per division for lower pressures.

This was the most difficult system to operate because static electricity would cause the sample to stick to the sides of the tube. To prevent this problem, if possible, the sample was outgassed overnight, and then in the morning, great care was taken not to touch the tube prior to or during the experiment. It was also noticed that if the liquid nitrogen Dewar was emptied and refilled occasionally and if

only cotton clothing was worn, the frequency of static problems was reduced.

The reasons for the choice of a microbalance as the major analytical tool for this work can now be summarized. With the addition of a few peripherals, the final system was capable of yielding reaction rate, phosgene chemisorption, and nitrogen adsorption data. Had the system been designed slightly differently, all of these experiments could have been done without even changing the reaction tube. Finally, due to the balance sensitivity, the reaction rate, phosgene chemisorption isotherm, and nitrogen adsorption isotherm of the same small sample (25-150 mg) could be measured.

Diffusion cell system

The experimental determination of an effective diffusion coefficient was discussed as part of the reaction model development. Figure 5 shows the system built for this work. The major components were the gas flow controllers (described earlier), manometer, diffusion cell, sampling valves, and gas chromatograph. The manometer, filled with water, was used along with a pressure control valve to null the pressure across the pellet. The diffusion cell, pictured in greater detail in Figure 6, was constructed of 316 stainless steel with lids sealed to the center body by copper o-rings. Gases entered at the edge of the pellet perpendicular to its surface and exited parallel to the surface across from the entrance. Cylindrical pellets, 1 inch in diameter, were formed directly in the cell.

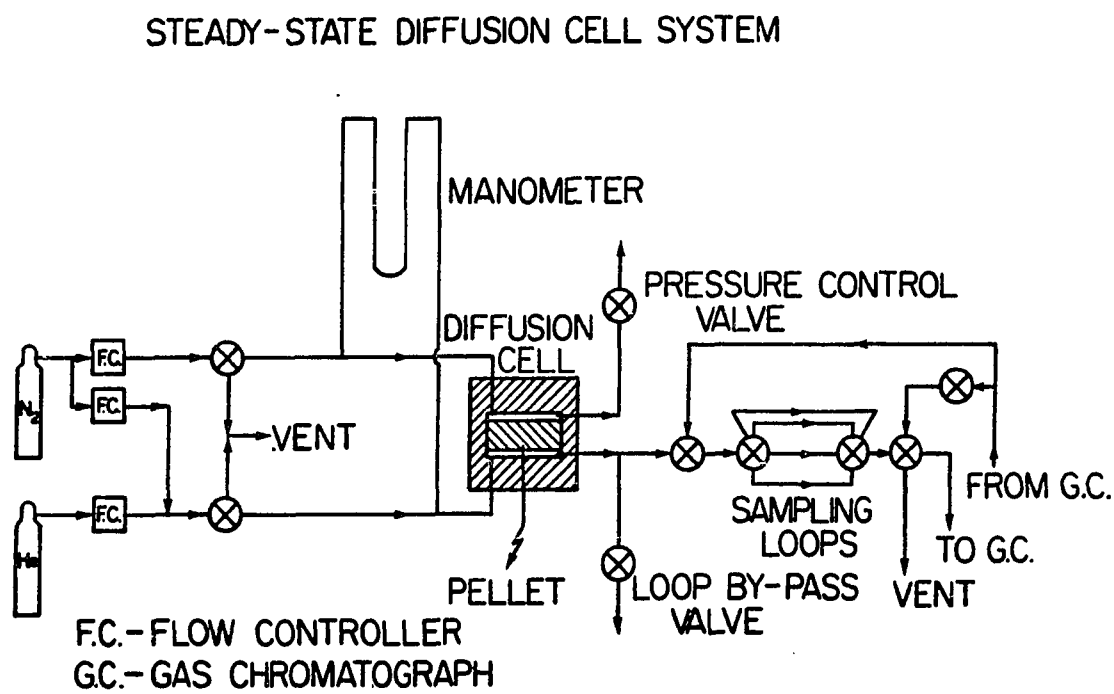

Figure 5. Steady-state diffusion cell and gas-sampling loop system

The gas sampling system pictured in Figure 5 was used to collect three samples within seconds for analysis later. The samples were passed directly from the loops to the thermal conductivity cell of a gas chromatograph.

The diffusion cell system (Figure 5) was designed for steady-state operation. Had the gas sampling loops been incorporated ahead of the cell, the resulting system would have worked well for injecting pulses of tracer gas into a carrier gas stream for nonsteady-state measurements. Effective diffusion coefficients from nonsteady-state measurements are thought to be more accurate (64), one reason being that dead-end pores are taken into account. This measurement was not done

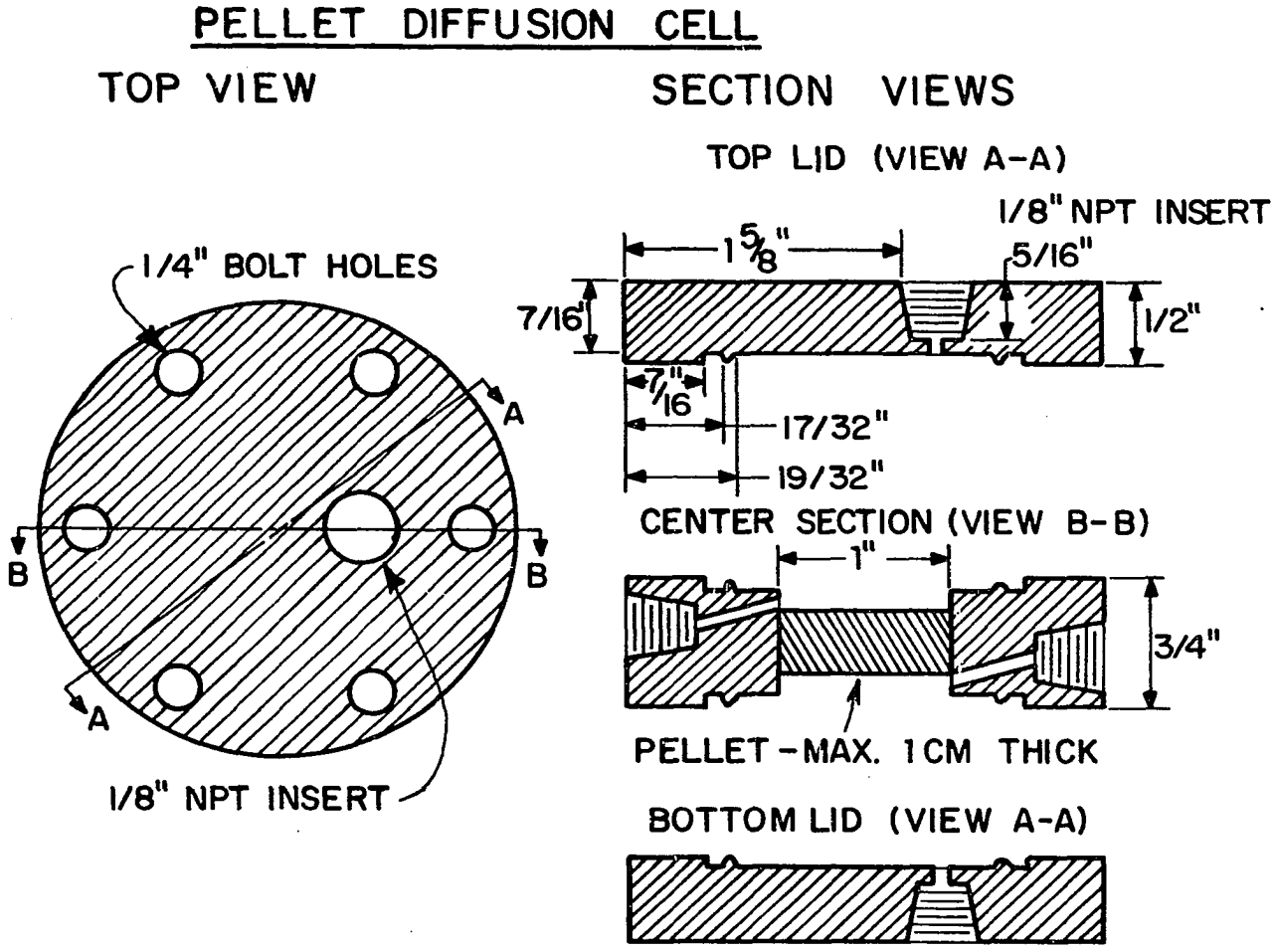

Figure 6. Full-scale top and sectioned views of diffusion cell

here because the resulting increase in computational complexity could not be justified for the limited amount of diffusion information required in this work.

Gas chromatograph

In addition to the application in the diffusion coefficient work, the F&M model 720 gas chromatograph was used in phosgene dissociation experiments to measure the composition of the reactor exit stream. Carbon monoxide, chlorine, and phosgene were separated in a column which consisted of a 10-foot long, 1/8-inch diameter teflon tube packed with 15 grams of 60/80 mesh Carbopack B coated with 10 weight percent phosphoric acid. The column, submerged in an ice bath, resolved the three gases within seven minutes. Helium was used as the carrier gas at a flow rate of 60 cc/min. The chromatograph was equipped with a thermal conductivity detector and the peak areas were measured by a Hewlett-Packard model 3880A integrator.

Other systems

A Knudsen-cell mass spectrometer was employed for the identification of surface gaseous species. Mass to charge numbers of 18 to 138 were monitored as the sample was heated, under vacuum, from 25 to 900 ^{o}C. Grain size distributions were determined by a Coulter counter and grain morphological changes, resulting from reaction, were observed using a scanning electron microscope. Also, minerals present in fly ash were identified using an x-ray diffractometer. Only the Knudsen cell mass spectrometer was operated by the author.

Experimental Procedures and Data Analysis

Initial reaction rates

Either a powder sample (45 or 90 mg) or a pellet (12.7mm diameter by 1 mm thick, 140mg) was loaded into the reactor and suspended from the balance beam. The sample was outgassed at a pressure of 10^{-6} torr and a temperature of 400 ^{o}C until no further weight loss was detected. The balance system was then slowly repressurized with purified helium while the furnace temperature was adjusted to the desired level. The balance jar and reactor purge flows were established along with the phosgene partial pressure and flow. The latter was vented to the scrubber until the chlorination was started.

When the temperature and weight were stable, the four-way ball valve stem (Figure 3) was rotated which directed the reaction gas to the sample. The pressure and temperature were monitored during the experiment. A rise in pressure could signal the presence of a block in the reactor exit tube. While this never happened, it would be disastrous because the phosgene would then leave the system via the jar, exposing the balance mechanism enroute.

The sample was exposed to phosgene until the weight versus time line was long enough to be used for the measurement of a slope. The four-way valve stem was again rotated to restore the helium reactor purge and vent the reaction gas stream. The furnace was opened, the reactor and sample were removed, and the sample was weighed. Another sample could then be loaded for the next experiment.

Kinetic parameters determination

The initial conversion rate was calculated by dividing the slope of the weight versus time line by the initial sample weight. Such results were employed in the determination of the phosgene partial pressure dependence and in the calculation of rate constants. At the outset, it was assumed that the surface reaction rate controlled when powder samples were reacted. The individual grains would then react according to the shrinking core model (SCM) which is the form the grain model assumes under surface reaction control. The following relationship between conversion (X) and reactive core radius (r) is used in applying the SCM.

$$X = 1 - \frac{r^3}{r_o^3} \qquad (15)$$

where X = fly ash conversion (mass fraction reacted).

Limits associated with this equation are:

At X = 0 $\quad r = r_o$

At X = 1 $\quad r = 0$

It was assumed for the reaction of fly ash that the reactive core radius approached zero but that the conversion approached a value less than one due to the presence of the inert material. Equation 15 and its limits were adjusted then for use with fly ash to yield:

$$X_A = 1 - \frac{r^3}{r_o^3} \qquad (16)$$

with $$X_A = \frac{X}{X_F} \qquad (17)$$

at $X_A = 0$ $\quad r = r_o$

at $X_A = 1$ $\quad r = 0$

where X_A = active phase conversion;

X_F = final conversion.

When equation 16 is solved for r and the result is differentiated with respect to X_A, application of the chain rule, assumption of ideal gas behavior ($C_A = P_A/R_GT$), and substitution into equation 4 results in the following:

$$\frac{dX_A}{dt} = \frac{3kbM_AC_A(1 - X_A)^{2/3}}{r_o\rho_s} \qquad (18)$$

To obtain an expression useful in testing the applicability of the SCM, equation 15 was integrated to give:

$$1 - (1 - X_A)^{1/3} = \frac{kbM_AP_At}{r_o\rho_sR_GT} \qquad (19)$$

It was assumed that the variables, k, b, and ρ_s, are not functions of conversion. Linear plots of the l.h.s. versus time should result upon successful application of this equation to fly ash reaction data. In the absence of external mass transfer or pore diffusion rate limitations, equation 18 could be used to predict fly ash reaction rates and equation 19 for prediction of fly ash conversion-time results.

Equation 19 then would represent the fly ash reaction model.

Reaction order As a test for first order dependence, conversion rates and corresponding phosgene partial pressures were plotted according to equation 18. A linear correlation indicates first order phosgene partial pressure dependence. Only initial conversion rates were used in these determinations. Thus, no attempt was made to determine if the reaction order changed as a function of fly ash conversion.

In addition to the reaction order, a reaction stoichiometric coefficient, an average grain radius, and a fly ash density had to be determined prior to the calculation of rate constants according to equation 18. The stoichiometric coefficient determination is reviewed first.

Stoichiometric coefficient To obtain the necessary data, fly ash samples were reacted to a given conversion (0 to 0.375), the partially reacted samples fused into solution (16), and the solutions analyzed for silicon, aluminum, and iron using an atomic absorption spectrophotometer. Since the original fly ash composition was known, metal losses could be calculated. Empirical relationships were fit to the mass fractions of the alumina and silica reacted versus fly ash conversion. With the relative amount of iron oxide reacted being insignificant, the stoichiometric coefficient, as a function of fly ash conversion, was defined as the ratio of the sum of the differential masses of alumina and silica reacted to the differential mass of phosgene reacted, all at the same average fly ash conversion. The

derivatives of the alumina and silica conversion versus fly ash conversion lines were multiplied by the original sample weight and divided by their respective original weight percent compositions to obtain the terms needed for the first half of the definition. The second half was obtained by multiplying the first terms by the appropriate reaction stoichiometric coefficient and then dividing by the respective oxide molecular weight. The resulting equation is:

$$b(x) = \frac{C\,B'(X) + E'(X)}{M_A\left(\frac{3C\,B'(X)}{M_{Al}} + \frac{2E'(X)}{M_{Si}}\right)} \qquad (20)$$

where $b(X)$ = reaction stoichiometric coefficient as a function of fly ash conversion, $g_{\text{fly ash}}\,(g_{COCl_2})^{-1}$;

C = ratio of alumina to silica initial weight percent composition;

$B'(X), E'(X)$ = derivatives of alumina and silica versus fly ash conversion expressions;

M_{Al}, M_{Si} = molecular weights of alumina and silica, respectively, g g-M^{-1}.

Grain radius and density The fly ash average grain radius was calculated from a particle size distribution obtained using a Coulter counter. The equation used was:

$$r_o = \frac{\sum_{i=1}^{I} J_i d_i}{2\sum_{i=1}^{I} J_i} \qquad (21)$$

where d_i = average diameter of component i of grain size distribution, cm;

J_i = number of grains in component i of the distribution.

The fly ash density was measured using a LeChatelier flask and an established procedure (63). High-purity kerosene served as the liquid medium. Since the microporosity of the grains had been found to be insignificant, the density obtained in this way should be accurate.

Activation energies and frequency factors Experimental procedures and calculations applied in the determination of the reaction order, stoichiometric coefficient, average grain radius, and powder density have been described. With values of these parameters available, it was possible to calculate rate constants needed in the determination of an activation energy and a frequency factor. Initial conversion rate data were determined using the methods described previously. Rate constants were then calculated using equation 18 and plotted versus temperature according to the Arrhenius equation. The slope of the resulting line should be proportional to the activation energy and the y-intercept should be the logarithm of the frequency factor.

An alternate technique was also used to determine rate constants. Samples were reacted to much higher conversions and the resulting conversion versus time data were plotted according to equation 19. The rate constants were calculated from the slope of the lines and then again were plotted versus the experimental temperatures according to the

Arrhenius equation to yield an activation energy and a frequency factor.

Effective diffusion coefficient

Pellets used in the diffusion and chlorination work were all formed at a pressure of 7,640 lb/in^2. After a pellet was pressed into the diffusion cell and the cell was reassembled and connected into the flow system, helium and nitrogen streams were passed over the separate faces of the pellet. The pressure control valve was adjusted until the manometer was nulled and then samples from the helium-rich side were analyzed intermittently for nitrogen until the composition became constant.

The effective diffusion coefficient was calculated according to the following equation:

$$D_{e_N} = \frac{2N_N R_G T L \alpha}{P \ln\left(\frac{1 + \alpha Y_{N_2}}{1 + \alpha Y_{N_1}}\right)} \tag{22}$$

where

$$\alpha = 1 - \frac{N_H}{N_N} \tag{23}$$

and D_{e_N} = effective diffusion coefficient of nitrogen, $cm^2 s^{-1}$;

$N_{N,H}$ = flux of nitrogen, helium across pellet, g-M $cm^{-2} s^{-1}$;

P = total pressure, atm;

Y_{N_2} = exit mole fraction of nitrogen in helium-rich side;

Y_{N_1} = exit mole fraction of nitrogen in nitrogen-rich side.

As pictured in Figure 5, the helium-rich side is the lower half of the

cell and the nitrogen-rich side is the upper half. The temperature, pressure, and half-thickness used in solving equation 22, were measured directly. The remaining factors, Y_{N_1}, Y_{N_2}, and α were calculated from experimental data according to the following set of equations.

$$N_N = \frac{PY_{N_2}F_{T_2}}{15R_GTD^2} \tag{24}$$

$$Y_{N_1} = \frac{F_N - Y_{N_2}F_{T_2}}{F_T - F_{T_2}} \tag{25}$$

$$\alpha = 1 - \frac{F_T - F_{T_2} - F_N + Y_{N_2}F_{T_2}}{Y_{N_2}F_{T_2}} \tag{26}$$

where F_{T_2} = flow rate of gases exiting the helium-rich side, cm^3s^{-1};

D = pellet diameter, cm;

F_N = flow rate of nitrogen into nitrogen-rich side, cm^3s^{-1};

F_T = total flow entering cell, cm^3s^{-1}.

The three flows defined above were measured using a bubble flowmeter after the nitrogen concentration in the helium-rich side became constant. An effective diffusion coefficient was then calculated according to equation 22. This value was used with equations 9, 10, and 11 to calculate a value for the tortuosity factor.

B.E.T. surface area

A sample, powder or pellet, was cleaned to a constant weight at 10^{-6} torr and 400 °C. The system pressure and sample weight were

recorded after the sample was cooled to room temperature while still under vacuum. The system was then pressurized to about 30 torr with nitrogen and a Dewar flask, containing liquid nitrogen, was raised up around the sample tube. After equilibration, the pressure and weight were recorded again to give the second set of data. The nitrogen pressure was then increased by another 30 torr, the system allowed to equilibrate, and another set of readings taken. This process was repeated until a pressure of 210 torr was reached. The liquid nitrogen bath temperature, required in the surface area calculations, was measured using a thermistor before and after each experiment.

A weight data point at ambient pressure where pores with radii of less than 300 Å are filled was required to determine a microporosity. The initial clean sample weight was subtracted from this final weight to give the total weight of nitrogen adsorbed. This value, along with the liquid nitrogen density, the fly ash density, and the clean sample weight were needed in the calculation of a microporosity. However, correction for buoyancy effects was required before any of the nitrogen weight data could be used in microporosity or surface area calculations. The sample was replaced by a comparable volume of quartz rod (55) and the same measurements at the same conditions and nitrogen pressures were carried out. The correction was completed by subtracting the blank weight differences, measured at corresponding pressures, from the nitrogen weight differences.

The following form of the B.E.T. (66) equation was used in determining sample surface areas.

$$\frac{P_{ad}}{V_{ad}(P_s - P_{ad})} = \frac{1}{V_m c} + \frac{(c - 1)P_{ad}}{V_m c P_s} \qquad (27)$$

where P_{ad} = nitrogen pressure, torr;

V_{ad} = volume of nitrogen on fly ash surface, cm^3;

P_s = saturated vapor pressure of nitrogen in contact with fly ash, torr;

V_m = volume of nitrogen monolayer, cm^3;

c = B.E.T. constant.

The saturated vapor pressure, required in equation 27, was calculated from the bath temperature according to the following empirical equation (35,71):

$$P_s = 729.398 + 89.744(T_s - 77.0) \qquad (28)$$

where T_s = temperature of liquid nitrogen bath, K.

A plot of the l.h.s. of equation 27 versus P_{ad}/P_s yielded a straight line between 30 and 210 torr with a slope (a) and intercept (b) equal to:

$$a = \frac{c - 1}{V_m c} \quad \text{and} \quad b = \frac{1}{V_m c} \qquad (29)$$

Combining these two expressions gave:

$$V_m = \frac{1}{a + b} \qquad (30)$$

With V_m known, the specific surface area was calculated according to:

$$S = \frac{V_m N_o A_N}{2.2415E04W} \tag{31}$$

where S = fly ash specific surface area, $m^2 g^{-1}$;

N_o = Avogadro's number, molecules $g\text{-}M^{-1}$;

A_N = area per nitrogen molecule, 16.2 $\AA^2$;

W = clean sample weight, g.

A computer program was written to do the calculations outlined above. Sample and blank weights, nitrogen pressures, the bath temperature, and the clean sample weight were entered. Calculated and output were the specific surface area and the line slope and intercept, all with corresponding standard deviations and a correlation coefficient. The results were stored on disk for reference and plotting purposes. A listing of the program is included in Appendix A.

Chemisorption

Phosgene chemisorption results were not incorporated into the reaction model for the reasons mentioned earlier. However, phosgene chemisorption isotherms were measured over a range of fly ash conversions for comparison to B.E.T. surface area results. Samples were cleaned at a temperature of 700 °C and a pressure of 10^{-5} torr until a constant weight was recorded. The system was repressurized with helium while the sample temperature was adjusted to 250 °C. Chemisorption isotherms could not be measured at higher temperatures because the rate

of reaction became significant. When a constant weight and a temperature of 250 ^{o}C were established, the sample was exposed to a stream of pure phosgene. The flow was maintained until a constant sample weight was reached. The sample was then exposed to pure helium at the same temperature until a constant weight was recorded. A gross phosgene chemisorption weight was calculated by subtracting the clean sample weight from the sample weight recorded immediately after the phosgene flow was replaced by helium. A net phosgene chemisorption weight was obtained similarly except that the initial sample weight was subtracted from the weight following desorption.

RESULTS AND DISCUSSION

Fly Ash Characteristics

The composition of the fly ash utilized in this study is listed in the third column of Table 1. This composition was obtained as a result of leaching a Texas lignite ash (column 2) with 6 M aq HCl at 100 ^{o}C for two hours. A liquid to solid weight ratio of 40 to 1 was used. As column 4 indicates, large percentages of the calcium and iron oxides were removed. The leached material contained a total of 97 weight percent silica and alumina; the nearly pure alumina-silica material desired.

Fly ash physical characteristics are listed in Table 2. The techniques used in obtaining some of these results have not been mentioned. The pellet porosity was calculated from the powder density and the pellet volume and weight. A nitrogen desorption isotherm was measured and used to determine a powder micropore distribution (9) which consisted of one peak at 23 Å. In measuring the maximum conversion, a fly ash sample was exposed to phosgene at 625 ^{o}C until further sample weight loss was difficult to detect. This occurred at a conversion of 0.375. The resulting weight versus time data were used to calculate specific reaction rates at known average fly ash conversions. A plot of these rates versus the average conversions was constructed and the resulting curve was extrapolated from the rate measured at the conversion of 0.375 to a rate of zero at a conversion of 0.40.

Table 1. As received and leached compositions of Texas lignite fly ash

Oxide	Wt. %[a]	Wt. %[b]	Wt. % removed
Al_2O_3	33.44	34.40	2.13
CaO	2.26	0.32	86.53
Fe_2O_3	1.94	0.93	54.38
K_2O	0.39	0.39	4.93
MgO	0.04	0.04	4.93
Na_2O	0.36	0.32	15.48
SiO_2	55.38	57.26	1.63
TiO_2	0.76	0.71	11.16
LOD	0.16	0.15	
LOI	4.61	4.37	
Total	99.34	98.89	
Total impurities[c]	6.08	2.87	
Wt. % $Al_2O_3 + SiO_2$[d]	93.92	97.1	

[a]As received fly ash composition.

[b]Leached fly ash composition.

[c]Normalized weight percent totals for nonalumina/silica constituents.

[d]Normalized weight percent total of alumina and silica.

Table 2. Leached Texas lignite fly ash physical properties

Property	Value
Powder density	2.04 g cm^{-3}
Powder specific surface area	3.47 m^2g^{-1}
Pellet specific surface area	3.10 m^2g^{-1}
Pellet porosity	0.42
Average micropore radius	23 Å
Microporosity	0.005
Average grain radius	3.96E-04 cm
Maximum conversion	0.40

Phosgene Rate Dependence

Initial conversion rate data were measured and plotted versus the corresponding phosgene partial pressures. As shown in Figure 7, the measurements were done at three temperatures with two samples sizes. In accordance with equation 18, the linear behavior seen in Figure 7 indicates that the reaction was first order with respect to the phosgene partial pressure at all three temperatures. There was no mechanism change with temperature. The sample pan geometry was the same regardless of the sample size used so when the sample size was doubled, the diffusion distance to the center of the sample was also doubled. The conversion rates, however, were independent of the sample size indicating intergrain powder diffusion was not a limiting factor at the conditions used.

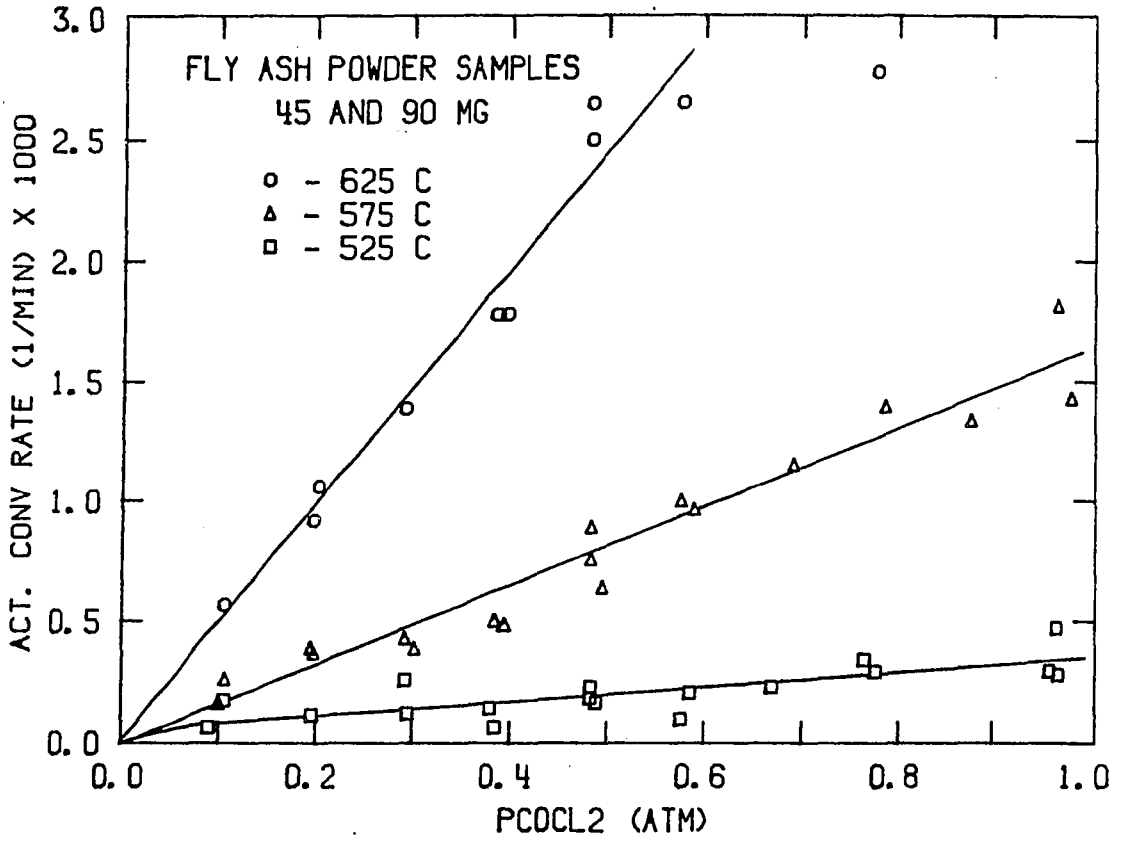

Figure 7. Fly ash powder conversion rates as a function of phosgene partial pressure

Stoichiometric Coefficient

The stoichiometric coefficient was defined earlier as the weight ratio of fly ash to phosgene reacted. Figure 8 is a plot of the data used in the calculation of this coefficient (equation 20). The weight of iron oxide reacted represents at most 2 percent of the total reacted weight. This amount was assumed to be insignificant and so iron oxide contributions to fly ash conversion rates were disregarded.

The linear relationships between the alumina and silica conversions

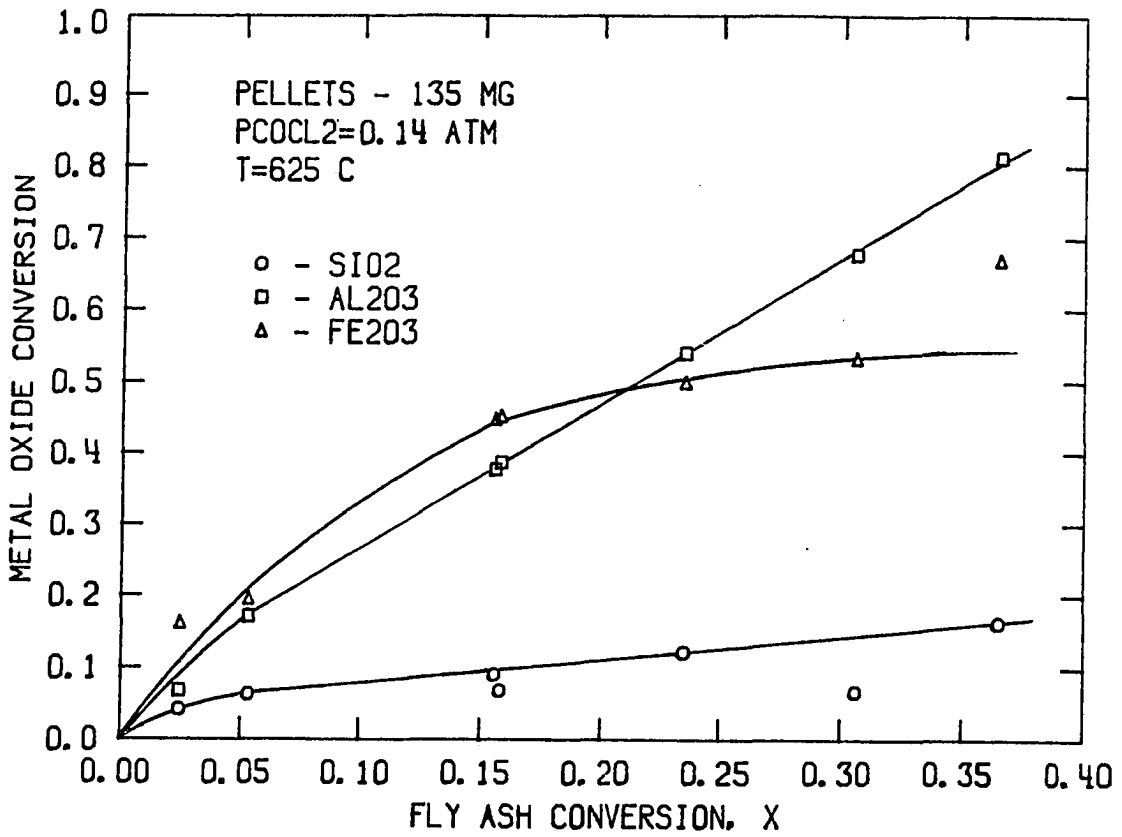

Figure 8. Metal oxide conversions versus fly ash conversion for fly ash pellets reacted with phosgene

and the fly ash conversion shown in Figure 8 for fly ash conversions of 0.05 to 0.37 greatly simplified the modelling of the reaction system. These results mean that the silica to alumina molar reaction ratio and the stoichiometric coefficient were constant over the fly ash conversion range of 0.05 to 0.37. As a result of the linear behavior, equal sized fly ash conversion steps along each oxide-fly ash conversion line corresponded to the reaction of the same amounts of alumina and silica and yielded a constant alumina to silica molar reaction ratio of 1.86.

Since the number of moles of phosgene reacted per mole silica or alumina was assumed constant, a constant stoichiometric coefficient with a value of 0.333 resulted.

The data in Figure 8 are also important with regard to fly ash processing considerations. At the largest fly ash conversion (0.375), 16 percent of the silica and 80 percent of the alumina have reacted which corresponds to the alumina to silica molar reaction ratio of 1.86 to 1. The ratio obtained in a previous study in which a bituminous fly ash was reacted with carbon and chlorine (1) decreased from a value of 1.8 down to 1.2 as the fly ash conversion increased. This difference could result from use of different fly ashes but it could also be a function of the carbon and chlorine source employed. Being gaseous, phosgene can diffuse to the inner surfaces of fly ash grains. With carbon and chlorine, on the other hand, the fly ash inert matrix is likely to serve as a barrier to reactive intermediates travelling from the carbon surface to the interior of fly ash grains. This may result in the reaction of more silica as the outer grain surface is depleted of alumina.

Phosgene Dissociation

With a stoichiometric coefficient and the data in Table 2 available, rate constants were calculated from initial conversion rate data according to equation 18 and used in an Arrhenius plot to obtain an activation energy and a frequency factor. Reasonable values for these parameters were obtained using the linear section of an Arrhenius plot.

At temperatures greater the 625 ^{o}C, the slope of the line started to lessen. In the literature, this is attributed to the dissociation of phosgene (14).

Accepting dissociation as a valid explanation, additional experiments were done in which fly ash pellets were reacted to higher conversions and the conversion versus time data were plotted according to the integrated form of the SCM equation (equation 19). Linear relationships resulted and so rate constants, calculated from the slopes of the lines, were used to construct the Arrhenius plot shown in Figure 9. The partial pressure dependence shown was not understood and curved lines of this shape generally result from the increasing influence of diffusion or mass transfer control as a function of increasing temperature. At comparable temperatures, this behavior was not seen during previously completed initial rate studies.

Since the higher conversion experiments required much greater reaction times, it was decided that the phosgene flow rates could be reduced to conserve phosgene and the scrubbing solution. The only difference then between the initial and the high conversion experiments was that the flow rates were changed. Possible flow related causes of the anomalous behavior included: external mass transfer rate limitations, phosgene dilution due to the back diffusion of the upper helium purge stream, and nonequilibrium dissociation of phosgene. It was estimated using the highest reaction rate and the lowest flow rate that a phosgene mole fraction gradient of only 10^{-5} existed across the pellet stagnant gaseous boundary layer. This meant that the bulk and

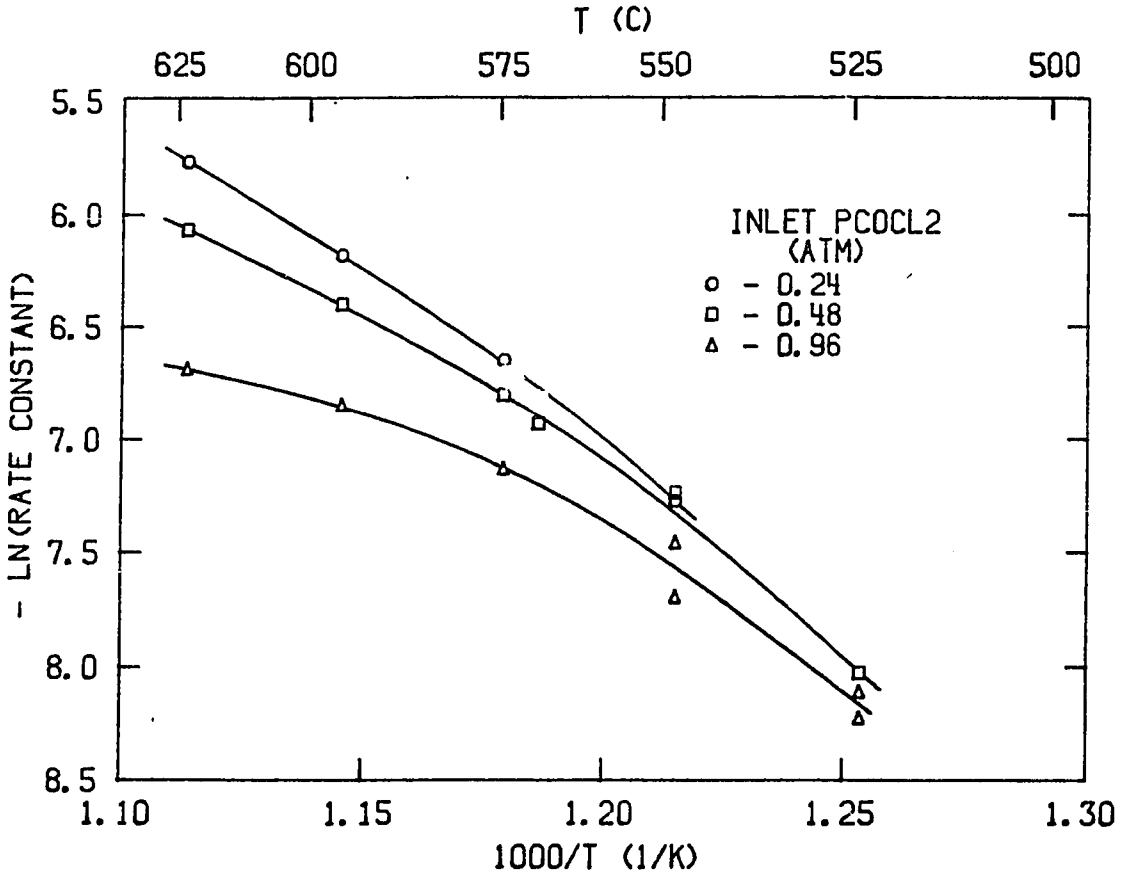

Figure 9. Arrhenius plot resulting from integral fly ash reaction data uncorrected for phosgene dissociation

surface phosgene concentrations were essentially the same and that the external mass transfer rate was not a limiting factor.

A check for helium dilution required the development of a mathematical model of the experimental reactor. Laminar flow was known to exist, but for simplicity, a flat velocity profile was assumed. A computer program, listed in Appendix A, was written and used for the calculation of phosgene mole fraction profiles. The results for the

worst case indicated that helium back-diffusion did not dilute the phosgene in the sample area. It was also predicted that phosgene would only rise to within 45 cm of the venturi.

Equilibrium phosgene partial pressures calculated at experimental temperatures are listed in Table 3. Very high degrees of dissociation

Table 3. Equilibrium phosgene partial pressures calculated at the temperatures indicated with a total phosgene pressure of 0.96 atm

T (^{o}C)	P_{COCl_2} (atm)
525	0.162
575	0.076
625	0.036
700	0.013

are predicted. Observations, discussed earlier, indicated that the curved Arrhenius lines (Figure 9) resulted upon lowering the reactant gas flow rate. The flow dependence suggested that the phosgene dissociation reaction did not reach equilibrium at all conditions. With kinetics then involved, the direct measurement of phosgene concentrations at the chlorination experimental conditions was required. The results are listed in Table 4.

Since the sample was positioned approximately 9 cm below the point where the gaseous composition was measured, the concentration of phosgene in contact with the sample was still unknown. It was noticed,

Table 4. Inlet and outlet phosgene partial pressures as a function of temperature and total reaction gas flow rate. Helium was used as the diluent

T (°C)	Total Flow (cm^3/min)	$P_{COCl_2 in}$ (atm)	$P_{COCl_2 out}$ (atm)
525	20	0.96	0.90
	40	0.48	0.46
575	20	0.96	0.54
	40	0.48	0.37
	40	0.24	0.23
	100	0.96	0.81
	200	0.48	0.44
625	20	0.96	0.12
	40	0.48	0.14
	40	0.24	0.09
	100	0.96	0.41
	200	0.48	0.29
700	100	0.96	0.05
	200	0.48	0.04

however, that quartz chips located upstream of the sample in the reactor preheating section became coated with a layer of carbon. If most of the dissociation occurred on the chip surfaces then the concentration of phosgene in contact with the sample would be the same as that measured at the exit. This was assumed correct and the exit phosgene partial

pressures were used to recalculate rate constants resulting from powder initial rate measurements. The uncorrected data are represented in Figure 10 by the dotted line. The slope and y-intercept of the solid line through the corrected data yield the activation energy and the frequency factor given in Figure 10.

The accuracy of the assumption that most dissociation occurred on the surface of the quartz chips was reinforced by the linear Arrhenius relationship obtained over the temperature range of 525-650 ^{o}C. If the levels of dissociation listed in Table 4 were achieved throughout the heated volume of the reactor at all temperatures, then the resulting Arrhenius line would be the mirror image of the dotted line shown in Figure 10. A positive deviation is seen, however, beginning with the 675 ^{o}C data. At the higher temperatures, either the phosgene continued to dissociate as it flowed through the reactor above the sample or the carbon monoxide and chlorine, present as a result of dissociation, reacted with the sample to enhance the conversion rate. The phosgene gas-phase dissociation rates could have been fast enough starting at 675 ^{o}C so the reactor residence time above the sample was great enough to allow for significant dissociation. This would lead to a positive deviation since, in using equation 18 to calculate the rate constants, phosgene partial pressures smaller than the actual values would have been employed.

The positive deviations of the data points from the solid line in Figure 10 could also result from enhancement of the fly ash chlorination rate due to its reaction with carbon monoxide and chlorine. The

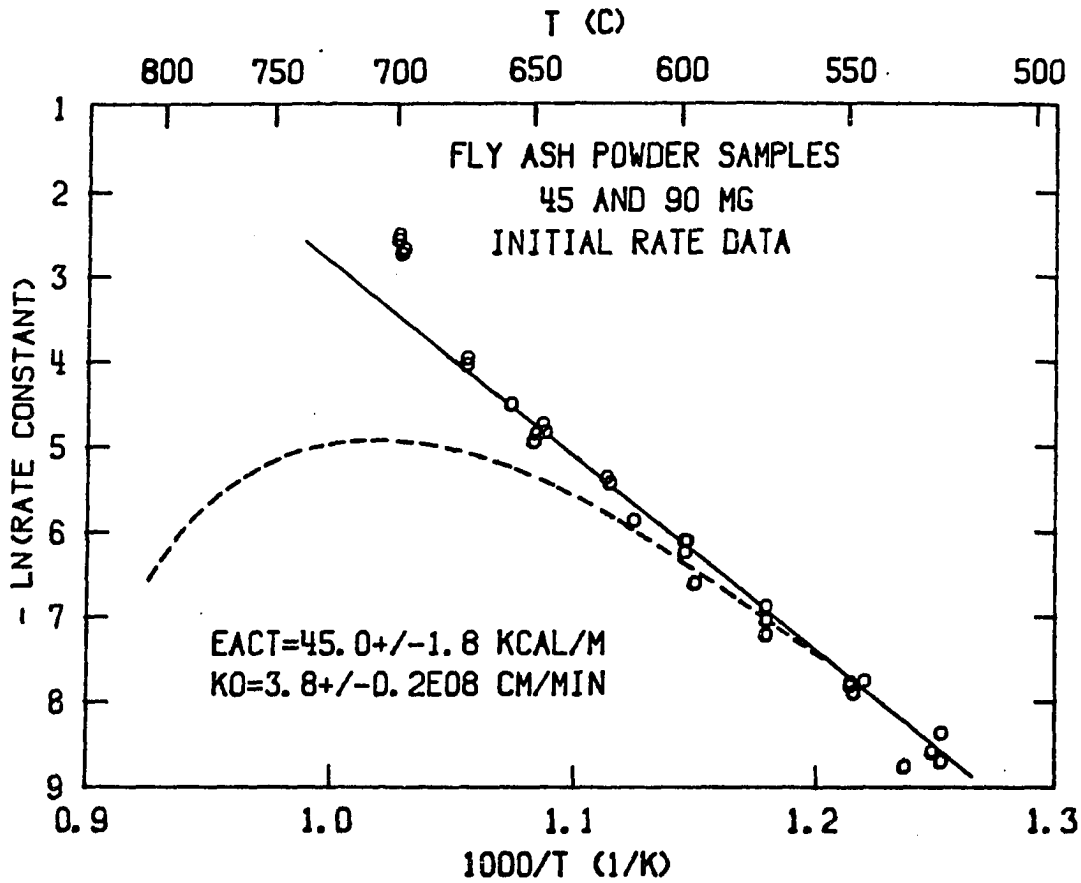

Figure 10. Arrhenius plot resulting from fly ash powder initial conversion rate data

fraction of the fly ash surface covered by phosgene was probably a function of the phosgene partial pressure. Since small phosgene partial pressures were measured at the temperatures where the deviations occur, free sites could have been available for reaction with carbon monoxide and chlorine. This enhancement reaction would yield a positive deviation from the Arrhenius line since, when calculating rate constants according to equation 18, the conversion rate would be greater than if

only phosgene were reacting with the sample. Both options, phosgene gas-phase dissociation and carbon/chlorine reaction, are reasonable causes for the positive deviations from the Arrhenius line. Unfortunately, the data available are too limited to establish the relative importance of the two effects.

Activation Energy and Frequency Factor

Powder and pellet initial rate data

The results of the powder chlorination experiments were presented earlier in Figure 10. The magnitude of the activation energy would suggest surface reaction control. This is supported by the fact that the rate constants are independent of sample size (diffusion distance).

Pellets 1 mm thick and 12.7 mm in diameter were reacted under the same conditions as the powder samples. Rate constants were calculated from initial conversion rate data according to equation 18 and plotted versus inverse Kelvin in Figure 11. The sample porosity was decreased in the pellet experiments from the powder value of approximately 0.8 to a value of 0.42. Further evidence for surface reaction control is provided here since the decrease in porosity did not significantly affect the value of the activation energy. It was possible then using only the kinetic parameters and equation 18 to calculate initial reaction rates over a temperature range of 450-650 ^{o}C for any phosgene partial pressure of up to one atmosphere.

Pellet integral data

To determine if the variables, k, b, and ρ_s on the r.h.s. of

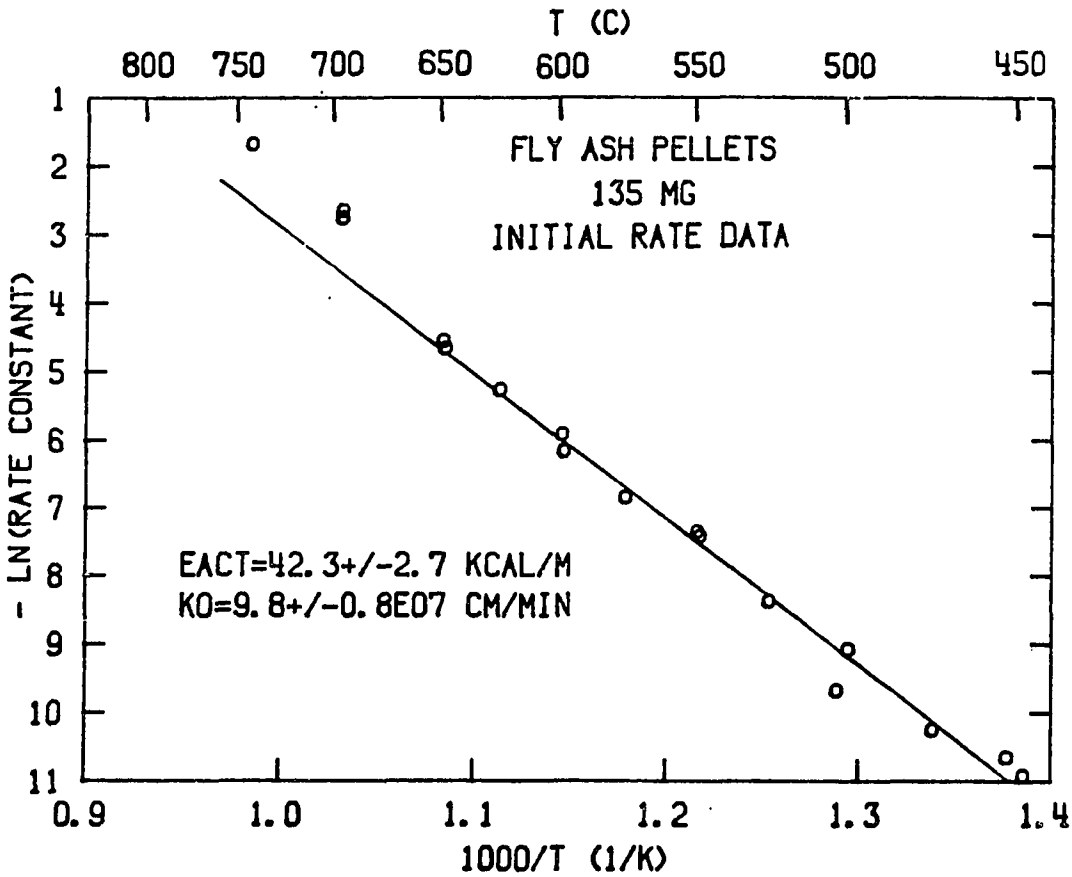

Figure 11. Arrhenius plot resulting from fly ash pellet initial conversion rate data

equation 18 were constant as a function of conversion, extended fly ash reaction experiments were conducted. The resulting conversion versus time data were plotted according to equation 19. Seventeen of the extended pellet chlorination experiments were completed and almost all of the data sets were as linear as those shown in Figure 12. The linear correlations indicate that the shrinking-core model can be used to represent the reaction of fly ash and that the variables which comprise

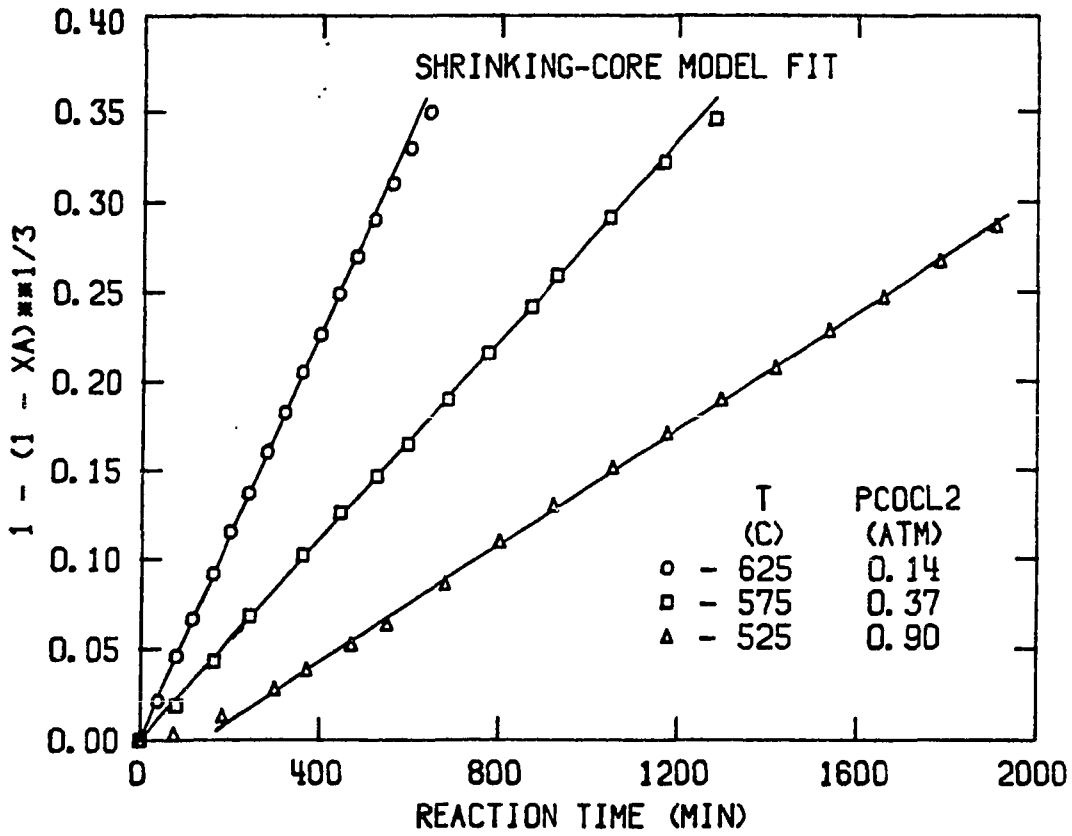

Figure 12. Fly ash conversion versus time data plotted according to the shrinking-core model

the slope are constant as a function of fly ash conversion. It was already known (Figure 8) that a constant composition reacted over most of the conversion range (0.05 to 0.375). The activation energy was then not expected to change as a result of chemical effects. The change in fly ash density as a function of conversion should be small since the initial density is not greatly different from that of quartz, a prominent component of the inert matrix.

Rate constants were then calculated from the slopes of lines such

as those shown in Figure 12. The original Arrhenius plot constructed from these results was presented in Figure 9. After correction for phosgene dissociation, the plot in Figure 13 was obtained. Phosgene partial pressure dependence is no longer seen. The activation energy and frequency factor listed in Figure 13 were calculated using the data in the temperature range of 525-600 ^{o}C.

Kinetic Parameter Comparison

The activation energy and frequency factor values given in Figures 10, 11, and 13 differ. In an attempt to determine if these differences are significant, all of the data were plotted together in Figure 14. The initial powder and pellet data are indistinguishable and the only integral data which deviate from the line are the points at 625 ^{o}C. This deviation could be a consequence of calculating rate constants using the measured exit phosgene partial pressures. Since dissociation in the tube above the sample was shown to be a function of temperature and the phosgene residence time, lowering the flow rate at a temperature where an appreciable gas-phase dissociation rate exists would yield a phosgene exit concentration which is less than that seen by the sample. Division of the reaction rates by the smaller exit phosgene partial pressures would result in larger rate constants and thus a positive deviation from the Arrhenius line.

If the integral results at 625 ^{o}C are not used, an activation energy and a frequency factor are calculated (Figure 14) which fall in the middle of the range defined by the individual sets of data to

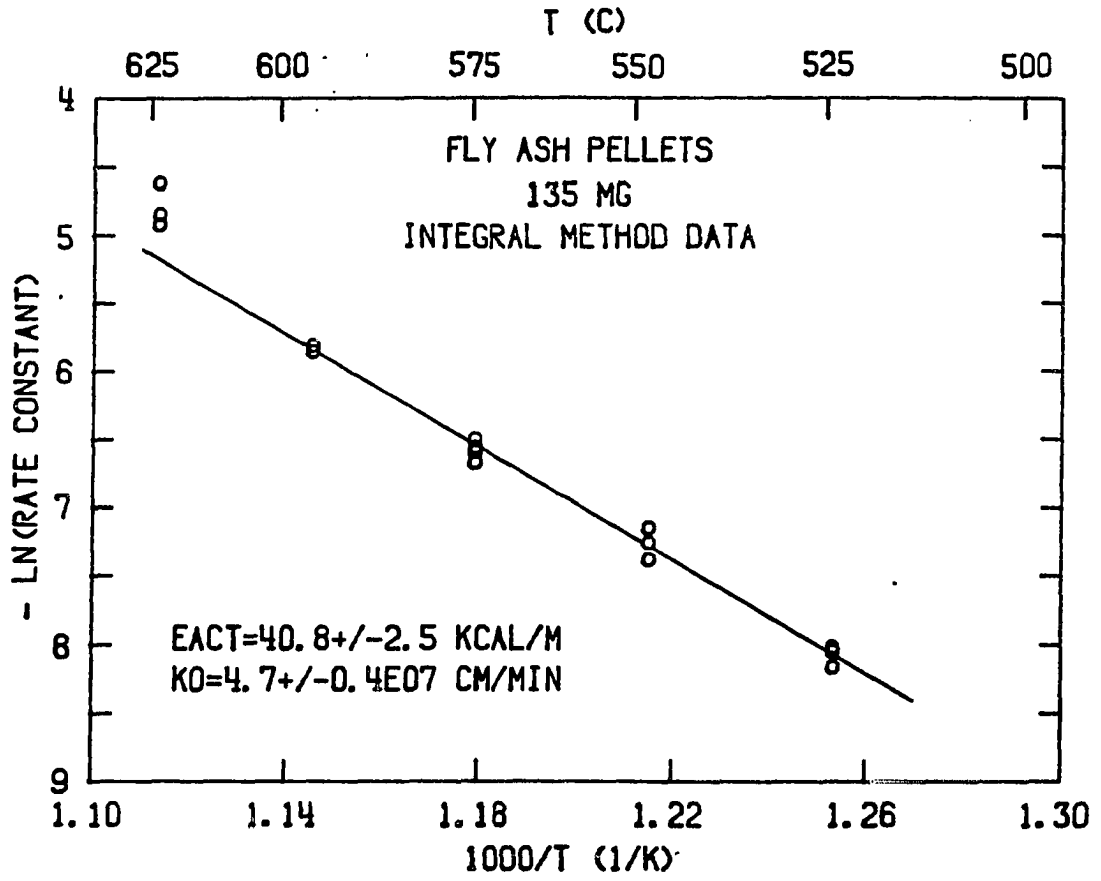

Figure 13. Arrhenius plot resulting from extended fly ash chlorination data corrected for phosgene dissociation

suggest that the differences between the initial and integral data are insignificant. It is possible then to use equation 19 to predict fly ash conversion-time results over a phosgene partial pressure range of 0.03 to 0.9 atm and a temperature range of 450 to 700 ^{o}C.

Fly Ash Reaction Model

A computer program, listed in Appendix A, uses the values of the kinetic parameters of Figure 13 in equation 19 to calculate fly ash

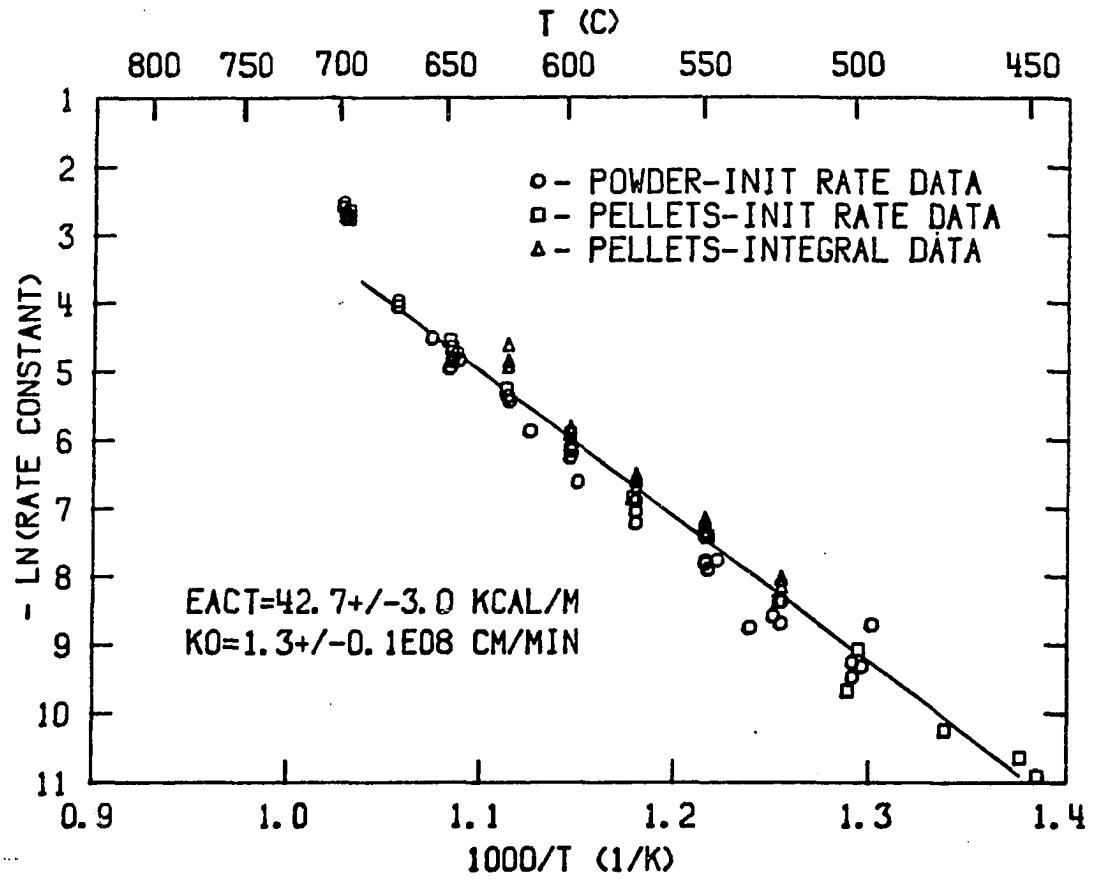

Figure 14. Arrhenius plot of powder and pellet initial conversion rate data and pellet extended conversion data

conversions as a function of time. Figures 15 and 16 are plots of the calculated data overlayed onto corresponding experimental data. The predictions are excellent for all but the 625 °C data. The failure at 625 °C was expected since the rate constants at the same temperature deviated from linearity in the Arrhenius plot of Figure 13. As was mentioned earlier, the positive deviation of the integral results is probably due to the method used to correct for phosgene dissociation at

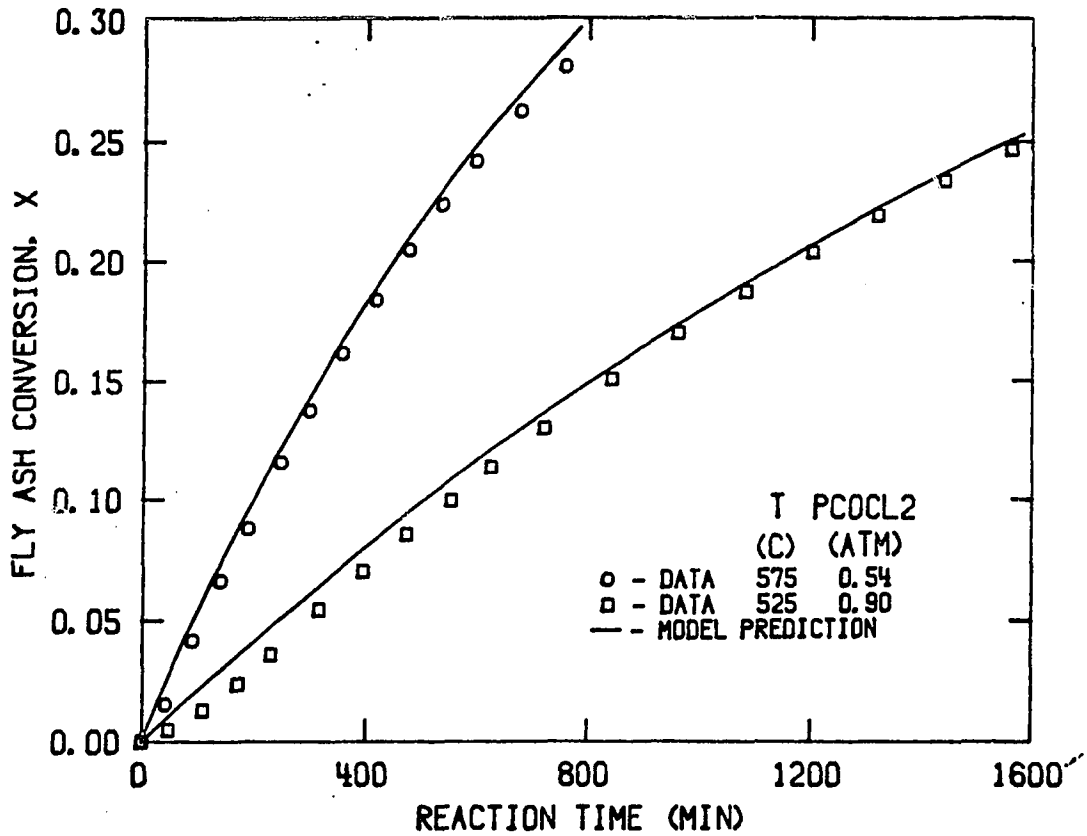

Figure 15. Comparison of reaction model predictions to experimental fly ash conversion-time data at the specified conditions

the lower flow rates.

Tortuosity and Reaction Modulus Results

The relationships between tortuosity, diffusion coefficients, and the reaction modulus are given by equations 8, 9, 10, and 11. A detailed description of the application of these equations for the calculation of reaction modulus values is given in Appendix B so only a brief review of the results are included here.

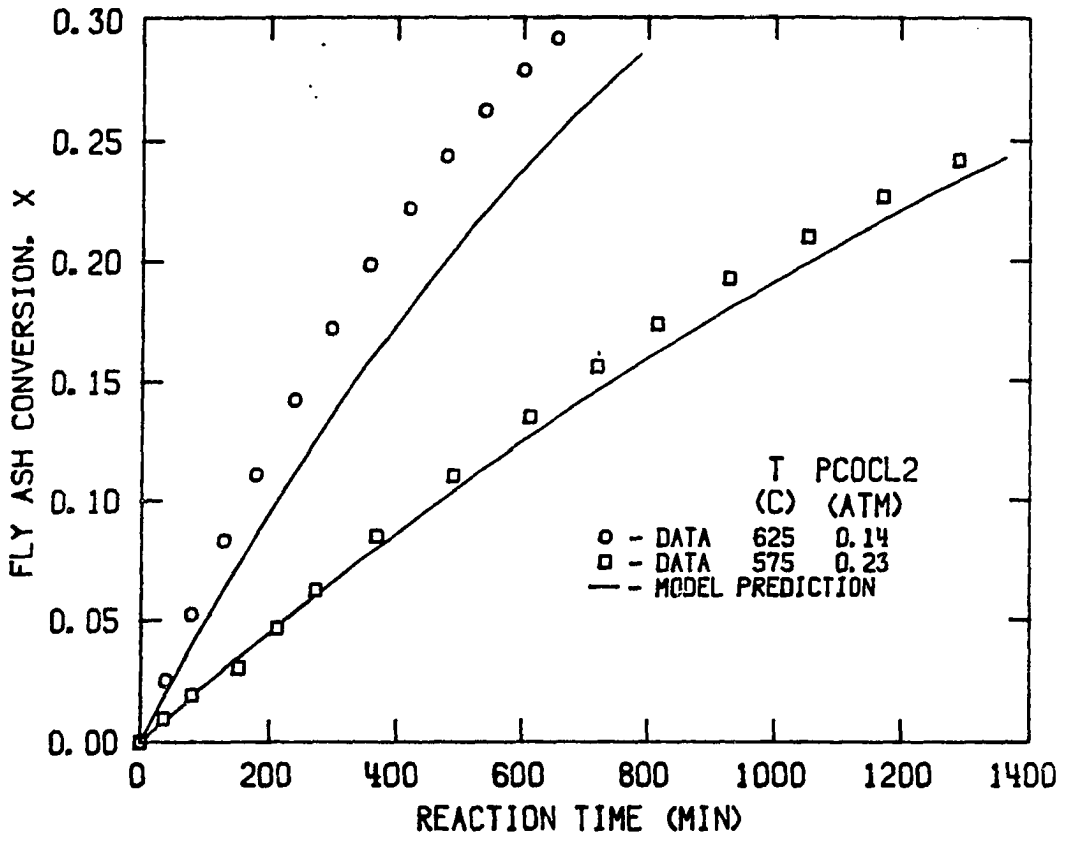

Figure 16. Comparison of reaction model predictions to experimental fly ash conversion-time data at the specified conditions

The effective diffusion coefficient for nitrogen/helium diffusion in a fly ash pellet at 24 ^{o}C and 0.97 atm was determined experimentally as 0.103+/-0.003 cm^{2}/s. Using this value, a tortuosity factor of 2.71 was calculated and applied in the estimation of phosgene effective diffusion coefficients. These values along with rate constants calculated using the powder kinetic parameters and the Arrhenius equation yielded modulus values of 0.12 at 700 ^{o}C and 0.04 at 625 ^{o}C. Values of less than 0.3 are indicative of a reaction system limited by

its surface reaction rate (65). The reaction rates at 700 °C were the largest measured in this work so it is clear that, based both on the modulus value and the previous kinetic parameter results, intragrain diffusion rates never limited the fly ash reaction rates. This further supports the view that intrinsic kinetic parameters have been determined. Since the reaction modulus is directly proportional to the pellet thickness, pellets with a minimum dimension of up to 2.5 mm (0.1 inch) can be reacted at 700 °C without risking significant diffusion limitations. This information was used in the chlorination reactor design.

B.E.T. Surface Areas

The data described in the remaining parts of this section were not used directly in the reaction model. They are mostly analytical in nature and were collected for the characterization of the fly ash as it reacted.

Nitrogen adsorption isotherms of fly ash samples reacted to conversions of 0 to 0.375 were obtained. The data from each isotherm were plotted according to equation 27 (B.E.T. equation) and the slopes and y-intercepts of the resulting lines were used in the calculation (equations 30 and 31) of specific surface areas. An example of a B.E.T. plot for one fly ash sample is shown in Figure 17. The data from all other samples fit the B.E.T. equation equally well to give a high degree of confidence in the accuracy of the surface areas computed.

Fly ash specific surface areas as a function of conversion are

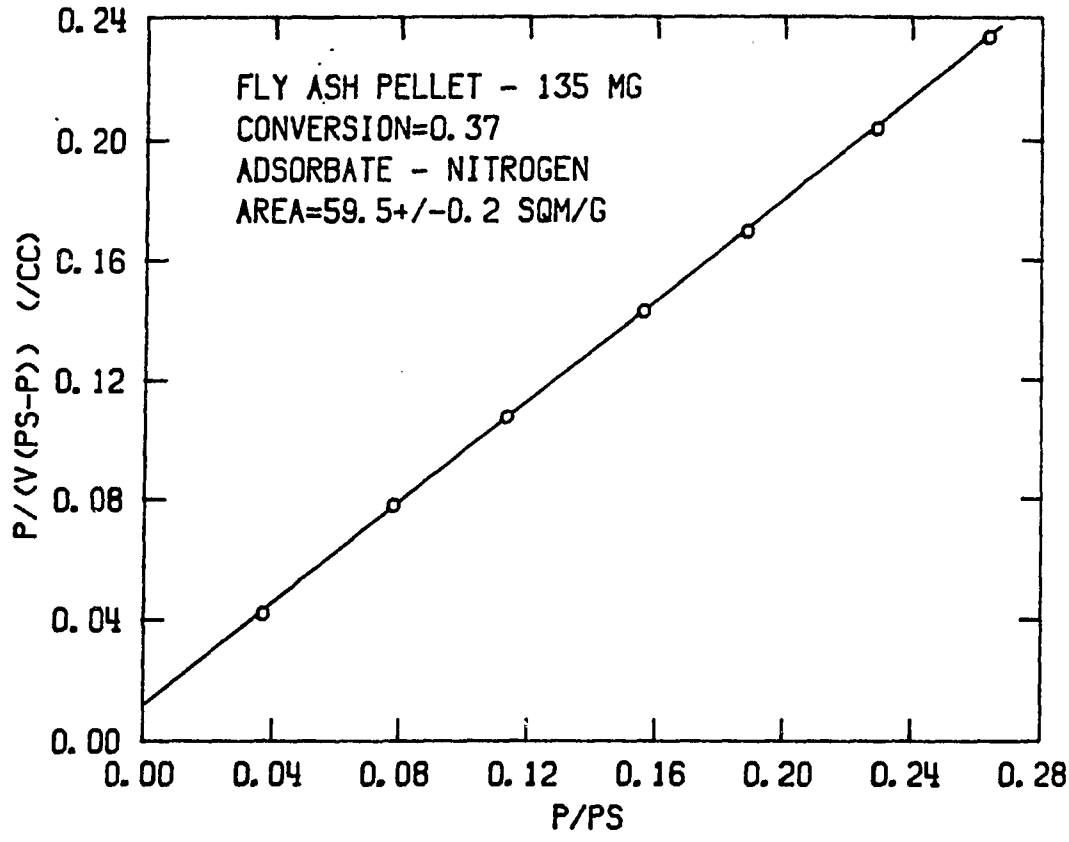

Figure 17. Nitrogen adsorption isotherm plotted according to the B.E.T. equation

plotted in Figure 18. These results indicate that the fly ash specific surface area is a strong function of conversion. Reaction according to the SCM would result in an increase in the specific surface area as a function of conversion but not nearly of the magnitude shown in Figure 18. To verify this, a simple relationship between conversion and specific surface area was developed. The initial sample weight, divided by the fly ash density and average initial grain volume, yields a relationship between the number of grains in a sample and the sample

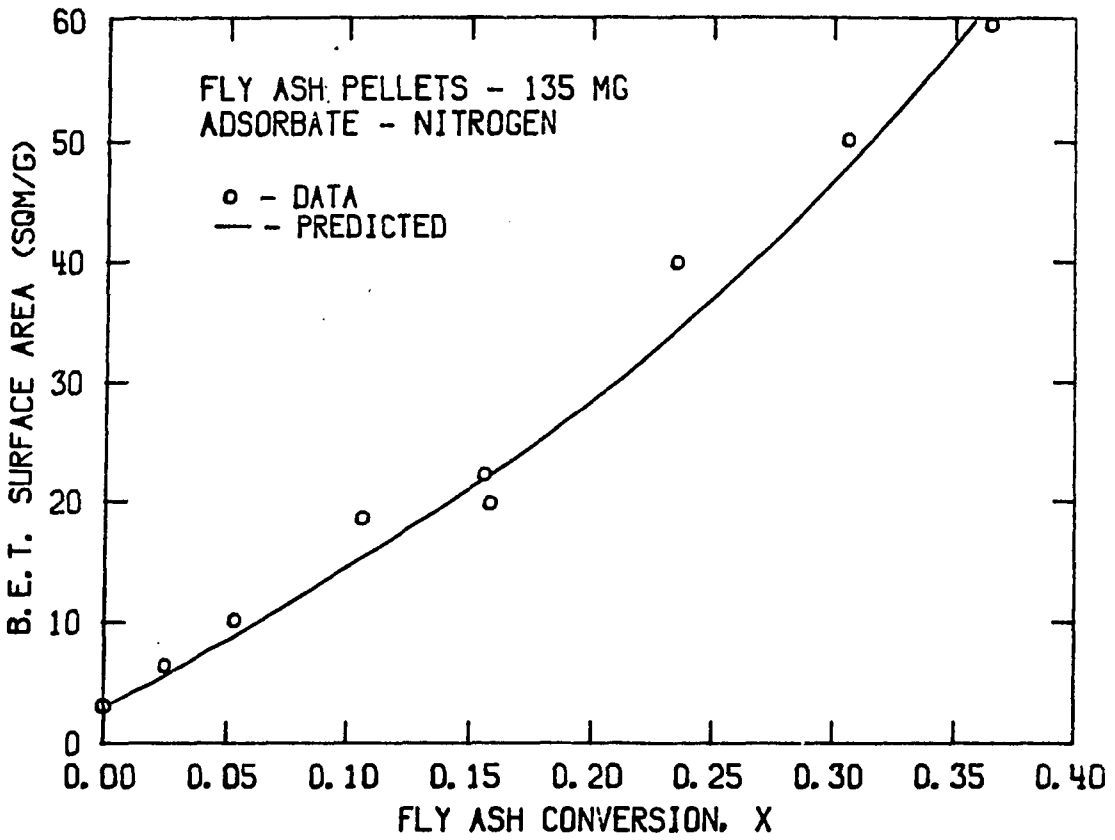

Figure 18. Comparison of measured to predicted fly ash pellet surface areas

weight. Assuming the grains react as hard spheres, an expression relating the average grain area to conversion can be developed using equation 15. This expression combined with the previous equation results in a relationship between sample area and conversion. To obtain a specific surface area-conversion equation, the sample area-conversion expression must be divided by the sample weight as a function of conversion. It was assumed that the sample weight can be related to conversion by:

$$W = W_i(1 - X) \tag{32}$$

where W_i = initial sample weight, g;

Division of the sample area-conversion expression by equation 32 yields the following specific surface area-conversion relationship:

$$S = \frac{3(1 - X)^{-1/3}}{1E04\rho_s r_o} \tag{33}$$

Specific surface areas as a function of conversion, calculated according to equation 33, are listed in Table 5. The surface area increase with conversion is insignificant relative to the magnitude of the increase shown in Figure 18.

The SEM pictures (Figures 1 and 2) and the results listed in Table 5 suggest the fly ash grains develop an inert shell as reaction proceeds. To account for development of the inert matrix, a semi-empirical relationship between specific surface area and conversion was developed. It was assumed that the inert area predominated over the whole conversion range and that the inert phase had a constant specific surface area. Furthermore, it was assumed that the fraction of the inert exposed was equal to the fraction of the active material reacted. The relationship between the sample surface area and conversion is then:

$$A_s = W_i(1 - X_F)A_I X_A + W_i A_o \tag{34}$$

Table 5. Specific surface area as a function of conversion as predicted by assuming fly ash reacts as shrinking, hard spheres

Conversion	Area (m^2/g)
0.0	0.372
0.2	0.402
0.4	0.441
0.6	0.504
0.8	0.636

where A_s = sample area, m^2;

A_I = inert specific surface area, $m^2 g^{-1}$;

A_o = initial specific surface area; $m^2 g^{-1}$.

The second term on the r.h.s. of equation 34 represents the initial sample surface area. The sample weight in the first term is multiplied by the factor $(1 - X_F)$ so that only the inert weight is used. The sample weight as a function of conversion is given by equation 32. Dividing equation 34 by equation 32 yields the following relationship between specific surface area and conversion:

$$S = \frac{(1 - X_F)A_I X_A + A_o}{1 - X} \qquad (35)$$

A value for A_I was estimated from the specific surface area (59.5 m^2/g) of the pellet reacted to the highest conversion (0.375) because it was expected that the active area contribution to the total area of this

sample would be small. The specific surface area of unreacted fly ash pellets (A_o) was measured as 3.13+/-0.06 m^2/g.

With values for the constants in equation 35 available, specific surface areas as a function of conversion were predicted and plotted in Figure 18 as a solid line. The positive deviations of the data points seem reasonable since the active surface area was not considered in developing the equation. The general agreement between the shape of the data and the predicted line supports the idea that an inert matrix of constant specific surface area develops as reaction proceeds. It does not, however, confirm or refute whether the physical changes which occur as fly ash reacts are consistent with the shrinking-core mode of reaction.

Chemisorption Results

Phosgene chemisorption isotherms of the same samples used in the B.E.T. work were measured. As was explained earlier, two sets of phosgene weight data were collected. The net weight was the amount of phosgene which remained adsorbed after the sample weight was allowed to reequilibrate in the presence of helium. The gross weight was recorded immediately after the flow of phosgene was stopped. The spontaneous desorption of phosgene cannot be attributed to the desorption of physically adsorbed phosgene since the experiments were performed at 250 ^oC and the critical temperature of phosgene is 182 ^oC (32). The gross specific weights are plotted as a function of solid conversion in Figure 19. The data, above a conversion of 0.05, appear to approximate a straight line. The point at zero conversion is assumed correct since it

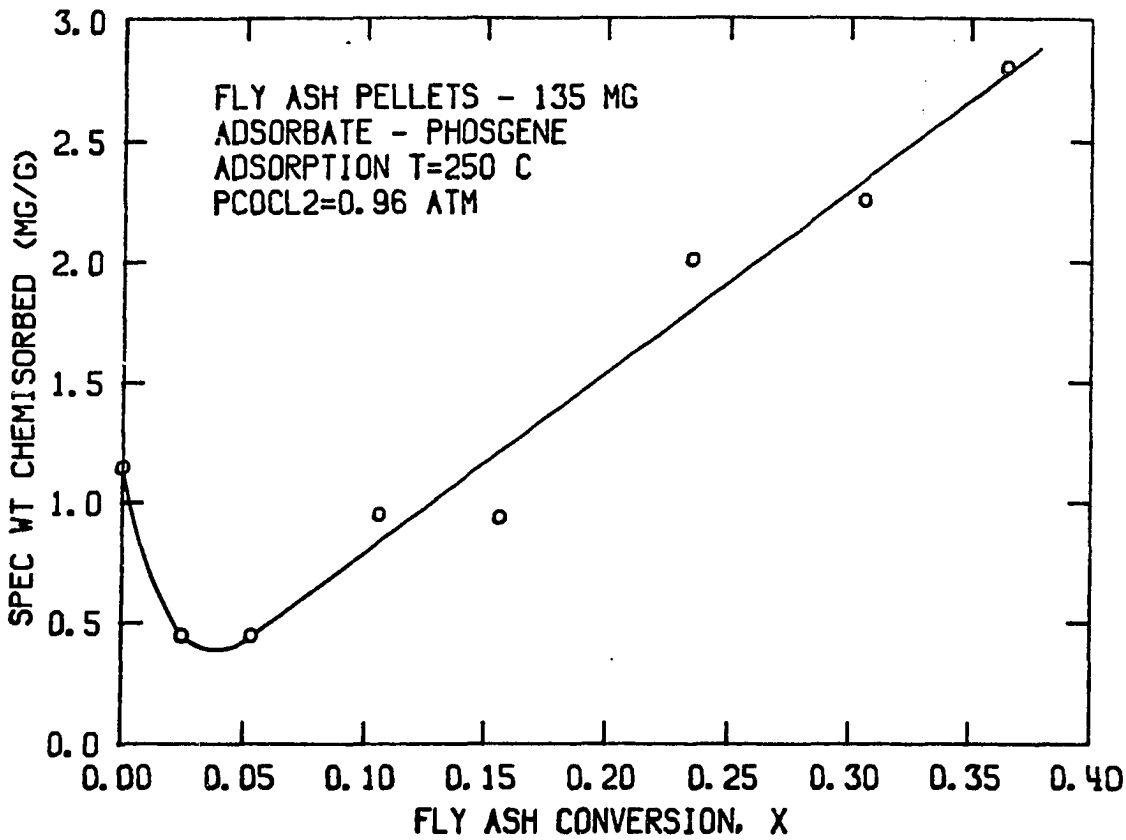

Figure 19. Specific weight of phosgene chemisorbed as a function of fly ash conversion

was reproduced four times with as many samples. The shape of the curve at low conversions cannot be explained. However, this could be due to a change in the fly ash surface composition since the oxide-fly ash conversion lines (Figure 8) deviated over the same fly ash conversion range.

If the inert matrix has a constant surface composition and if it represents most the exposed surface, then the ratio of the B.E.T. areas to the specific weight of phosgene chemisorbed should be a constant.

The ratios of the data points at corresponding conversions were computed and averaged to obtain a nearly constant value of 21.2 +/- 0.1 m^2/(mg phosgene). The ratio was used to estimate an effective phosgene molecular area of 350 $Å^2$. This is greatly different from the value of 35 $Å^2$ predicted by a literature correlation (27). Assuming the latter is correct, a phosgene surface coverage of only 10 percent at 250 °C is estimated. This very low coverage will likely decrease further as temperature increases since chemisorption is generally an exothermic process.

X-ray Diffraction Results

In two previous fly ash chlorination studies (1,42) and in this work, it has been found that only 80 percent of the alumina present in fly ash will chlorinate. It was thought that the presence of a nonreactive alumina mineral could be the cause of the upper limit. To identify minerals present in fly ash as a function of conversion, an unreacted sample along with several reacted samples were analyzed using x-ray diffraction. Figure 20 is a plot of some of the results. The degree of conversion decreases upon moving away from the x-axis. All major peaks were identified as either quartz or mullite. The quartz peaks remain about the same size but the mullite peaks shrink appreciably as conversion increases. The sample used in obtaining scan D was exposed to phosgene for 10 hours past the time when reaction was predicted to stop; however, a significant amount of mullite still remains.

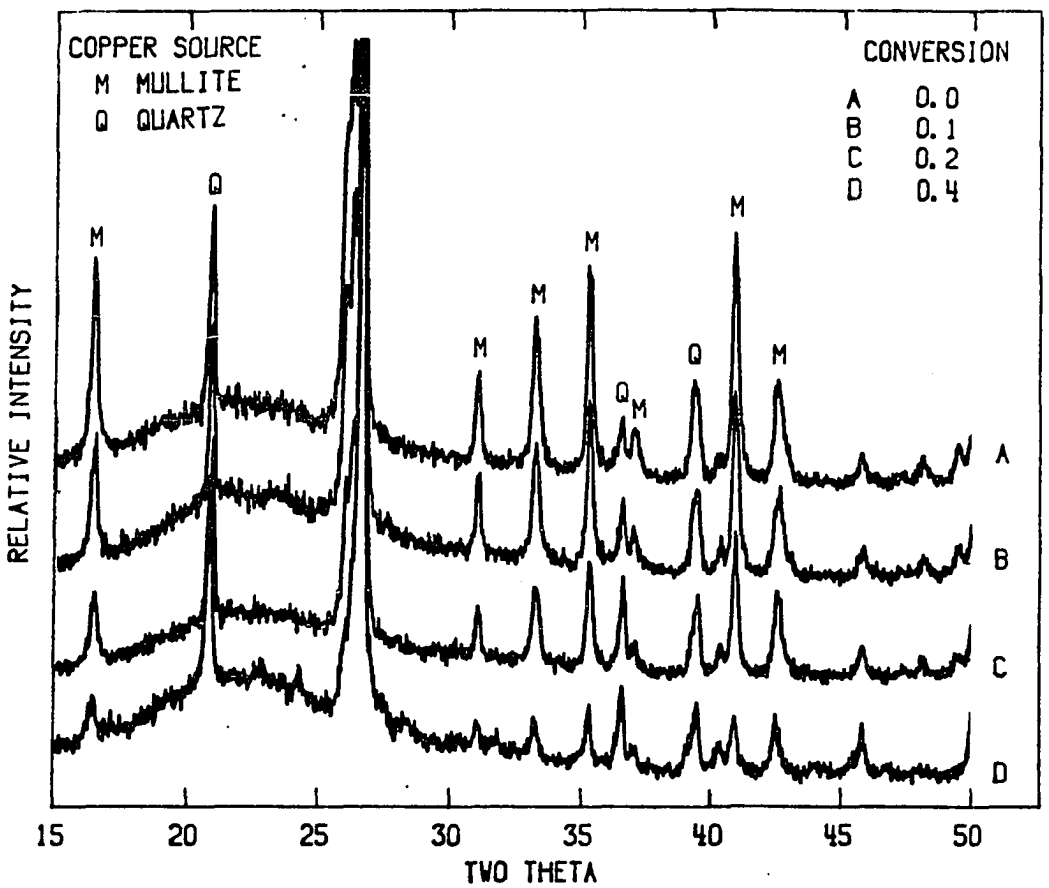

Figure 20. Comparison of x-ray diffraction spectra as a function of fly ash conversion

The amorphous peak appearing over the two theta range of 18 to 25 does not appear to shrink with conversion. Had the glass reacted, a decrease in the intensity of the amorphous peak with conversion should have resulted. The location of this peak, to the left of the large merged quartz-mullite peak, is characteristic of a silica rich glass (21). This glass is expected to contain low concentrations of alumina and balancing ions (calcium, sodium). There was, however, probably a

finite amount of alumina present which appears to have not reacted since the intensity of the amorphous hump did not change with conversion. The x-ray diffraction data do not explain why an alumina conversion limit exists, however, species containing the residual alumina are identified.

Knudsen-Cell Mass Spectrometer Results

This technique was employed to determine whether phosgene molecules exist on the surface of fly ash during chlorination. Two separate fly ash samples were reacted to conversions of about 0.15 and then placed, without cleaning, inside the vacuum chamber of a Knudsen-cell mass spectrometer system. Mass to energy numbers of 18 to 138 were monitored by a quadrupole mass spectrometer as the sample was heated from room temperature to 900 ^{o}C under vacuum.

Qualitative results were obtained so it was not possible to estimate the abundance of any of the products. Chlorine and the carbon oxides desorbed over the temperature range of 250 to 600 ^{o}C. As higher temperatures of 610 to 920 ^{o}C were approached, phosgene, aluminum chloride, silicon tetrachloride, and iron chloride desorbed. Finally, sodium chloride, potassium chloride, and calcium chloride were detected at 900 to 920 ^{o}C. A hydrogen chloride peak was prominent over the whole temperature range. Blank scans indicated that water existed in the system making it possible for water to react with any of the chlorine containing compounds at the ion source to form hydrogen chloride. The positive identification of phosgene verifies that phosgene molecules exist on the surface of fly ash during chlorination.

Identification of the many metal chlorides is very interesting, however, quantitative measurements are needed to determine if the amounts are significant. The system resulting from the coupling of a mass spectrometer to the Cahn balance would be very useful in the study the reaction of individual oxides.

FLY ASH CHLORINATION REACTOR DESIGN

The process design of a reactor for an ash chlorination plant is proposed. Plant capacity is based on processing the quantity of ash collected from a 1000 megawatt power station. Since approximately 272,000 metric tons of ash are collected annually by such a station, more than one chlorination reactor will be required. Results of the fly ash-phosgene reaction study are applied in the design of a chlorination reactor. It is assumed that the chlorination plant will operate 24 hours a day, 330 days a year. Phosgene will be produced by passing an equimolar mixture of CO and Cl_2 over a bed of charcoal located upstream of the chlorination reactor (47,50).

The design of a product separation system is not included. However, a scheme (61) has been developed which employs anhydrous distillation to recover $SiCl_4$, $TiCl_4$, CO, CO_2, $COCl_2$, and CO_2 and solvent extraction to separate $FeCl_3$ and $AlCl_3$. The final products are TiO_2, Al_2O_3, SiO_2, and an $FeCl_3$ solution.

Assumptions

Additional design assumptions used are:

1. Spherical fly ash pellets with a diameter of 0.25 cm enter the top of a cylindrical reactor and flow countercurrent to the phosgene/products stream.
2. No pellet fracture occurs as a result of reaction.
3. The fly ash has a weight percent composition of 56-SiO_2,

28-Al_2O_3, 10-Fe_2O_3, 5-CaO, and 1-TiO_2.

4. A reactor unit consists of a steel shell lined with a 0.6 meter thick layer of refractory brick.
5. Phosgene dissociates only in the void volume of the reactor and not on the surface of the fly ash or the reactor.
6. The fly ash reaction rate is not limited by pore diffusion effects.
7. The reactor operates at a specified temperature but the pressure is allowed to vary as a function of the bed height.
8. Component concentrations do not vary with radial position in the reactor.
9. Gaseous products do not affect the fly ash reaction kinetics.
10. The alumina to silica molar reaction ratio is constant at 1.86 and a maximum of 80 weight percent of the alumina reacts.

Some of these assumptions are based on available information while others were chosen to simplify the design problem.

The reaction of fly ash as pellets is required for achievement of optimal reaction rates. It has been reported that fly ash powder fluidizes at a linear velocity of only 0.4 cm/s (49). This rate along with the fact that 1.6 moles of gas are produced per mole of phosgene reacted greatly limit the fly ash-phosgene contacting rate. The use of powder would result in phosgene starvation mode operation. The uncovering of small particles on the surface of grains as conversion increases also supports the use of pellets. Most of the uncovered

particles would remain trapped within pellets, lessening the possibility of an elutriation problem.

A pellet thickness of 0.25 cm was discussed earlier as the primary dimension of a pellet whose reaction rate would not be limited by pore diffusion at 700 °C. Pellets must be formed which can withstand handling operations and the bed static pressure. In a recent experimental study (26), 0.4 cm spherical fly ash pellets were formed and then fired at 1000 °C in the presence of air yielding pellets with compressive strengths of 8.2 lb_f at fracture. This would be sufficient strength for delivery of 0.4 cm pellets to a reactor since for normal handling operations a strength of 2.5-5 lb_f is recommended (26). The fracture of pellets due to the weight of the bed will be discussed later after a bed height is computed.

Loss of pellet strength as a result of chlorination has also been investigated (26). The strength of 0.75 cm fly ash-coke pellets decreased by 50 percent at a conversion of 0.4. This conversion is the same as the upper limit expected in the fly ash-phosgene reaction. For the 0.4 cm pellets, a 50 percent strength decrease would leave the pellets with 4.2 lb_f of compressive strength which would likely be sufficient for handling. The degradation of reacted pellets after they leave the reactor is not a concern. However, their fracture within the reactor would result in a large bed pressure drop and also powder elutriation.

The changes in fly ash physical characteristics as a result of the firing step were also considered. The fly ash pellet B.E.T. surface area

decreased from a green state value of 2.31 m^2/g to 0.67 m^2/g after only 5 minutes of heating at 1000 ^oC. The loss of area could result from collapse of internal structure or the fusion of grains. Based on an observed parallel decrease in the microporosity, it would appear that a large fraction of the internal grain structure was destroyed.

Since the kinetic results and SEM pictures (Figures 1 and 2) support a fly ash shrinking-core mode of reaction, the surface area decrease would not be expected to affect the chlorination rates. As direct evidence for this, Feisel (26) reports that coke-fly ash powder and fired-pellet (0.75 cm diameter) samples reacted under identical conditions reached the same conversion at equal reaction times. The decrease in surface area from 2.31 to 0.67 m^2/g did not appear to affect the reaction rate.

The initial porosity of the fired pellets was measured as 0.48 by a mercury porosimeter. Pores with radii centered around 2000 Å account for almost all of the void volume. This size of pore would not lead to pore diffusion limitations for the range of reaction rates measured in this work.

Since the fly ash reaction rate is a function of both the fly ash conversion and the phosgene mole fraction, contacting opposite extremes of these variables is desirable as this tends to average the reaction rates and therefore the local heat production rates. Use of a countercurrent gas-solid flow configuration achieves this goal since at the bottom of the reactor fly ash containing a small reactive fraction contacts a gas phase with a high phosgene partial pressure and at the

top, fly ash containing a large reactive fraction contacts a gas phase with a small phosgene mole fraction.

Contacting gas with a small phosgene partial pressure and nearly unreacted fly ash at the top of the reactor is advantageous for another reason which concerns the reaction of iron, calcium, and titanium oxides. These components are present in most fly ashes and have been shown to react at much higher rates than the alumina and silica (1). Limiting the phosgene partial pressure in contact with them would decrease their reaction rates and thus, the local heat production rates.

The fly ash composition was chosen based on an average for magnetically separated bituminous ashes (48). Lignite ashes are usually not considered for chlorination processing because phosgene is wasted in chlorinating the large amount of calcium oxide often present in these ashes. The materials of construction specified in assumption 4 are based on information given in a rutile chlorination patent (51).

Even though the assumption that phosgene dissociates only in the gas phase is probably unrealistic it was applied in the absence of surface dissociation kinetic information. The uncertainty associated with this assumption compromises the accuracy of the preliminary design and makes it impossible to propose a detailed final design. Gas-phase dissociation rates are computed according to a literature expression (37).

The pressure is assumed to be 1 atm at the top of the reactor while at the bottom, the pressure is a function of bed porosity, bed depth, and gaseous flux rate. With regard to the energy balance, it is assumed that all components enter, leave, and react at the specified temperature. The

design model developed calculates and outputs a net heat flux as a function of bed height. Excess heat of reaction could be used to preheat input streams but no attempt was made to incorporate this into the design model.

Another simplification concerns radial concentration and temperature profiles. Flat profiles lessen the computational complexity since one spatial variable is eliminated. The constant temperature assumption makes the computational system much more stable. Without this assumption, small fluctuations in the temperature give rise to very large changes in the reaction rate which in turn affect the heat production rates, all of which lead to computational instability.

The last two assumptions are necessary for the application of the fly ash-phosgene reaction kinetics in the reactor design program. Single pellets are not exposed to the same gaseous environment as pellets in a bed. However, in the absence of experimental information, it is assumed that the products do not affect the fly ash reaction rate. The need for the values listed in assumption 10 will become apparent later.

Reactor Design Model

The reactor is designed as a series of cylindrical slices of equal thickness. Mass and energy balances computed for each slice are used in predicting concentration and net heat production profiles, respectively. Additional expressions are utilized which yield phosgene fractional dissociation data and the reactor pressure as a function of bed height. The bed height is measured starting from the bottom of the reactor. The

development and application of a FORTRAN program used for these computations follows.

Fly ash reaction

The difference in the rate at which fly ash enters and leaves a slice is equal to its reaction rate in that slice. Multiplication of equation 18, the fly ash conversion rate relationship, by the solid density, slice volume, and occupied fraction yields an expression for the fly ash reaction rate in a slice:

$$R_F = \frac{72kbM_A Y_A C_T V(1 - \epsilon_T)(1 - \frac{X}{0.4})^{2/3}}{r_o} \tag{36}$$

with $$V = \pi R_i^2 \Delta Z \tag{37}$$

$$C_T = \frac{P}{R_G T} \tag{38}$$

$$k = 4.7E07\exp(-4.0E04/(R_G T)) \tag{39}$$

where R_F = fly ash reaction rate in a slice, kg hr^{-1};

Y_A = phosgene mole fraction;

C_T = total gaseous molar concentration, kg-M m^{-3};

V = slice volume, m^3;

ϵ_T = total void fraction of slice;

R_i = reactor inner radius, m;

ΔZ = slice thickness, m;

One result of the design program is a fly ash conversion profile. In accordance with the fly ash reaction model, the design program calculates

fly ash conversions in terms of the silica-alumina reaction rate. The fly ash input rate is adjusted by subtracting from it the nonsilica-alumina input rate. The conversion in a slice is equal then to the silica-alumina reaction rate of the slice divided by the rate at which the silica-alumina fraction enters the reactor.

Phosgene reaction and dissociation

The phosgene consumption rate in a slice results from both its reaction and dissociation. The fly ash reaction rate divided by the reaction stoichiometric coefficient and the phosgene molecular weight is equal to the phosgene molar reaction rate.

$$R_A = \frac{R_F}{bM_A} \tag{40}$$

The gas-phase dissociation rate is given by the following expression (92):

$$R_{A_{dv}} = 3.332E12\exp(-49580/(R_G T))C_T^{3/2} Y_A Y_{Cl_2}^{1/2} \tag{41}$$

where $R_{A_{dv}}$ = phosgene molar dissociation rate, g-M liter^{-1}s^{-1};

Y_{Cl_2} = chlorine mole fraction.

Equation 41 is the result of a fit to data obtained over the temperature range, 380-505 ^{o}C. The dissociation data collected in this study (Table 4) were used to estimate rates at 625 and 700 ^{o}C which were a factor of three less than those predicted by equation 41. The dissociation rate expression was, therefore, divided by three and used in the reactor design model.

The dissociation rate for a slice is equal to $R_{A_{dv}}$ from equation 41 multiplied by the slice void fraction and total volume. The result is:

$$R_{A_d} = 4.0E15\exp(-49580/(R_G T))C_T^{3/2} Y_A Y_{Cl_2}^{1/2} V\epsilon_T \qquad (42)$$

where R_{A_d} = phosgene molar dissociation rate per slice, kg-M hr^{-1}.

The phosgene dissociation rate is a function of both the phosgene and chlorine mole fractions. To obtain an initial value for the latter, a mass fraction of chlorine not reacting to form phosgene is estimated.

The fly ash and phosgene reaction rates in a given slice are both functions of the fly ash conversion and the phosgene mole fraction. To calculate either reaction rate, a simplifying assumption was made with respect to one of these variables. Since the phosgene dissociation rate is also a function of the phosgene mole fraction, further complicating its mole fraction dependence, it was assumed that the phosgene and chlorine mole fractions at the exit of the previous slice are the same as those in the current slice. Phosgene reaction and dissociation are then assumed to occur at these mole fractions. This is not a particularly inaccurate assumption if a small step size is used. The fly ash reaction rate is calculated for the current slice using this same phosgene mole fraction and an estimated average fly ash conversion. The fly ash conversion is then computed and compared to the estimated value. If the estimate differs from the calculated value by more than one-half of a percent, a new average fly ash conversion is computed from the difference and the cycle is repeated.

Upon satisfying the one-half percent condition, the phosgene reaction and dissociation rates are computed and used to calculate the phosgene total consumption rate for that slice. The phosgene reaction rate is further utilized in calculating production rates of CO_2, $AlCl_3$, and $SiCl_4$ according to the following equations:

$$R_{CO_2} = -R_A \tag{43}$$

$$R_{Al} = -0.5655R_A \tag{44}$$

$$R_{Si} = -0.1517R_A \tag{45}$$

where R_{CO_2} = carbon dioxide molar production rate, kg-M hr^{-1};
R_{Al} = aluminum chloride molar production rate, kg-M hr^{-1};
R_{Si} = silicon tetrachloride molar production rate, kg-M hr^{-1}.

The numerical prefixes in equations 44 and 45 were calculated from the respective reaction stoichiometric coefficients and the experimentally determined alumina to silica molar reaction ratio. The production rate of chlorine and carbon dioxide are each equal to the dissociation rate of phosgene:

$$R_{CO} = -R_{A_d} \tag{46}$$

$$R_{Cl_2} = -R_{A_d} \tag{47}$$

where R_{CO} = carbon monoxide molar production rate, kg-M hr^{-1};
R_{Cl_2} = chlorine molar production rate, kg-M hr^{-1}.

The total molar flow rate at any position in the reactor is equal to the sum of the production rates of all previous slices. The phosgene molar flow rate as a function of axial position is equal to the initial input rate minus the sum of the reaction and dissociation rates of all previous slices. Cumulative total flows of all components are calculated, saved, and used to compute $COCl_2$, Cl_2, CO, CO_2, $AlCl_3$, and $SiCl_4$ mole fractions for the next slice.

Phosgene input requirements

A fly ash processing rate is chosen as a program input parameter. In the absence of phosgene dissociation, it would be possible to calculate directly the required phosgene input rate from the fly ash composition, the oxide conversions, and the fly ash input rate. To account for dissociation, excess phosgene is added and the design input calculations are repeated while varying the phosgene input rate until a phosgene exit conversion of 0.95 is computed upon reaching the specified alumina-silica conversion.

The quantity of phosgene needed for reaction is the sum of that which reacts with the nonsilica-alumina materials, Fe_2O_3, CaO, and TiO_2, and with alumina and silica. A final conversion of 0.9 was chosen for iron, calcium, and titanium oxide based on previous experimental results (1). These components are assumed to chlorinate near the top of the reactor so they are not a limiting factor in determining a bed depth. The fractions of alumina and silica which react are chosen and input into the design program. The molar flow rate of phosgene needed to react the

nonsilica-alumina components is calculated according to:

$$F_{A_{nsa}} = 0.9 M_A F_I \left(\frac{(3)(0.10)}{M_{Fe}} + \frac{(1)(0.05)}{M_{Ca}} + \frac{(2)(0.01)}{M_{Ti}}\right) \tag{48}$$

where $F_{A_{nsa}}$ = phosgene mass input rate for reaction of nonsilica-alumina components, kg hr^{-1};

F_I = fly ash input rate, kg hr^{-1};

M_{Fe}, M_{Ca}, M_{Ti} = molecular weights of Fe_2O_3, CaO, and TiO_2, respectively, kg $kg\text{-}M^{-1}$.

The numerical prefix pairs are the reaction stoichiometric coefficient and the initial fly ash weight fraction, respectively, for each component. The alumina-silica phosgene requirement is given by:

$$F_{A_{as}} = \frac{0.84 F_I X_F}{b} \tag{49}$$

where $F_{A_{as}}$ = phosgene mass input rate required for reaction with alumina and silica, kg hr^{-1}.

The numerical prefix in this equation is the sum of the alumina and silica initial weight fractions. The total phosgene input required then for a given fly ash input is given by:

$$F_A = \frac{F_{A_{nsa}} + F_{A_{as}}}{\bar{Y}_A} \tag{50}$$

where F_A = phosgene input rate, kg hr^{-1};

$\bar{Y}_A$ = phosgene input stream mass fraction.

The factor, γ_A, adjusts the phosgene input rate for the incomplete reaction of chlorine and carbon monoxide to form phosgene.

The phosgene conversion in a slice is calculated by dividing the sum of the reaction and dissociation rates in the slice by an adjusted phosgene reactor input rate. The adjusted rate is the total input rate minus the phosgene needed for reaction of the nonsilica-alumina components.

Bed and pellet porosities

The initial porosities of the bed and pellets are also required as program inputs. A bed porosity of 0.57 was determined according to the following scheme. The bulk volume of a known number of 0.25 cm diameter pellets was measured using a graduated cylinder. This bulk volume along with the computed pellet volume were used to obtain the bed porosity. As was mentioned earlier, an initial pellet porosity of 0.48 was measured using a mercury porosimeter. The total bed porosity is assumed to vary according to the following expression:

$$\epsilon_T = (1 - \epsilon_b)(\epsilon_{p_o} + (1 - \epsilon_{p_o})X) + \epsilon_b \qquad (51)$$

where ϵ_b = initial interpellet bed porosity;

ϵ_{p_o} = initial intrapellet porosity.

It is assumed that the interpellet porosity is constant throughout the reactor but that the intrapellet porosity varies as a function of the fly ash conversion.

Heat flux

The heat generation term is calculated by multiplying the heat of reaction per kg fly ash by its reaction rate. The heats of reaction of only alumina and silica are considered. It is assumed that the other components chlorinate near the top of the reactor and that their heats of reaction are used to partially preheat the fly ash. The following expression is used then to calculate the heat flux due to generation:

$$Q_C = \frac{\Delta H_{rxn} R_F}{2\pi R \Delta Z} \tag{52}$$

where Q_C = heat generation rate, kcal $hr^{-1}m^{-2}$;

ΔH_{rxn} = heat of reaction per kg of alumina-silica fly ash, kcal kg^{-1}.

The alumina and silica heats of reaction at 700 °C (7) and their fixed molar reaction ratio were used to compute a H_{rxn} of 145.7 kcal/kg.

The wall heat loss flux is given by:

$$Q_L = \frac{K(T_i - T_o)}{R_i \ln \frac{R_o}{R_i}} \tag{53}$$

where Q_L = wall heat loss rate per slice, kcal $hr^{-1}m^{-2}$;

K = thermal conductivity of wall material, kcal $m^{-1}hr^{-1}\,°C^{-1}$;

T_i, T_o = inner and outer reactor wall temperatures, respectively, °C;

R_i, R_o = inner and outer reactor wall radii, respectively, m.

A fused alumina brick thermal conductivity of 1.5 kcal/m/hr/^{o}C is used (18) along with an outer wall temperature of 25 ^{o}C.

Reactor pressure

The reactor pressure is computed as a function of the axial position in the bed. The adding of slices beginning at the bottom of the reactor leads to an iterative pressure drop solution. A pressure at the bottom of the reactor is estimated and then the pressure drop contribution of each slice is subtracted from this value until a specified fly ash or phosgene test condition is satisfied or until the pressure falls below 1 atm. New initial pressure estimates are input until a pressure of 1 atm at the top of the reactor is calculated at the same time that the fly ash and phosgene conversions are at the desired levels.

The pressure drop across a slice of spherical pellets is given by (19):

$$\Delta P = \frac{2f_m G^2 \Delta Z (1 - \epsilon_b)^{3-m}}{Dg \rho_g \epsilon_b^3} \qquad (54)$$

where ΔP = pressure drop across slice, kg m^{-2};

f_m = friction factor;

G = gaseous superficial mass velocity, kg $hr^{-1}m^{-2}$;

m = exponent;

D = pellet diameter, m;

g = gravity acceleration constant, m hr^{-2};

ρ_g = gaseous density, kg m^{-3}.

The pressure in the previous slice minus the pressure drop across the current slice yields the pressure in the current slice. The parameters, f_m and m, are functions of the following modified Reynolds number:

$$N'_{Re} = \frac{DG}{\mu_m} \tag{55}$$

where N'_{Re} = modified Reynolds number;

μ_m = viscosity of gaseous mixture, kg $m^{-1}hr^{-1}$.

Relationships between the modified Reynolds number and f_m and m were developed from available graphs (19) and were incorporated into the design model.

The pressure drop calculations require the computation of a gaseous superficial velocity, density, and viscosity. The superficial velocity is the sum of the products of the molar flow rates and their respective molecular weights. The density is computed by multiplying the total molar concentration by the gaseous molecular weight. The latter is obtained by summing the products of the component mole fractions and respective molecular weights.

The viscosity of an individual component is given by (19):

$$\mu = \frac{27.0M^{1/2}T^{3/2}}{V_b^{2/3}(T + 1.47T_b)} \tag{56}$$

where μ = viscosity of a single component, micropoise;

V_b = molar volume, $cm^3g\text{-}M^{-1}$;

T_b = boiling point temperature, K.

The mixture viscosity is then given by (19):

$$\mu_m = \frac{\sum_{i=1}^{I} Y_i \mu_i M_i^{1/2}}{\sum_{i=1}^{I} Y_i M_i^{1/2}} \qquad (57)$$

where Y_i = component i mole fraction.

The gaseous concentration, molecular weight, density, and viscosity are computed for a slice and are used then to estimate the pressure drop for that slice.

Design program summary

The assumptions and relationships used in developing the design program have been presented. A list of the general operations performed by the program follows. A program listing, complete with comments, is given in Appendix A.

1. Input reactor radius, slice thickness, initial phosgene mass fraction, fly ash and phosgene flow rates, fly ash final conversion, temperature, and pressure estimate.
2. Estimate fly ash conversion in first slice.
3. Calculate total gaseous molar concentration.
4. Calculate total porosity of slice i.
5. Calculate phosgene input mole fraction and use with estimated

fly ash conversion to compute fly ash conversion rate.

6. Calculate fly ash conversion and use to estimate new value for average slice conversion.
7. Apply one-half percent deviation test to fly ash conversions; if satisfied, continue, otherwise repeat steps 4, 5, and 6.
8. Calculate phosgene reaction and dissociation rates using most recent fly ash conversion value.
9. Calculate phosgene total conversion in slice i.
10. Calculate heat production rate and wall heat loss rate and subtract the latter from the former for a net flux.
11. Calculate new phosgene flow rate.
12. Calculate gaseous component production rates and add to respective total rates from the previous slice.
13. Add all gaseous cumulative flows together to obtain a total gaseous flow rate.
14. Calculate new gaseous mole fractions.
15. Calculate gaseous superficial velocity, molecular weight, density, and viscosity.
16. Calculate pressure drop for current slice and subtract from previous value to obtain the pressure for the current slice.
17. Estimate fly ash average conversion for the next slice.
18. Increment reactor height by slice thickness.
19. Repeat cycle starting at step 4 until the fly ash conversion is calculated to be less than or equal to zero, the phosgene conversion is within 1 percent of 0.95, and the pressure is

within 1 percent of 1 atm.

20. Output final reactor height and initial conditions.
21. Store to disk fly ash and phosgene conversions, heat fluxes, reactor pressures, and phosgene fractions dissociated, all as a function of reactor height.
22. End computation or begin again at 1.

Reactor Design Results

A reactor design optimization study would be premature at this time in the absence of phosgene surface dissociation information. Another approach, wherein values of many parameters were simply chosen, was used to arrive at the design specified in Table 6. A discussion of these preliminary results is followed by suggestions for an alternate reactor design.

Preliminary reactor design

While the results in Table 6 do not represent an optimal design, they will be used to demonstrate the effects of several variables. To arrive at these results, the bed radius, pressure drop, and porosity, the pellet diameter and porosity, and the reaction temperature were chosen and the fly ash and phosgene input rates were varied until a fly ash conversion of 0.3 and a phosgene conversion of 0.95 were computed.

The bed height to diameter ratio of 0.8 computed is much less than was desired. The high level of phosgene dissociation and the production of 1.6 moles of gas per mole of phosgene reacted results in such a large gaseous flow rate that the bed height had to be small to limit the

Table 6. Results of fly ash reactor design calculations

Variable	Value
Bed diameter	3.0 m
Bed height	2.36 m
Bed porosity	0.57
Initial pellet porosity	0.48
Pellet diameter	0.25 cm
Fly ash input rate	10020 kg hr^{-1}
Fly ash final conversion	0.3
Phosgene input rate	31968 kg hr^{-1}
Phosgene final conversion	0.95
Fraction phosgene dissociated	0.69
Temperature	700 ^{o}C
Pressure drop	2.0 atm
$AlCl_3$ Production Rate	4916 kg hr^{-1}
$SiCl_4$ Production Rate	1934 kg hr^{-1}
$FeCl_3$ Production Rate	1832 kg hr^{-1}
$TiCl_4$ Production Rate	213.8 kg hr^{-1}

pressure drop to 2 atm. The reactor pressure as a function of bed height is shown in Figure 21. The bottom of the reactor is at a bed height of zero. An explanation of the influence of total pressure on the phosgene reaction and dissociation rates follows.

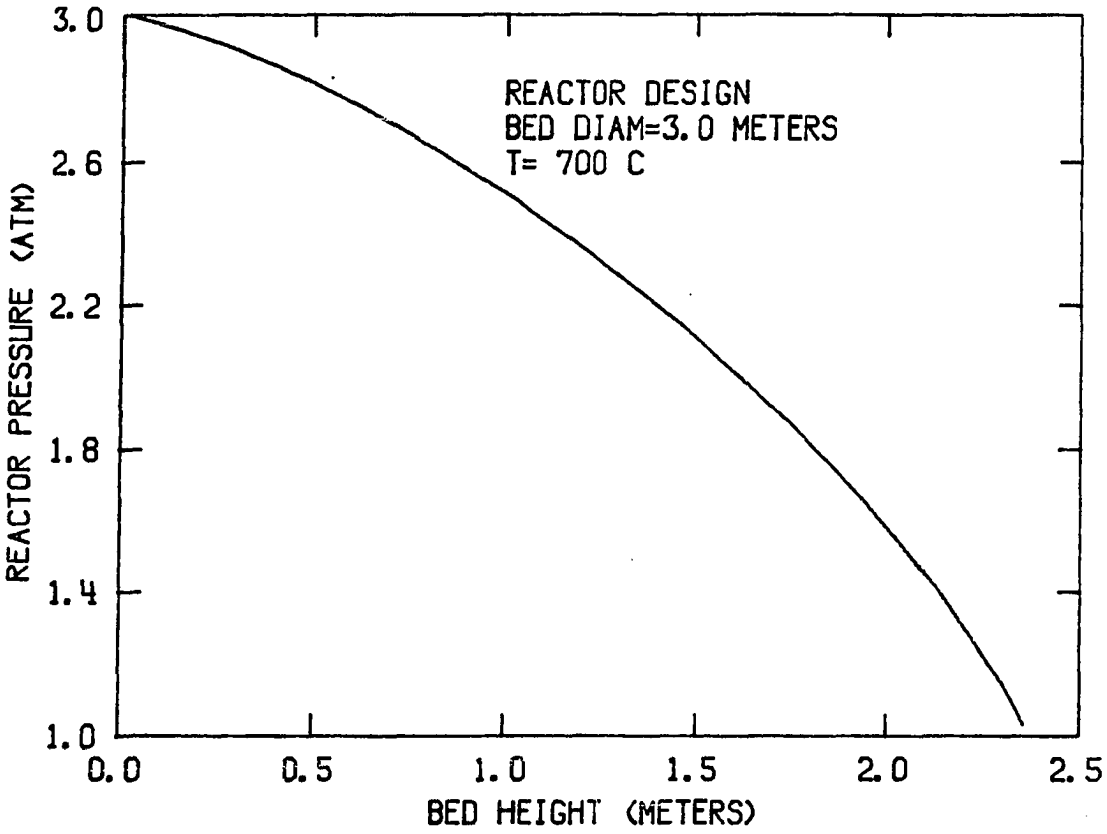

Figure 21. Reactor pressure as a function of bed height

Assuming that the phosgene dissociation and reaction equations apply at pressures greater than 1 atm, phosgene dissociation is favored at pressures greater than one 1 atm because it is one and one-half order with respect to pressure while the reaction rate is first order. Evidence is seen for this upon considering the results of Figures 22 and 23. The former is a plot of the fraction of the phosgene dissociated as a function of bed height and the latter shows the fly ash and phosgene conversions also as a function of bed height. At small bed heights, the

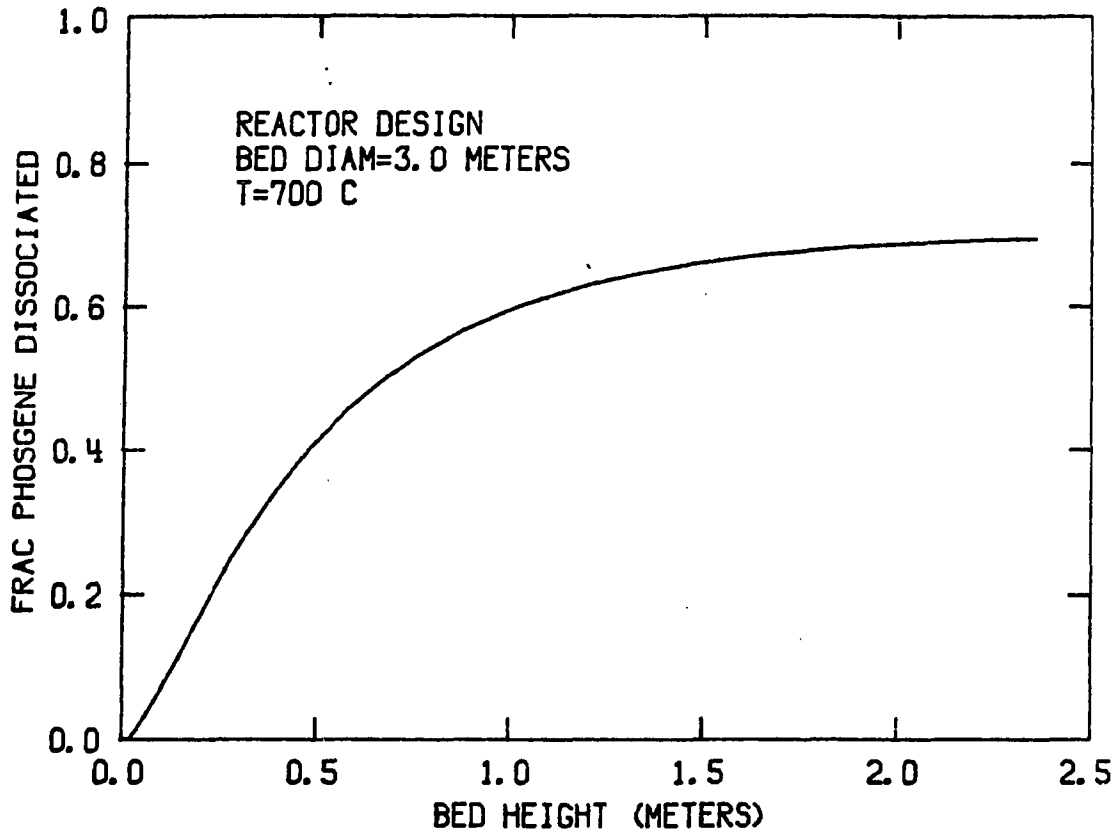

Figure 22. Fraction of phosgene dissociated as a function of bed height

fractional conversion and dissociation of phosgene are nearly equal. This is verified upon comparing the phosgene dissociation line in Figure 22 and the conversion line in Figure 23. However, upon moving up the column, the pressure decreases causing a shift in the relative rates of the two processes. This results in a gradual separation of the two lines which indicates that an increasingly larger fraction of the phosgene is reacting instead of dissociating.

The data in Figure 23 indicate that most reaction occurs within the

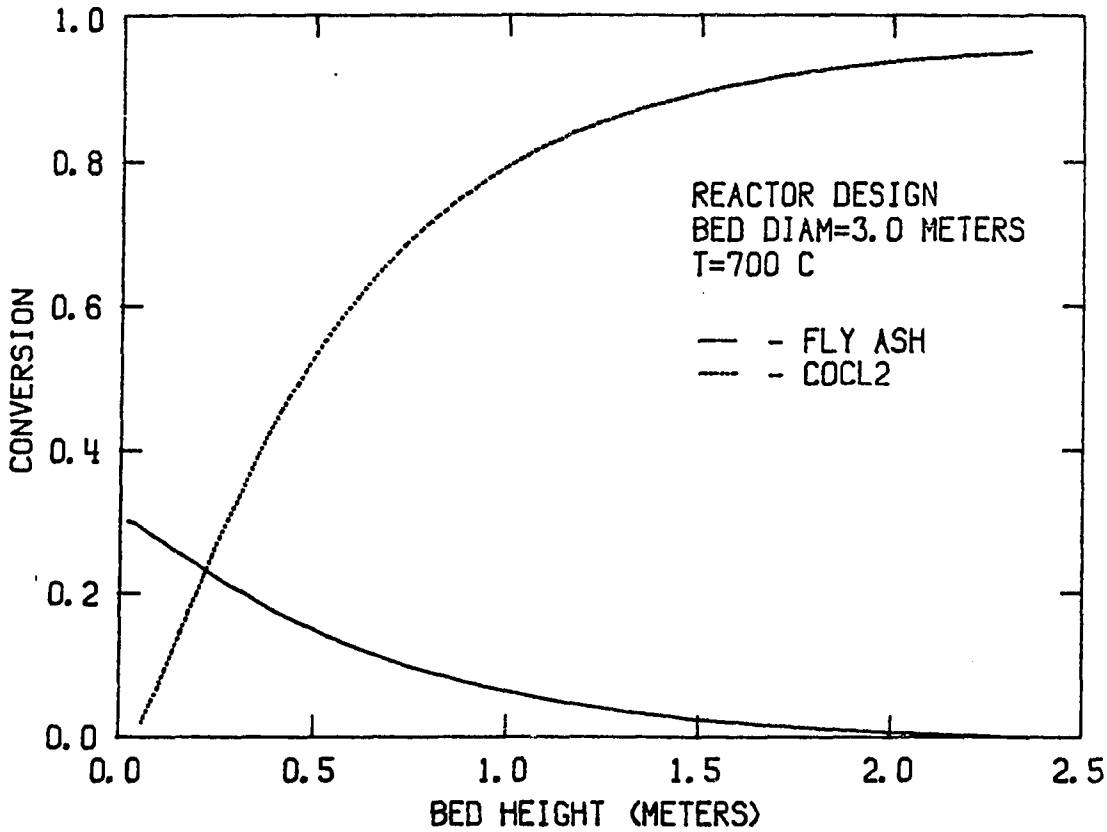

Figure 23. Phosgene conversion (dissociation and reaction) and fly ash conversion versus bed height

first meter of the bed. It is expected then, and shown in Figure 24, that most of the heat is produced near the bottom of the reactor. Dissipation of this heat could be achieved by circulating coolant within loops embedded in the reactor or in the reactor walls, or by feeding the phosgene at a temperature below the reaction temperature. Coolant loops in the reactor would have to be constructed of a corrosion resistant metal. For the reactor conditions specified, the modified Reynolds number lies within the turbulent range ensuring rapid convective heat

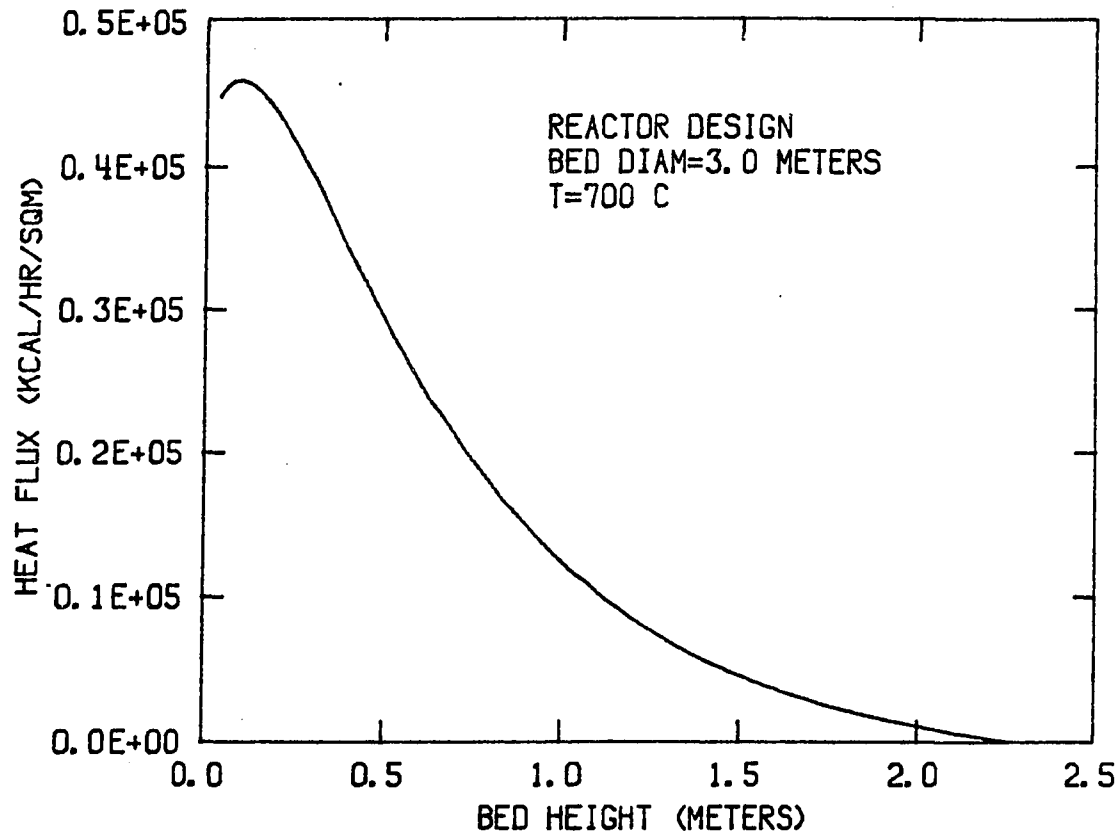

Figure 24. Reactor heat flux as a function of bed height

transfer.

The static pressure felt by pellets lying in the bottom of the reactor was calculated by multiplying the weight of an unreacted pellet by the number of pellets which could be stacked from the bottom to the top of the reactor. A value of 0.02 lb_f was computed to indicate that fracture due to static pressure is not likely. Powder accumulation due to abrasion, however, is still possible.

The value of the input phosgene mass fraction strongly affects the

reactor design results. As it approaches one, the chlorine mole fraction in the phosgene dissociation expression (equation 42) approaches zero. To demonstrate the effect of increasing the phosgene mass fraction, design calculations were done in which the fly ash input rate, reactor radius, and temperature values listed in Table 6 were entered along with a phosgene mass fraction of 0.995. Since a mass fraction of 0.95 was used previously, the chlorine mass fraction was reduced by a factor of 10. Relative to the results listed in Table 6, the phosgene input requirement decreased by 16 percent and the total bed pressure drop decreased by 25 percent. The bed height (2.40) was only slightly larger and the total fraction of the phosgene dissociated decreased by 5 percent. The input then of a chlorine-free phosgene feed would greatly enhance the efficiency of the reactor. Mass fractions in the range of 0.995 are easily attainable since one phosgene production patent (47) specifies an impurity level of only 100 ppm carbon tetrachloride.

The processing of 272,000 metric tons of fly ash annually was chosen as a basis for a chlorination plant design. Since a single reactor can process 80,000 metric tons per year, a minimum of 3.5 units would be required. Employment of at least 4 units would be necessary to allow for some down-time.

The production rates of $AlCl_3$, $SiCl_4$, $FeCl_3$, and $TiCl_4$ are listed in Table 6. These are based on conversions of 0.67, 0.13, 0.9, and 0.9 for aluminum, silicon, iron, and titanium oxides, respectively. At these conversions and if it is assumed that there is no product loss in

the separation step, a plant processing 272,000 metric tons of fly ash annually would produce, 27,000 metric tons aluminum, 17,000 metric tons iron, 9,300 metric tons silicon, and 1,500 metric tons titanium. The components are listed as metals for comparison reasons only. The final products would be an iron chloride solution, titania, alumina, and silica. The iron chloride solution could be further processed to yield a high-purity iron ore. The silica, while not of great value, could be used in the glass industry. The alumina and titania could be used in these forms or processed for use as metals.

Alternate reactor design

The most disturbing result of the design calculations is the high level of phosgene dissociation. The phosgene dissociation to reaction rate ratio would have to be minimized to optimize phosgene utilization. The two variables common to both kinetic expressions are total pressure and temperature. Since the dissociation is a stronger function of pressure, a minimization of the pressure drop would be advantageous. The reaction of larger pellets would reduce the pressure drop somewhat since the porosity of the bed would be increased. This gain would be offset somewhat by the need to use a taller column to process the same amount of fly ash per reactor unit. Also, the use of larger pellets could possibly introduce reaction diffusion control.

Reaction of a thin bed of pellets would lessen the pressure drop. A staged column in which product gases are withdrawn and phosgene is added at each level is a possibility. By withdrawing some of the

products, the pressure drop across each stage would be minimized and the dilution of the phosgene by dissociation and gaseous reaction products would be reduced. As is shown in Figure 23, the fly ash conversion rate with respect to the bed height is very small above 1 meter. The major cause for this was the very low phosgene concentration.

Advantageous temperature effects could also be exploited in a staged reactor. The ratio of the temperature dependent parts of the reaction and dissociation expressions increases from a value of 142 at 700 ^{o}C to 250 at 600 ^{o}C. If the fly ash processing capacity is held constant upon decreasing the temperature, design program results show that the bed depth increases causing as increase in the pressure drop to offset any temperature advantage. However, if a staged design were employed, a decrease in the temperature would only require the addition of more stages.

The construction and operation of a staged chlorination reactor may be difficult. The input and withdrawal of gases at each stage as well as the transport of the fly ash from stage to stage would require special design consideration. Also, a major concern which will be associated with any reactor design is the large amount of energy needed to separate and recycle the carbon monoxide, chlorine, and phosgene and to heat the fly ash.

CONCLUSIONS

Results of the fly ash-phosgene kinetic study and the reactor design program have been presented and discussed separately. The same approach is used in presenting the conclusions. Lists of what are considered to be the most significant conclusions of each section follow.

Fly Ash-Phosgene Kinetic Study

1. Small unreactive particles are uncovered as fly ash reacts. This results in the development of an inert matrix beginning on the grain surfaces.
2. Some fly ash grains are formed by the agglomeration of small particulates.
3. The microporosity of unreacted fly ash grains is very small causing chlorination to begin on the outer grain surfaces.
4. The chlorination of fly ash is first order with respect to the phosgene partial pressure over the temperature range of 525 to 625 ^{o}C and at a total pressure of approximately 1 atm.
5. The fly ash pellet chlorination rate is surface reaction controlled for the temperature range of 450 to 700 ^{o}C.
6. A constant alumina to silica molar ratio of 1.86 reacts over the fly ash conversion range of 0.05 to 0.375.
7. The activation energy (42.7 kcal/g-M) and the frequency factor (1.3×10^{8} cm/min) are independent of fly ash conversion.
8. Phosgene nondissociatively chemisorbs on fly ash at a reaction

temperature of 625 °C.

9. Phosgene covers a small fraction of the fly ash surface.
10. Alumina in mullite and possibly in the glass phase of fly ash does not react with phosgene.
11. The shrinking core model accurately predicts fly ash conversion versus time data for temperatures of 525 to 600 °C and phosgene partial pressures of 0.02 to 0.9 atm.
12. Pellets with a porosity of 0.42 and a primary axis of 0.1 inch can be reacted with phosgene at temperatures of up to 700 °C without rate limitation due to diffusion or mass transfer.

Reactor Design

1. Phosgene gas-phase dissociation will be a major problem in the design and operation of any chlorination reactor employing phosgene as the primary reactant.
2. Minimization of the phosgene dissociation to reaction rate ratio is required for the optimal utilization of phosgene. This is best achieved by lowering the reactor bed pressure.
3. The chlorination of alumina and silica at 700 °C is highly exothermic which would make dissipation of excess heat in a chlorination reactor necessary.
4. Results of the preliminary design indicate that 4 reactors, 3 m in diameter and 2.36 m tall operated at 700 °C would react 67 percent of the alumina present in the fly ash (272,000 metric tons) produced annually by a typical 1000 megawatt power station.

RECOMMENDATIONS

Several assumptions were made during development of the fly ash-phosgene reaction model and the reactor design program. The list of recommended experiments which follows is proposed with the intention that the results would provide the information needed to eliminate some of the assumptions. It would be possible then to specifiy a more accurate reactor design.

1. Investigate the gas-phase and surface dissociation kinetics of phosgene. This could be done by exposing a bed of pellets to phosgene until reaction stops (carbon dioxide concentration in the product stream approaches zero). The temperature, total pressure, chlorine mole fraction, and gaseous residence time would be varied while the concentrations of carbon monoxide, chlorine, and phosgene in the exit stream were monitored. The same tests would then be repeated at identical conditions with an empty reactor and the data obtained used to correct the previous results for gas-phase dissociation contributions. The surface area of the pellets would next be determined and used to calculate the surface dissociation rate in terms of moles per area-time. Additional experiments would then be performed in which phosgene, chlorine, and carbon monoxide and dioxide concentrations would be measured as a function of fly ash conversion. These data and the kinetic expression developed in this study along with a gas phase dissociation expression and

fly ash surface areas as a function of conversion would be used to determine if the surface dissociation rate is proportional to the exposed surface area. As a result of these experiments, the surface dissociation information needed in the reactor design would be available.

2. Expose beds of pellets or single pellets to different product gases ($AlCl_3$, $SiCl_4$, CO_2) to assess effects of these gases on the fly ash reaction kinetics.
3. React several sets of fly ash samples with different initial compositions to a range of conversions, analyze the samples for alumina and silica losses, and calculate alumina to silica molar reaction ratios. These data would indicate whether the alumina to silica reaction ratio is a function of the fly ash initial composition and thus, whether a given reactor design could be used to process different fly ashes.
4. Measure the specific reaction rates of different sized (diameters of 0.25 to 1.3 cm) spherical pellets at identical conditions. The data could be used to determine the maximum size of pellet which can be processed in the absence of mass transfer and pore diffusion rate limitations.
5. Use the results of the dissociation experiments and the design program to develop a staged reactor design. Maximization of the phosgene reaction to dissociation ratio and the phosgene final conversion could be important considerations.

BIBLIOGRAPHY

1. Adelman, D. J. High-temperature chlorination of coal fly ash. Ames, IA: Iowa State University; 1980. 105 p. M. S. Thesis.

2. Adelman, D. J.; Burnet, G. The status and potential of metals recovery from coal fly ash by high-temperature chlorination. Proc. Iowa Acad. Sci. 87(4): 129-133; 1980.

3. Alder, H. P.; Geisser. H.; Baiker, A.; Richarz, W. The chlorination of alumina. A comparison of the kinetics with different reduction agents. Light Metals 3: 337-352; 1979.

4. Alder, H. P.; Muller, H. P.; Richarz, W. Kinetic study of the alumina chlorination with carbon monoxide and chlorine. Light Metals 1: 219-232; 1977.

5. Anvaer, B. I.; Drugov, Y. S. Gas chromatography in the analysis of inorganic materials (Review). Zh. Anal. Khim. 26: 1180-1201; 1971.

6. Ash production ash utilization - 1982. Ash at Work XV(3). National Ash Association, Washington, D. C.; 1982.

7. Barin, I.; Knacke, O. Thermochemical properties of inorganic substances. New York: Springer-Verlag; 1973.

8. Barin, I.; Schuler, W. On the kinetics of the chlorination of titanium dioxide in the presence of solid carbon. Metall. Trans. B 11B: 199-207; 1980.

9. Barrett, E. P.; Joyner, L. G.; Halenda, P. P. The determination of pore volume and area distributions in porous substances. I. Computations from nitrogen isotherms. J. Am. Chem. Soc. 73(Jan.): 373-380; 1951.

10. Bergholm, A. Chlorination of rutile. Trans. Metall. Soc. AIME 221(Dec.): 1121-1129; 1961.

11. Bertoti, I.; Pap, I. S.; Szekely, T.; Toth, A. Kinetics of gamma-alumina chlorination by carbon tetrachloride. Thermochim. Acta 41: 27-32; 1980.

12. Bertoti, I.; Pap, I. S.; Toth, A.; Szekely, T. Kinetics of gamma-alumina chlorination by tetrachloroethylene. Thermochim. Acta 44: 333-336; 1981.

13. Bertoti, I.; Podor, B.; Mink, J.; Pap, I. S.; Szabo, A.; Szekely,

T. TG, MS, and IR study on the chlorination reaction of gamma-aluminum oxide with carbon tetrachloride. Trav. Com. Int. Etude Bauxites, Alumine Alum. 17: 185-193; 1982; Chem. Abstr. 99: 108555t (1983).

14. Bertoti, I.; Toth, A.; Szekely, T.; Pap, I. S. Kinetics of gamma-alumina chlorination by phosgene. Thermochim. Acta 44: 325-331; 1981.

15. Bird, R. B.; Stewart, W. E.; Lightfoot, E. N. Transport phenomenon. New York: John Wiley and Sons, Inc.; 1960.

16. Boar, P. L.; Ingram, L. K. Comprehensive analysis of coal ash and silicate rocks by atomic-absorption spectrophotometry by a fusion technique. Analyst 95(Feb.): 124-130; 1970.

17. Cahn, L.; Peterson, N. C. Conditions for optimum sensitivity in thermogravimetric analysis at atmospheric pressure. Anal. Chem. 39(Mar): 403-404; 1967.

18. Chemical engineers' handbook. 4th ed. Perry, J. H., ed. New York: McGraw-Hill Book Co.; 1963.

19. Chemical engineers' handbook. 5th ed. Perry, J. H., ed. New York: McGraw-Hill Book Co.; 1973.

20. DeCarlo, V. A.; Seeley, F. G.; Canon, R. M.; McDowell, W. J.; Brown, K. B. Evaluation of potential processes for the recovery of resource materials from coal residues: fly ash. NTIS ORNL/TM-6126; 1978. 99 p.

21. Diamond, S. On the glass present in low-calcium and in high-calcium fly ashes. Cement and Concrete Research 13: 459-464; 1983.

22. Doubovetzky, P.; Forschner, P.; Montazeau, F. Phosgene. Ger. patent 2,600,387. 1975 Jan. 4; Chem. Abstr. 85: P178184 (1976).

23. Dunn, W. E., Jr. High-temperature chlorination of titanium bearing minerals. Trans. Metall. Soc. AIME 218(Feb.): 6-12; 1960.

24. Dunn, W. E., Jr. High-temperature chlorination of titanium bearing minerals: Part III. Metall. Trans. B 10B: 293-294; 1979.

25. Dunn, W. E., Jr. High-temperature chlorination of titanium bearing minerals: Part IV. Metall. Trans. B 10B: 271-277; 1979.

26. Feisel, B. C. Granulation of nonmagnetic fly ash-coke mixtures. Ames, IA: Iowa State University; 1984. 114 p. M. S. Thesis.

27. Gregg, S. J.; Sing, K. S. W. Adsorption, surface area, and porosity. London: Academic Press; 1967.

28. Henry, J. P., Jr.; Cunningham, R. S.; Geankoplis, C. J. Diffusion of gases in porous solids over a thousand-fold pressure range. Chem. Eng. Sci. 22: 11-20; 1967.

29. Holliday, R. D.; Milne, D. J. Experimental evaluation of routes for purification of bauxite by gas-solid reactions. Ind. Eng. Chem., Process Des. Dev. 14(4): 447-452; 1975.

30. Hulett, L. D., Jr.; Weinberger, A. J.; Northcutt, K. J.; Ferguson, M. Chemical species in fly ash from coal-burning power plants. Science 210(Dec.): 1356-1358; 1980.

31. Industrial hygiene and toxicology II. Patty, F. A. ed. New York: Interscience Publishers, Inc.; 1949; 624-626.

32. International critical tables of numerical data physics, chemistry, and technology. Washburn, E. W. ed. New York: McGraw-Hill Book Company, Inc.; 1928.

33. Ishii, T.; Tsuchida, T.; Furuichi, R.; Haga, H.; Kudo, K. DTA study of the chlorination of fly ash and bauxite in the presence of carbon. Themochim. Acta 53: 89-103; 1982.

34. Ivashentsev, Y. I.; Pogonina, L. N. Mechanism of titania chlorination. Zh. Prikl. Khim. 48(8): 1837-1838; 1975; Chem. Abstr. 83: 184176 (1975).

35. Johnson, V. J. A compendium of the properties of materials at low temperature (Phase I). WADD Technical Report 60-56; 1960.

36. Kellog, H. H. Thermodynamic relationships in chlorine metallurgy. J. Metall. Trans. AIME 188(June): 862-872; 1950.

37. Kowalczyk, K. J. Kinetic study of the thermal formation and dissociation of phosgene in a tubular reactor. Ames, IA: Iowa State University; 1968. 62 p. M. S. Thesis.

38. Kuruvilla, J.; Dadape, V. V. Studies in the chlorination of Indian bauxite ores. Indian J. Technol. 3(81): 244-248; 1965.

39. Landsberg, A. Chlorination kinetics of aluminum bearing minerals. Met. Trans. B 6B(June): 435-441; 1977.

40. Landsberg, A. Some factors affecting the chlorination of kaolinic clay. Met. Trans. B 8B(Sept.): 435-441; 1977.

41. Longatte, J. M. E.; Charles, R.; Courbin, G. Phosgene manufacture. S. African patent 7,106,693. 1972 May 15; Chem. Abstr. 78: P60333 (1973).

42. Mehrotra, A. K.; Behie, L. A.; Bishnoi, P. R.; Svrcek, W. Y. High-temperature chorination of coal ash in a fluidized bed. 1. Recovery of aluminum. Ind. Eng. Chem. Process Des. Dev. 21: 37-44; 1982.

43. Milne, D. J. Chlorination of bauxite in the presence of silicon tetrachloride. Met. Trans. B 6B(Sept.): 486-488; 1975.

44. Milne, D. J. The chlorination of alumina and bauxite with chlorine and carbon monoxide. Proc. Australas. Inst. Min. Metall. 260(Dec.): 23-31; 1976.

45. Milne, D. J.; Wibberley, L. J. The removal of iron from bauxite using anhydrous HCl. Light Metals (NY) 2: 125-45; 1977.

46. Milne, D. J.; Wibberley, L. J. Chlorination of alumina and bauxite using pyrolytic carbon as reductant. Light Metals 2: 147-162; 1978.

47. Mitsubishi Gas Chemical Co. Inc. Manufacture of phosgene. Jpn. patent 14,044. 1980 Dec. 26; Chem. Abstr. 94: P65095 (1981).

48. Murtha, M. J.; Burnet, G. Power plant fly ash as a resource for aluminum and cement. NTIS IS-M-298. 1978. 21 p.

49. Nguyen, C. T. Fluidization characteristics of power-plant fly ashes and fly ash-charcoal mixtures. Ames, IA: Iowa State University; 1979. 96 p. M. S. Thesis.

50. Obrecht, R. P. Phosgene manufacture. U.S. patent 878,032. 1979 Feb. 15; Chem. Abstr. 91: P210922 (1979).

51. Powell, R. Titanium oxide and titanium tetrachloride. Park Ridge, NJ: Noyes Development Corporation; 1968.

52. Raval, R. P.; Dixit, S. G. Some aspects of the chlorination of bauxite. J. Chem. Tech. Biotechnol. 29: 107-115; 1979.

53. Reid, R. C.; Prausnitz, J. M.; Sherwood, T. K. The properties of gases and liquids. 3rd ed. New York: McGraw-Hill, Inc.; 1977.

54. Reynolds, J. E.; Williams, A. R. Process for recovery of aluminum and other metal values from fly ash. U.S. patent 4,159,310. 1979 Jun. 26.

55. Robens, E. Errors in thermogravimetric experiments resulting from adsorption on the counterweight. Thermal Analysis ICTA 80. Basel: Birkhaeuser Verlag; 1980; 213-218.

56. Rodriguez-Vazquez, J. A. Quantitative inorganic analysis by gas chromatography. A review. Anal. Chim. Acta 73: 1-32; 1974.

57. Scholz, H.; Decker, M.; Neumayr, F. Removal of phosgene from waste gases. Ger. patent 2,632,138. 1975 Jul. 18; Chem. Abstr. 86: 176578j (1977).

58. Shapatina, E. N.; Kuchaev, V. L.; Temkin, M. I. The kinetics of catalytic synthesis of phosgene. Kinet. and Catal. 17(3): 559-566; 1976.

59. Shapatina, E. N.; Kuchaev, V. L.; Temkin, M. I. Kinetics of the catalytic synthesis of phosgene. Kinet. and Catal. 18(4): 800-809; 1977.

60. Shapatina, E. N.; Kuchaev, V. L.; Temkin, M. I. Kinetics of phosgene synthesis at low chlorine concentrations. Kinet. and Catal. 20(5): 972-976; 1979.

61. Sheng, Z,; Murtha, M. J.; Burnet, G. Some recent results in the separation of metal chlorides by solvent extraction. Proc. Third Symp. Sep. Sci. and Tech. for Energy Applications, Gatlinburg, TN; 1983; in press.

62. Smith, K. A.; Riemer, S. C.; Iwasaki, I. Carbochlorination of aluminum from non-bauxite sources. J. Metals 34(9): 59-62; 1982.

63. Standard test method for specific gravity of hydraulic cement. ASTM ANSI, C188-72; 1972.

64. Szekely, J.; Evans, J. W.; Sohn, H. Y. Gas-solid reactions. New York: Academic Press; 1976.

65. Szekely, J.; Sohn, H. Y. Effect of structure on the reaction between a porous solid and a gas. Inst. Mining Met. Trans. C C82: C92-C100; 1973.

66. Thomas, J. M.; Thomas, W. J. Introduction to the principles of heterogeneous catalysis. London: Academic Press; 1967.

67. Trapnell, B. M. W. Chemisorption. New York: Academic Press; 1955.

68. Turkdogan, E. T.; Olosson, R. G.; Vinters, J. V. Pore

characteristics of carbons. Carbon 8: 545-564; 1970.

69. Ulrich, G. D.; Riehl, J. W.; French, B. R.; Desrosiers, R. Mechanism of sub-micron fly-ash formation in a cyclone, coal-fired boiler. Ash Deposits Corros. Impurities Combust. Gases, (Proc. Int. Conf). Washington D.C.: Hemisphere Publ. Corp.; 1977; 253-268.

70. Ulrichson, D. L.; Yake, D. E. Numerical analysis of a finite cylindrical pellet model in solid-gas reactions. Chem. Eng. Sci. 35: 2207-2212; 1980.

71. Ziegler, W. T.; Mullins, J. C. Calculation of the vapor pressure and heats of vaporization and sublimation of liquids and solids, especially, below one atmosphere. IV. Nitrogen and Fluorine. Report No. 1 to NBS, Project A-663, Georgia Inst. of Tech., Atlanta; 1963.

ACKNOWLEDGMENTS

I would like to thank Dr. George Burnet for the advice and guidance offered throughout the course of this study. The stable working environment which has been a part of working with Dr. Burnet allowed me to concentrate almost solely on research. In addition, the opportunities and encouragement he provided to write and present papers have been greatly appreciated.

Thanks are also due to Harvey Jensen for his help in building and finding available equipment and for his advice on operation of the balance. Mike Murtha's encouragement and interest in this work are also appreciated along with his knowledge of the operation of Ames Laboratory.

Mike Dobbins and Jim Voigt are also thanked for their very significant contributions. The discussions with Mike throughout this study answered many questions and solidified many ideas. Besides being founder of the Ames Laboratory Gazelles, Jim's collection of the Coulter counter data, shooting of the SEM pictures, and help running the LSI-11 computer were greatly appreciated.

Thanks are also given to Dr. Dean Ulrichson for his advice and questions concerning the experimental results.

Most importantly, I would like to thank my wife Sylvia for her constant companionship and encouragment.

APPENDIX A: SOFTWARE

B.E.T. Surface Area

```
10  HOME
15 D$ =  CHR$ (4)
20  PRINT "THIS PROGRAM  USES THE
      B.E.T.EQUATION "
25  PRINT "FOR CALCULATION OF SUR
     FACE AREAS"
26  PRINT : PRINT : PRINT
27  INPUT "ENTER FILE NAME,NUMBER
      , ETC... ";F$
30  PRINT
40  INPUT "ENTER THE NUMBER OF DA
     TA POINTS ";N
45 F = N - 1
47  DIM X(N),Y(N),D(7,N),MB(N),P(
     N),M(N),MC(N),T(N),V(N),PS(N
     ),YC(N),TS(N)
50  PRINT
60  PRINT "ENTER SAMPLE WEIGHTS (
     MG), STARTING WITH M(1)."
70  FOR J = 1 TO N
80  INPUT M(J)
85 D(1,J) = M(J)
90  NEXT J
100  PRINT
110  PRINT "ENTER SAMPLE PRESSURE
     S (TORR) STARTING WITH P(1).
     "
120  PRINT
130  FOR J = 1 TO N
140  INPUT P(J)
145 D(3,J) = P(J)
147  NEXT J
150  PRINT "ENTER BLANK WEIGHTS
     (MG) STARTING  WITH MB(1)."
160  PRINT
170  FOR J = 1 TO N
180  INPUT MB(J)
185 D(2,J) = MB(J)
190  NEXT J
200  PRINT "ENTER SAMPLE TEMPERAT
     URE"
201  INPUT TM
202  FOR J = 1 TO N
203 T(J) = TM
204 D(7,J) = T(J)
205  NEXT J
210  PRINT
220  INPUT "ENTER CLEAN SAMPLE WE
     IGHT (G).";W
230  PRINT
240  FOR J = 2 TO N
260 MC(J) = (M(J) - M(1)) - (MB(J
     ) - MB(1))
270 V(J) = 0.80015 * MC(J)
280 D(4,J) = V(J)
285 PS(J) = 729.398 + 89.744 * (T
     (J) - 77)
290 X(J) = P(J) / PS(J)
295 D(5,J) = X(J)
300 Y(J) = P(J) / (V(J) * (PS(J) -
     P(J)))
302 D(6,J) = Y(J)
305 Y2 = Y2 + Y(J) * Y(J)
310 SX = SX + X(J)
320 SY = SY + Y(J)
330 XY = XY + X(J) * Y(J)
340 X2 = X2 + X(J) * X(J)
350  NEXT J
360 D1 = F * X2 - SX * SX
370 B1 = (F * XY - SX * SY) / D1
380 A = (X2 * SY - SX * XY) / D1
390  FOR J = 2 TO N
400 YC(J) = A + B1 * X(J)
410 DE = DE + (YC(J) - Y(J)) * (Y
     C(J) - Y(J))
420  NEXT J
430 S1 = DE / (F - 2)
440 D2 = F * Y2 - SY * SY
460 SA =  SQR (S1 * X2 / D1)
470 SB =  SQR (F * S1 / D1)
480 SW = 2.5E - 9
485 D2 = F * Y2 - SY * SY
488 R2 = B1 * (XY - SX * SY / F) /
     (Y2 - SY * SY / F)
490 S = 4.353 / ((A + B1) * W)
500 SS = S *  SQR (SW / (W * W) +
     (SA * SA + SB * SB) / ((A +
     B1) * (A + B1)))
510  PRINT D$;"PR#1"
515  PRINT : PRINT : PRINT
```

```
520  PRINT "B.E.T.SURFACE AREA =
     ";S;" + / - ";SS
525  PRINT : PRINT : PRINT
530  PRINT "LINE SLOPE = ";B1;" +
     /-";SA
535  PRINT : PRINT : PRINT
540  PRINT "LINE Y INT= ";A;" +/-
     ";SB
545  PRINT : PRINT : PRINT
550  PRINT "LINE FIT COEFFICIENT,
      R@2 = ";R2
555  PRINT : PRINT : PRINT
560  PRINT D$;"PR#0"
570 G$(1) = "M(I)" + F$
580 G$(2) = "MB(I)" + F$
590 G$(3) = "P(I)" + F$
600 G$(4) = "V(I)" + F$
610 G$(5) = "X(I)" + F$
620 G$(6) = "Y(I)" + F$
630 G$(7) = "T(I)" + F$
640 NV = 7
645 P1 = 1
650 NT = N
2160  PRINT D$;"OPEN";F$
2170  PRINT D$;"WRITE";F$
2180  PRINT "TABLE": PRINT "0,1"
2190  PRINT  CHR$ (34);F$; CHR$ (
     34)
2200  PRINT "VECTORS": PRINT "0,"
     ;NV
2210  PRINT  CHR$ (34); CHR$ (34)

2220  PRINT "TUPLES": PRINT "0,";
     NT: PRINT  CHR$ (34)
2230  FOR J = 1 TO NV
2240  PRINT "LABEL": PRINT J;",1"

2250  PRINT  CHR$ (34);G$(J); CHR$
     (34)
2260  PRINT "PERIODICITY": PRINT
     J;",0"
2270  PRINT  CHR$ (34);P1; CHR$ (
     34)
2280  PRINT "MAJORSTART": PRINT J
     ;",0"
2290  PRINT  CHR$ (34);1; CHR$ (3
     4)
2300  PRINT "MINORSTART": PRINT J
     ;",0"
2310  PRINT  CHR$ (34);0; CHR$ (3
     4)
2320  PRINT "TRUELENGTH": PRINT J
     ;",0"
2330  PRINT  CHR$ (34);NT; CHR$ (
     34)
2340  NEXT J
2350  PRINT "DATA": PRINT "0,0": PRINT
      CHR$ (34); CHR$ (34)
2360  FOR N = 1 TO NT
2370  PRINT "-1,0": PRINT "BOT"
2380  FOR M = 1 TO NV
2410  PRINT "0,";D(M,N): PRINT "V
     "
2420  NEXT M
2430  NEXT N
2440  PRINT "-1,0": PRINT "EOD"
2450  PRINT D$;"CLOSE";F$
2460  END
```

Experimental Reactor Design

```
      IMPLICIT REAL*8(A-H,O-Z)
      REAL*8 X(1000),XX(1000)
      DOUBLE PRECISION STRING(4)
5     TYPE*,'ENTER REACTION T(C) AND PHOSGENE PARTIAL PRESSURE(ATM)'
      ACCEPT*,T,PA
      TYPE*,'ENTER TOTAL RXN GAS FLOW(CCPM) AND TOLERANCE'
      ACCEPT*,FT,TOL
      TYPE*,'ENTER TIME AND Z STEP SIZES AND AO'
      ACCEPT*,DT,DZ,AO
      XAO=PA/0.96
      RA=DT/DZ**2.
      TN=2.D-5
      BN=FT*3.33D-7
      CT=1.194D-2/(T+273.14)
      N=106/DZ
      NN=8/DZ+1
      A=2.011
      TIME=0.0
      DIFF2=0.0
C     TEST=XAO*FT/(60.+FT)
      DO 10 I=2, N+1
         X(I)=0.0
10    CONTINUE
      X(1)=XAO
      XX(1)=XAO
      TT=T/100.
      G=AO*DEXP(-24949.7/(T+273.14))*CT**.5*DT
      DAB=.454897+.0998095*TT+.033257*TT*TT-.0010667*TT**3.
15    DO 20 J=2, N
20    XX(J)=X(J)
      F=BN/CT*DT/DZ
      E=DAB*RA
      DO 30 K=2, NN
      GG=G*((XAO-X(K))/2.)**.5
      X(K)=E*XX(K-1)+(1.-2.*E+F-GG)*XX(K)+(E-F)*XX(K+1)
30    IF (X(K) .EQ. 0.0) GO TO 53
      NM=8/DZ+2
      F=(BN-TN)/CT*DT/DZ
      GG=G*((XAO-X(NM))/2.)**.5
      X(NM)=E*XX(NM-1)+(1.-2.*E+F-GG)*XX(NM)+(E-F)*XX(NM+1)
      IF (X(NM) .EQ. 0.0) GO TO 53
      MM=29/DZ+1
      F=-TN/CT*DT/DZ
      DO 40 L=NM+1, MM
      GG=G*((XAO-X(L))/2.)**.5
      X(L)=E*XX(L-1)+(1.-2.*E+F-GG)*XX(L)+(E-F)*XX(L+1)
40    IF (X(L) .EQ. 0.0) GO TO 53
      E=0.3377*RA
```

```
        DO 50 M=MM+1, N
        GG=G*((XAO-X(M))/2.)**.5
        X(M)=E*XX(M-1)+(1.-2.*E+F-GG)*XX(M)+(E-F)*XX(M+1)
50      IF (X(M) .EQ. 0.0) GO TO 53
53      DO 55 LL=1, N
        IF(X(LL) .EQ. 0.0) GO TO 56
55      TEST=TEST+X(LL)-XX(LL)
C55     TYPE*,LL,DZ*LL,X(LL)
56      TIME=TIME+DT
        AA=LL
        TESTER=TEST/AA
C       TESTER=(TEST-X(NM))/TEST*100.
        IF(TESTER .LE. TOL) GO TO 65
        GO TO 15
65      TYPE*,'TOTAL TIME = ',TIME
        DO 70 II=1, 21
        IF (X(II) .EQ. 0.0) GO TO 75
70      TYPE*,II-1,(II-1)*DZ,X(II)
75      TYPE*,'DO YOU WANT TO TRY AGAIN? (YES=0)'
        ACCEPT*,IJI
        IF (IJI .EQ. 0) GO TO 5
        STOP
        END
```

Fly Ash Reaction Model

```
      IMPLICIT REAL*8(A-H,O-Z)
      REAL*8 X(200),Y(200)
      DOUBLE PRECISION STRING(4)
      INTEGER*2 FILE1(15)
      DATA FILE1(4),FILE1(5)/'.I','NT',/
8     TYPE*,'ENTER TEMPERATURE AND PHOSGENE PRESSURE:'
      ACCEPT*,Q,XF
      TYPE*,'ENTER XMIN, XMAX, STEP:'
      ACCEPT*,XMIN,XMAX,STEP
      INC=(XMAX-XMIN)/STEP
10    DO 20 I=1, INC+1
         Y(I)=XMIN+STEP*(I-1)
         X(I)=4.28309D-11*(Q+273.14)*(1.-(1.-Y(I)/.4)**.33333)/XF
         X(I)=X(I)*DEXP(2.05264D04/(Q+273.14))
         TYPE*,I,X(I),Y(I)
20    CONTINUE
35    TYPE*,'DO YOU WISH TO SAVE? (0=YES):'
      ACCEPT*, II
      IF(II .NE. 0) GO TO 8
      TYPE*,'ENTER FILE NAME (MUST BE 6 CHARACTERS:______.INT):'
      ACCEPT 2000, FILE1(1), FILE1(2), FILE1(3)
      OPEN(UNIT=4,NAME=FILE1,TYPE='NEW')
      JJ=1
      WRITE(4,*) JJ
      WRITE(4,*) INC+1
      DO 50 I=1,INC+1
50    WRITE(4,*) X(I),Y(I)
70    CLOSE(UNIT=4)
900   TYPE*,'DO YOU WISH TO TRY AGAIN? (0=YES):'
      ACCEPT*, II
      IF(II .EQ. 0) GO TO 8
2000  FORMAT(3A2)
      STOP
      END
```

Chlorination Reactor Design

```
      IMPLICIT REAL*8(A-H,O-Z)
      REAL*8 X(600),XP(600),QNET(600),PD(600),Y(6)
     1 ,VB(6),TB(6),WMOL(6),P(600)
      DOUBLE PRECISION STRING(4)
      INTEGER*2 FILE1(15)
      DATA FILE1(4),FILE1(5)/'.I','NT',/
5     TYPE*,'ENTER T (DEG C) & P ESTIMATE (ATM)'
      ACCEPT*,T,PEST
      TYPE*,'ENTER PHOSGENE MASS FRACTION'
      ACCEPT*,YPMA
      TYPE*,'ENTER REACTOR RADIUS (METERS)'
      ACCEPT*,R
      TYPE*,'ENTER FLY ASH EXIT CONVERSION'
      ACCEPT*,XF
      TYPE*,'ENTER GASEOUS AND FLY ASH INPUT RATES (KG/HR)'
      ACCEPT*,GT,FI
      TYPE*,'ENTER HEIGHT STEP SIZE (METERS)'
      ACCEPT*,DZ
      AA=2.
      I=1
C
C     Set pellet diameter
      DP= 2.54D-03
C
C     Input gaseous specific molar volumes at Tb
      VB(1)=71.1
      VB(2)=40.0
      VB(3)=101.8
      VB(4)=93.1
      VB(5)=124.5
      VB(6)=114.6
C
C     Input gaseous boiling points
      TB(1)=281.3
      TB(2)=194.5
      TB(3)=456.0
      TB(4)=81.64
      TB(5)=239.1
      TB(6)=330.6
C
C     Input molecular weights of gaseous components
      WMOL(1)=98.92
      WMOL(2)=44.0
      WMOL(3)=133.3
      WMOL(4)=28.0
      WMOL(5)=70.9
      WMOL(6)=169.9
```

```
C       Set bed and pellet porosities
        EB=0.57
        EP=0.48
C
C       Initialize input pressure
        P(1)=PEST
C
C       Initialize CO2, AlCl3, and SiCl4 molar flows
        FCO21=0.0
        FAL1=0.0
        FSI1=0.0
C
C       Set fly ash and phosgene conv. in first slice
        X(1)=XF
        XP(1)=0.0
C
C       Initialize bed height counters
        Z=0.0
        ZT=0.0
C
C       Adjust fly ash input rate for only alumina and silica
        FI=0.84*FI
C
C       Calc. AlCl3, SiCl4, FeCl3, and TiCl4 mass prod'n rates
        ALP=0.5841*FI
        SIP=0.2298*FI
        FEP=0.2177*FI
        TIP=0.0254*FI
        TK=T+273.14
C
C       Calc. slice volume
        V=DZ*R*R*3.141593
C
C       Calc. wall heat flux
        QWALL=1.5*(T-25.)/DLOG((R+0.61)/R)/R
C
C       Adjust COCl2 molar flow for chlorination of alumina and silica only
        GIM=(YPMA*GT-0.3201*FI)/98.917
C
C       Calc. chlorine initial molar flow
        GIN=GT*0.00705*(1.-YPMA)
C
C       Constant part of fly ash mass reaction rate per slice
        CON=2.8194D14*V*DEXP(-20531.4/TK)
C
C       Constant part of COCl2 molar diss. rate per slice
        COD=1.2D16*DEXP(-24950./TK)*V/3.
C
```

```
C       Initialize COCl2, Cl2, CO, and total gaseous molar flows for slice i
        FP1=GIM
        FCL1=GIN
        FCO1=GIN
        FT=FP1+FCL1*2.
C
C       Calc. initial COCl2 and Cl2 mole fractions in slice i
        YP=FP1/FT
        YCL=FCL1/FT
        I=2
C
C       Estimate avg fly ash conv in slice i
        X(I)=X(I-1)-X(I-1)*0.005
C
C       Calc. total gaseous molar concentration
8       CT=12.19*P(I-1)/TK
C
C       Calc. total slice porosity
10      ET=(1.-EB)*(EP+(1.-EP)*X(I))+EB
C
C       Calc. fly ash mass reaction rate in slice i
        FARXN=CON*(1.-ET)*YP*(1.-X(I)/0.4)**0.666667*CT
C
C       Calc. fly ash conv. in slice i
        DX=FARXN/FI
C
C       Calc. deviation of calculated from estimated fly ash conv
        TEST=X(I-1)-DX/AA
C
C       Calc. frac deviation of calculated from estimated fly ash conv
        TOTES=(X(I)-TEST)/TEST
C
C       Apply one percent test
        IF(TOTES .LE. 0.005) GO TO 20
C
C       Estimate new fly ash conv
        X(I)=X(I)-0.5*(X(I)-TEST)
        GO TO 10
C
C       Calc. fly ash avg conv for slice i+1
20      X(I+1)=X(I)-DX
        AA=1.
C
C       Calc. heat generation flux
        QPROD=23.19*FARXN/DZ/R
C
C       Calc. net heat generation flux
        QNET(I)=QPROD-QUALL
C
```

```
C       Calc. phosgene molar diss'n rate for slice i
        FD=CT**1.5*ET*YP*YCL**0.5*COD
C
C       Calc. phosgene molar reaction rate for slice i
        FR=3.03497D-2*FARXN
C
C       Calc. phosgene frac conv in slice i
        PP=(FR+FD)/GIM
C
C       Calc. phosgene conv in slice i+1
        XP(I+1)=XP(I)+PP
C
C       Recalc. COCl2, CO, CO2, Cl2, AlCl3, SiCl4, and total molar flows
        FP2=FP1-FD-FR
        FCO2=FCO1+FD
        FCO22=FCO21+FR
        FCL2=FCL1+FD
        FAL2=FAL1+0.56553*FR
        FSI2=FSI1+0.1517*FR
        FT=FP2+FCO2+FCO22+FCL2+FAL2+FSI2
C
C       Calc. phosgene and chlorine mole frac's for slice i+1
        YP=FP2/FT
        YCL=FCL2/FT
C
C       Reassign mole fractions
        Y(1)=YP
        Y(5)=YCL
        Y(3)=FAL2/FT
        Y(4)=Y(5)
        Y(2)=FCO22/FT
        Y(6)=FSI2/FT
C
C       Calc. gaseous mass flux rate
        G=0.0
        DO 21 M=1,6
21         G=G+Y(M)*FT*WMOL(M)
        G=G*DZ/ET/V
C
C       Calc. gaseous avg molecular weight
        WMOLL=0.0
        DO 22 M=1,6
22         WMOLL=WMOLL+Y(M)*WMOL(M)
C
C       Calc. gaseous density
        RHO=CT*WMOLL
C
C       Increment reactor height
        Z=Z+DZ
C
```

```
C       Calc. viscosity of gas
        VIS1=0.0
        VIS2=0.0
        VISCOS=0.0
        DO 23 N=1,6
           VIS=27.*WMOL(N)**0.5*TK**1.5/VB(N)**0.66667/(TK+TB(N)*1.47)
           VIS1=VIS1+Y(N)*VIS*WMOL(N)**0.5
23         VIS2=VIS2+Y(N)*WMOL(N)**0.5
        VISCOS=VIS1/VIS2*3.6D-4
C
C       Calc. Reynolds number
        RE=DP*G/VISCOS
C
C       Estimate values of two parameters needed for delta P calculation
        IF(RE .GT. 10.) GO TO 24
        FM=100010.-1.D4*RE
        GO TO 25
24      FM=3.
25      IF(RE .GT. 100.) GO TO 26
        ETA=DLOG(RE)*0.3915-0.03171
26      ETA=1.85
C
C       Calc. delta P for slice i
        DELP= FM*G**2.*DZ*(1.-EB)**(3.-ETA)/(DP*RHO*EB**3.)*1.5945D-11
C
C       Calc. new bed pressure for slice i
        P(I)=P(I-1)-DELP
C
C       Calc. phosgene frac. conv. in slice i
        PD(I)=(FCL2-GIN)/GIM
C
C       Output to monitor fly ash and COCl2 conv's, COCl2 diss, and heat prod
        TYPE*,Z,X(I),XP(I),PD(I),QNET(I),P(I)
C
C       Fly ash conv test
        IF (X(I) .LE. 0.0) GO TO 150
C
C       Total pressure test
        IF (P(I) .LE. 1.) GO TO 28
        GO TO 30
28      TYPE*,'BED PRESSURE IS LESS THAN 1.0 ATM'
        GO TO 250
C
C       Phosgene conv test
30      IF (XP(I+1) .GE. 0.95) GO TO 40
C
        GO TO 60
40      TYPE*,'ONLY 5 PERCENT OF PHOSGENE REMAINS'
        GO TO 250
C
```

```
C       Reset COCl2, Cl2, CO, CO2, AlCl3, and SiCl4 molar flows
60      FP1=FP2
        FCL1=FCL2
        FCO1=FCO2
        FCO21=FCO22
        FAL1=FAL2
        FSI1=FSI2
C
C       Increment slice counter
        I=I+1
        GO TO 8
C
C       Print results and initial conditions
150     TYPE*,'ENTER ZERO TO PRINT REACTOR PARAMETERS'
        ACCEPT*,II
        IF(II .NE. 0) GO TO 180
        PRINT*,'          BED DIAM (M)=',2.*R,'           BED HGT (M)=',Z
        PRINT*,' '
        PRINT*,'   FLY ASH RATE (KG/H)=',FI/0.84,'      PHOS RATE (KG/H)='
     1  ,GT*YPHA
        PRINT*,' '
        PRINT*,'              BED POROS=',EB,'        INIT PEL POROS=',EP
        PRINT*,' '
        PRINT*, '           PEL DIAM (CM)=',0.25,'                 FRAC
     1 PHOS DISS=',PD(I)
        PRINT*,' '
        PRINT*,'   PRESSURE DROP (ATM)=',PEST-P(I),'             TEMP (
     1C)=',T
        PRINT*,' '
        PRINT*,'       AL-SI FLY ASH XF=',XF,'               PHOS XF=',
     1  XP(I)
        PRINT*,' '
        PRINT*,'ALCL3 PROD RATE (KG/H)=',ALP,'SICL4 PROD RATE (KG/H)=',SIP
        PRINT*,' '
        PRINT*,'FECL3 PROD RATE (KG/H)=',FEP,'TICL4 PROD RATE (KG/H)=',TIP
        PRINT*,' '
        PRINT*,' '
        PRINT*,' '
C
C       Save to disk fly ash and COCl2 conv and net heat prod rates all f(z)
180     TYPE*,'ENTER ZERO TO SAVE FLY ASH & PHOS XES & QES'
        ACCEPT*,III
        IF(III .NE. 0) GO TO 250
        TYPE*,'ENTER Z-X FILE NAME (MUST BE 6 CHARS)'
        ACCEPT 300, FILE1(1),FILE1(2),FILE1(3)
        OPEN(UNIT=4,NAME=FILE1,TYPE='NEW')
        WRITE(4,*) 1
        WRITE(4,*) I-1
        DO 190 J=1, I-1
        ZT=ZT+DZ
```

```
190     WRITE(4,*) ZT,X(J)
        CLOSE(UNIT=4)
        ZT=0.0
        TYPE*,'ENTER Z-XP FILE NAME (MUST BE 6 CHARS)'
        ACCEPT 300, FILE1(1),FILE1(2),FILE1(3)
        OPEN(UNIT=4,NAME=FILE1,TYPE='NEW')
        WRITE(4,*) 1
        WRITE(4,*) I-1
        DO 200 JJ=1, I-1
        ZT=ZT+DZ
200     WRITE(4,*) ZT,XP(JJ)
        CLOSE(UNIT=4)
        ZT=0.0
        TYPE*,'ENTER Z-Q FILE NAME (MUST BE 6 CHARS)'
        ACCEPT 300, FILE1(1),FILE1(2),FILE1(3)
        OPEN(UNIT=4,NAME=FILE1,TYPE='NEW')
        WRITE(4,*) 1
        WRITE(4,*) I-1
        DO 210 K=1, I-1
        ZT=ZT+DZ
210     WRITE(4,*) ZT,QNET(K)
        CLOSE(UNIT=4)
        ZT=0
        TYPE*,'ENTER Z-P FILE NAME (MUST BE 6 CHARS)'
        ACCEPT 300, FILE1(1),FILE1(2),FILE1(3)
        OPEN(UNIT=4,NAME=FILE1,TYPE='NEW')
        WRITE(4,*) 1
        WRITE(4,*) I-1
        DO 220 JJ=1, I-1
        ZT=ZT+DZ
220     WRITE(4,*) ZT,P(JJ)
        CLOSE(UNIT=4)
        ZT=0.0
        TYPE*,'ENTER Z-PHOS DISS FILE NAME (MUST BE 6 CHARS)'
        ACCEPT 300, FILE1(1),FILE1(2),FILE1(3)
        OPEN(UNIT=4,NAME=FILE1,TYPE='NEW')
        WRITE(4,*) 1
        WRITE(4,*) I-1
        DO 230 JK=1, I-1
        ZT=ZT+DZ
230     WRITE(4,*) ZT,PD(JK)
        CLOSE(UNIT=4)
250     TYPE*,'ENTER ZERO TO RESTART'
        ACCEPT*,KI
        IF(KI .EQ. 0) GO TO 5
300     FORMAT(3A2)
        STOP
        END
```

APPENDIX B: REACTION MODULUS DETERMINATION

It was necessary for the calculation of reaction modulus values to determine the tortuosity factor. Since the tortuosity factor is a function of pellet structure only, any change in the structure resulting from reaction will also change the tortuosity factor. The complexity of determining tortuosity factors as a function of conversion and the need to limit the scope of this study required that the factor be estimated for unreacted pellets only. The modulus values calculated then are useful only in the comparison of initial reaction and pellet diffusion rates.

An effective diffusion coefficient for a pellet pressed at the same force per unit area as the chlorination pellets was used in the determination of the tortuosity factor. Since the tortuosity factor is independent of the gases used in its determination, nitrogen-helium diffusion data, collected at 25 ^{o}C and 0.97 atm, were substituted into equations 22-26 to calculate an effective diffusion coefficient of 0.103 +/- 0.003 cm^2/s.

The tortuosity factor is related to the pellet porosity and the effective molecular and the molecular diffusion coefficients according to (64):

$$\tau D_{eM_N} = \epsilon_p D_{M_N} \qquad (B1)$$

where D_{eM_N} = effective molecular diffusion coefficient of nitrogen, $cm^2 s^{-1}$;

D_{M_N} = nitrogen molecular diffusion coefficient, $cm^2 s^{-1}$.

A value for ϵ_p of 0.42 was estimated using the pellet weight and volume and the fly ash density. The Chapman-Enskog equation (15) was used to compute a molecular diffusion coefficient of 0.72 cm^2/s. Values for the variables on the r.h.s. of equation B1 were then available but a value for D_{eM_N} was still required before τ could be calculated. The Bosanquet formula (equation 9) was multiplied by $1/\tau$ to give:

$$\frac{1}{\tau D_{e_N}} = \frac{1}{\tau D_{eM_N}} + \frac{1}{\tau D_{ek_N}} \qquad \text{(B2)}$$

where D_{ek_N} = effective Knudsen diffusion coefficient of nitrogen, $cm^2 g^{-1}$.

τD_{ek} was estimated using equation 10 and was redefined for further manipulation as:

$$D'_{ek_N} = \tau D_{ek_N} \qquad \text{(B3)}$$

Equations B1 and B3 were then substituted into equation B2 to give:

$$\tau = \frac{\epsilon_p D_{eM_N} D'_{ek_N}}{D_{e_N}(D'_{ek_N} + \epsilon_p D_{eM_N})} \qquad \text{(B4)}$$

With values for all variables on the right Known, a tortuosity factor of 2.7 was computed. This value is within the range seen in the literature (28,64).

The tortuosity factor was then used in the calculation of effective diffusion coefficients for the phosgene-fly ash pellet system. The effective diffusion coefficients were in turn used in equation 6 to estimate reaction modulus values and these results were applied to predict whether diffusion rates would limit fly ash reaction rates. Diffusion control is most likely at high temperatures so modulus values were estimated for temperatures of 625 and 700 ^{o}C.

It was assumed that a fly ash pellet was exposed to pure phosgene. From oxide versus fly ash conversion data (Figure 8), it was known that 1.86 moles alumina react per mole of silica. There were then 3.7 moles of $AlCl_3$ produced per mole of $SiCl_4$ which required the input of 7.6 moles phosgene and the exit of 7.6 moles of carbon dioxide. Phosgene was considered as component A of a binary system with the products comprising component B. The ratios at which the products were produced was used to calculate a mole fraction composition of: CO_2 - 0.61, $AlCl_3$ - 0.32, and $SiCl_4$ - 0.07. The component B parameters needed in the Chapman-Enskog equation were computed using the mole fractions as weighting factors in linear additions. Data for phosgene were obtained from the literature (53). In addition to the molecular diffusion coefficients, values for τD_{ek_A} were estimated using equation 10. Since τ was known, values for D_{eM_A} and D_{ek_A} were calculated and then substituted into the Bosanquet equation, to estimate values of D_{e_A}. The results are listed in Table 7. Rate constants, calculated using the kinetic parameter values from the powder measurements (Figure 10), and modulus values are listed in Table 8. Modulus values of less than 0.3 suggest

Table 7. Estimated initial values for the effective molecular, Knudsen, and overall diffusion coefficients as a function of temperature

T (°C)	D_{eM_A} (cm^2/s)[a]	D_{ek_A} (cm^2/s)[b]	D_e (cm^2/s)
625	0.062	1.305	0.091
700	0.071	1.358	0.067

[a]Phosgene effective molecular diffusion coefficient.

[b]Phosgene effective Knudsen diffusion coefficient.

Table 8. Initial rate constant and reaction modulus values calculated for the reaction of 0.1 cm thick fly ash pellets

T (°C)	k x 10^4 (cm/s)	σ
625	0.71	0.04
700	4.96	0.12

the absence of diffusion rate limitations for a reaction system. Since the modulus is directly proportional to the pellet half-thickness, the modulus value of 0.3 and the pellet thickness of 0.1 cm were used to predict that pellets with a primary axis of up to 0.25 cm (0.1 inch) would be surface reaction rate limited at 700 °C. It must be assumed, however, that the tortuosity does not change dramatically as a function of conversion.